

2

AD-A247 791



EOARD LR-91-037

DTIC
ELECTF
MAR 9 1992
S C D

PROCEEDINGS
of the
4th OGAMM MEETING

19-22 August 1991

Ilkley, Yorkshire, England

Approved for public release;
Distribution Unlimited

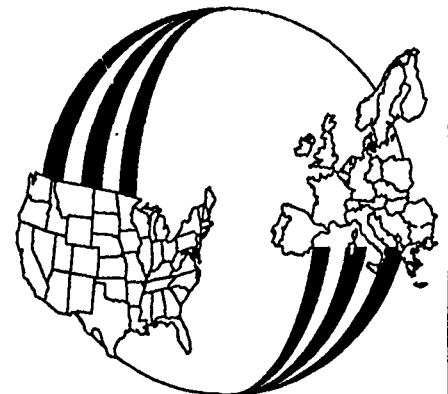
92-07042



LIAISON REPORT

Lt Col Chester J. Dymek
Air Force Office of Scientific Research

EUROPEAN OFFICE OF AEROSPACE
RESEARCH AND DEVELOPMENT



92 3 19 023

**PROCEEDINGS OF THE 1991 OPTICAL GLASS AND
MACROMOLECULAR MATERIALS (OGAMM) MEETING**

by

LtCol Chester J. Dymek

19-22 Sep 91

ABSTRACT

The Fourth OGAMM Meeting was held at the Craiglands Hotel in Ilkley in Yorkshire, England from 19 to 22 August 1991. The OGAMM program is a highly collaborative multidisciplinary effort designed to provide the technology base needed for the development of the highly sophisticated devices needed for advanced SDI systems. Because these devices are generally intended for imaging, detecting, photonics, tracking, and communications systems, the research focuses on material concepts combining various nonlinear optical, electrical, magnetic, thermal and mechanical functions. In the past year excellent progress has been made in understanding the influence of molecular structure and surface processes on these properties in a wide range of materials, including impregnated gel silica, multifunctional polymers, polymer blends, and polymer - glass composites. New device concepts and new insights into the role of local order on material processing and properties have also emerged. Greater control of material quality and the ability to predictably combine different functional groups to make truly multifunctional materials were identified as key program objectives at last year's OGAMM meeting. This year it is clear they have been achieved.



Accession For	
NTIS Grant	<input checked="" type="checkbox"/>
DTIC Tab	<input type="checkbox"/>
Unannounced	<input type="checkbox"/>
Justification	
Proc 91 Proceedings	
Distribution/	
Availability Codes	
Dist	Avail and/or Special
A-1	

TABLE OF CONTENTS

	Page no
The 1991 Optical Glass and Macromolecular Materials (OGAMM) Meeting - Overview by Lt Col C. J. Dymek, EOARD	1
<u>Organic Multifunctional Materials</u>	
Functional Polymers and Guest-Host Polymer Blends for Optical and Electronic Applications by <u>Prof. Graham Williams</u> , University College of Swansea, in collaboration with Professor F. E. Karasz, University of Massachusetts, and Dr. G. S. Attard, University of South Hampton	6
Control of Molecular Organisation in Side-Chain Polymers and Low Molar Mass Crystals by <u>G.S. Attard</u> , the University of Southhampton	12
Polyarylene Vinylene Copolymers by <u>F. E. Karasz</u> , University of Massachusetts	21
Thin Films of Functional Polymers by <u>Naoya Ogata</u> , Sophia University	26
Novel Electroactive and Nonlinear Optical Composites by <u>Paras N. Prasad</u> , Photonics Research Labratory, Suny Buffalo	32
Developement of Nonlinear Optical Devices by Improvement of Molecular Hyperpolarizabilities and Via Photoprocessing by <u>L. R. Dalton</u> , USC, Los Angeles CA	37
Multifunctional Macromolecules: Combining Photoconductivity and Electro- Optic Activity to Create Photorefractive Polymers. by M. J. Sanstone, K. Blatter, G. L. Breckenridge, A. J. East, <u>H. A. Goldberg</u> , M. S. Kwiatek, C. F. Shu, Hoechst Celanese Corporation	42
Applications of Photorefractive Polymers by <u>M. R. Worboys</u> and S. C. Gratzel, GEC- Marconi Research Centre, Chelmsford Essex UK	48
Local Electric fields in Poled Polymers as Probed by Photoconduction Experiments by <u>D. Haarer</u> , University of Bayreuth	53
The Effect of Mesogen Concentration on Pyroelectric Activity and on Dielectric and T.S.C Relaxation Phenomena by <u>Mr. P. L. Carr</u> , Dr. G. R. Davies and Professor I. M. Ward	60
Characterization and Kinnetics of Electric Field Alignment of Poly(MOxONS-CO-MMA) by <u>R. B. Findlay</u> and A. H. Windle	65

TABLE OF CONTENTS

Page no

Inorganic Multifunctional Materials

- Three Dimensional Packing Problems Associated with Molecular Materials 71
by D. Michael P. Mingos, University of Oxford
- Semiconductor Quantum Dot Materials 78
by Professor John D. Mackenzie and Chin Yen Li,
UCLA Professor Masayaki Yamane, Tokyo
Institute of Technology
- Second Harmonic Generation (SHG) in Inorganic Materials 85
by Professor John D. Mackenzie, Yuhuanan Xu
and Yu-Hua Kao, UCLA

Gel Silica Multifunctional Materials

- Structurally Engineered Porous Sol-Gel Silica for Optical Composites 90
by Larry L. Hench, University of Florida
- Progress in the Optical Technology of Gel-Silica and Polymer Materials 97
by Nicholas J Phillips, Spencer Modica, and Ce Wang,
Loughborough University
- Gel-Silica Lasers and Optics 105
by A. Charlton, M. A. Meneses-Nava, D. J. Shaw and T. A. King,
University of Manchester
- Structural Studies of Sol-Gel Glasses 114
Carole C. Perry and Xiaochun Li, Brunel University

LIST OF MEETING PARTICIPANTS 121**DISTRIBUTION** 126

**THE 1991 OPTICAL GLASS AND MACROMOLECULAR MATERIALS
(OGAMM) MEETING - AN OVERVIEW**

by

LtCol Chester J. Dymek

AIR FORCE OFFICE OF SCIENTIFIC RESEARCH

EUROPEAN OFFICE OF AEROSPACE
RESEARCH AND DEVELOPMENT

Introduction

The Fourth OGAMM Meeting was held at the Craiglands Hotel in Ilkley in Yorkshire, England from 19 to 22 August 1991. The OGAMM program is a highly collaborative multidisciplinary effort designed to provide the technology base for the development of the highly sophisticated devices needed for advanced SDI systems. Because these devices are generally intended for imaging, detecting, photonics, tracking, and communications systems, the research focuses on material concepts combining various nonlinear optical, electrical, magnetic, thermal and mechanical functions. In this overview the structure of the OGAMM program is reviewed and updated, and the results of the "wrap-up" session involving the participants are summarized. Funding support for this program comes primarily from the Innovative Science & Technology arm of the SDI Office, SDIO/IST (Dr. Len Caveny). Additional support is provided by AFOSR through the OGAMM Program Manager, Dr. Charles Lee, AFOSR/NC, and from the European Office of Aerospace Research & Development (LtCol Dymek, EOARD/LRC). George Gallagher-Daggitt is primarily responsible for the planning of the OGAMM meeting and is also a key player in the post meeting discussions with LtCol Dymek and Dr. Lee on the status of the program.

Structure of OGAMM

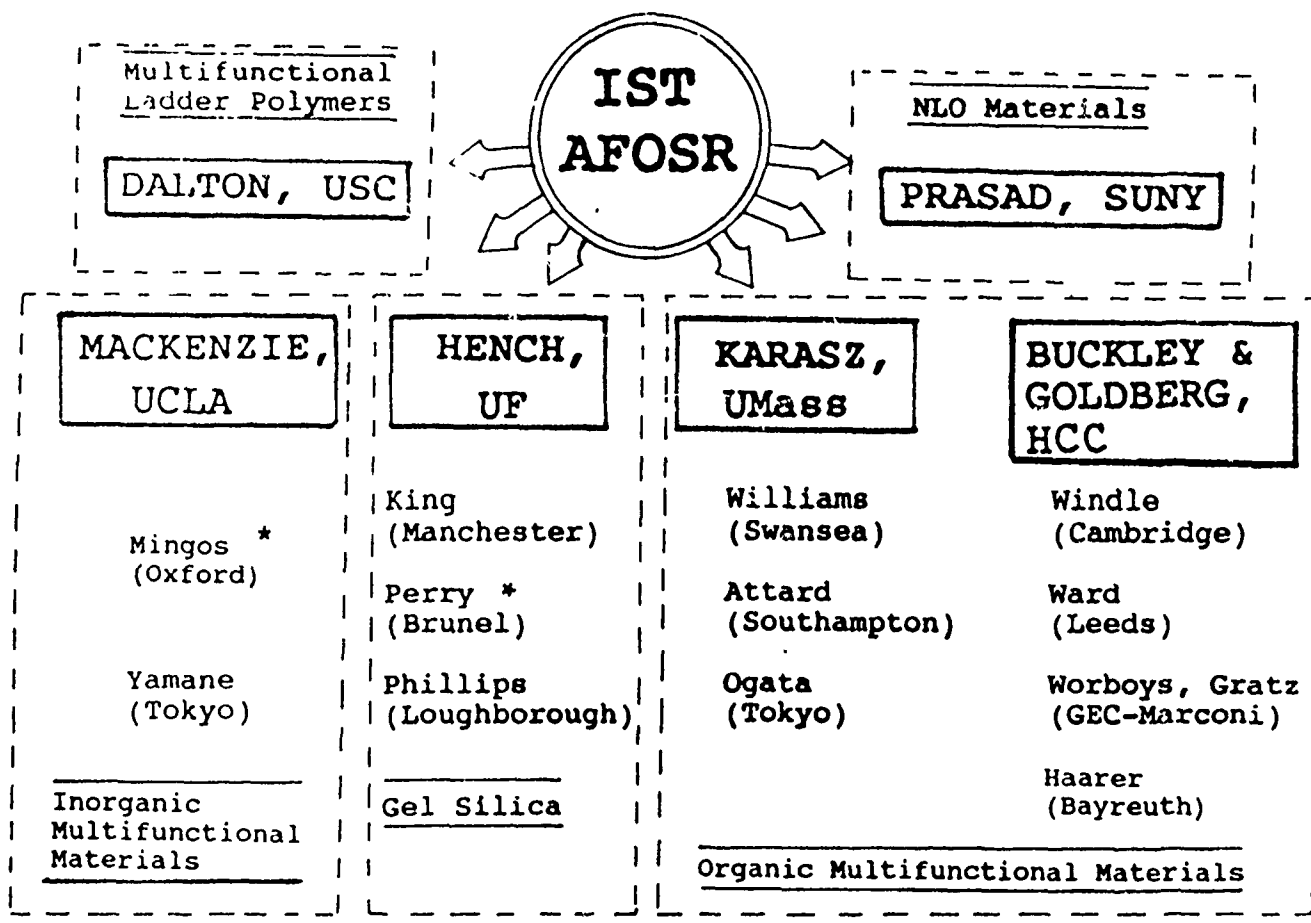
Following a reduction in the level of support from SDIO/IST in FY91, the structure of the OGAMM program has been slightly altered. Figure 1 shows the current organization. The six prime contractors from the US, who directly receive the IST funds, are listed in solid blocks. The general areas in which they work are indicated by the labels in the dashed blocks. Four of the primes have subcontractors from Europe and Japan.

The technical structure of the program is indicated in Figure 2. This gives a listing of key words which can be considered to characterize the phases in the progress from new materials ideas to device concepts. The starting point in the process is the production of interesting new materials. "Molecular engineering" of polymers and sol-gel processing of silica glass and composites of silica glass with organic materials have been the most highly visible activities at this stage. Once new materials are identified and created, the various electrical and optical properties expected for them are measured, and a range of other key aspects such as thermal stability and processibility are evaluated. As the reverse arrow suggests, information about the properties can be used to suggest modifications to the materials' chemistry or processing. Next, the behavior of systems with interesting properties is studied to determine their suitability for various functions. Finally the materials with suitable functionality or, preferably, multifunctionality are incorporated into laboratory devices to evaluate their performance. *These device concepts, along with the multifunctional materials used in them, represent the end products of the OGAMM program.* As the dashed "feedback arrow" indicates, the test devices also represent stimuli for new material developments by magnifying both the defects and special qualities of the materials incorporated into them.

Progress towards OGAMM Goals in FY91

The highly cooperative spirit of the OGAMM program participants, which has led to fruitful exchange of information and productive collaboration, continued despite any pressure that might have resulted from a diminished budget. This in itself is a major achievement and reflects the high level of professionalism of the scientists in the program.

While there were important advances in each of the research efforts within the program, three developments attracted particular attention from the participants. Doug MacKenzie's description of new amorphous $\text{LiNb}(\text{OC}_2\text{H}_5)_x\text{O}_{3-x/2}$ films exhibiting ferroelectric behavior was both surprising and interesting. The observation was confirmed by P-E hysteresis loop studies and pyroelectric current measurements. The discovery opens up new design possibilities for devices using the ferroelectric effect and is intriguing as a scientific question. Another impressive achievement is the enhanced control over laser densification of impregnated gel silica attained by Terry King's group. The capability to make devices with microlensing arrays using these materials now appears ready to enter the engineering stage. Finally, the synthesis and characterization of multifunctional polymers exhibiting the photorefractive effect by the Hoechst-Celanese group led by Harris



* - Direct AFOSR Grant

Figure 1.

OGAMM KEY WORDS

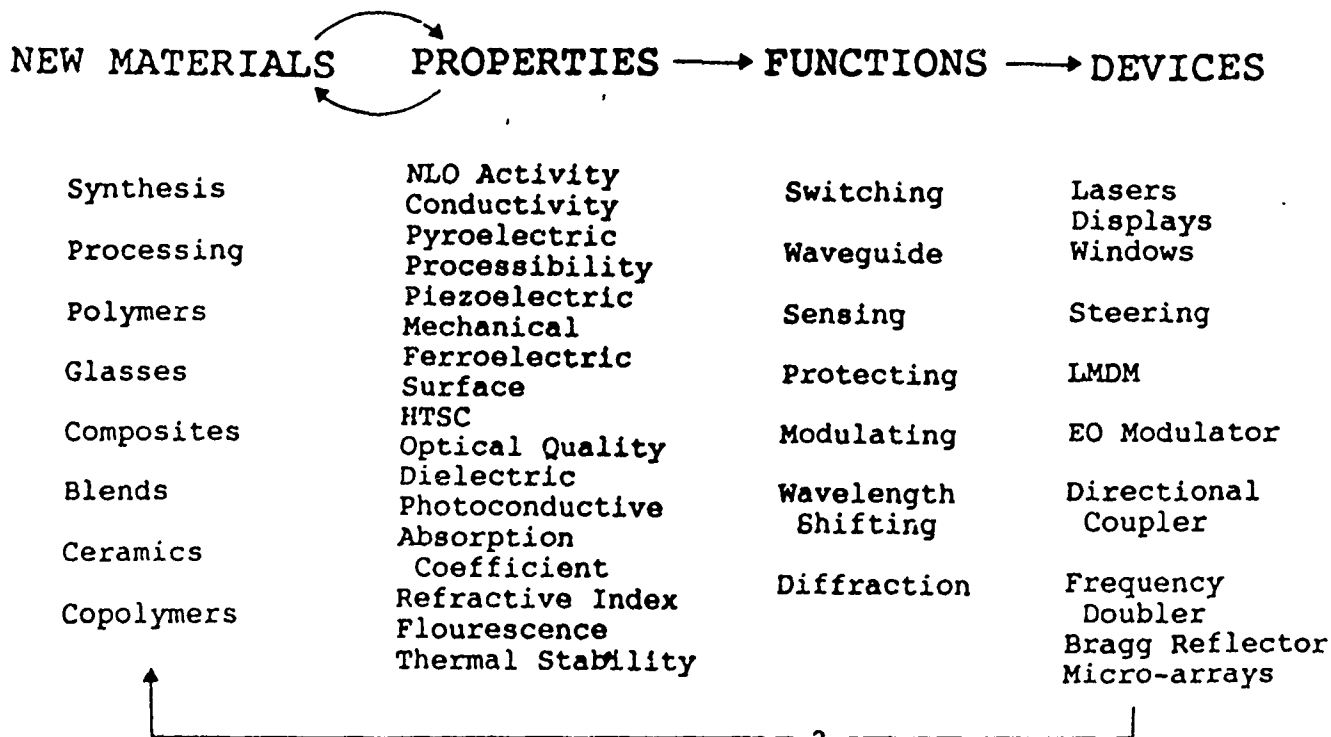


Figure 2.

Goldberg was widely recognized as a major advance. This combination of photoconductive and electrooptic functions to produce a multifunctional photorefractive material could lead to the realization of a number of device concepts, including beam steering.

The groups working on organic multifunctional materials have increased the understanding of the principles involved in "engineering" these materials. This includes greater understanding of the poling process and the role of local order in that process; how to orient "self assembled" multifunctional systems; and the synergistic multifunctionality in the photoconduction of oxynitrostilbene - carbazole copolymers. The ability of the Hoechst-Celanese group to produce well characterized multifunctional polymer films of high purity was underscored by reports of application of 1000 volt poling fields across 10 micron films. There have also been advances in the dielectric techniques used to study the effects on properties of copolymer ratios, spacer lengths, molecular weight and other subtle changes in molecular structure. Novel methods for producing NLO active polymer films, including formation at air-water interfaces by the Langmuir-Blodgett method, continue to emerge from collaborations among these groups. Larry Dalton's highly innovative team has used ultrastructural engineering (photo and thermal structural engineering) to realize "device quality" 2nd order NLO organic polymers, solving problems of lattice instability, phase matching and optical circuit integration. Paras Prasad's group has demonstrated that Kerr-scattering in liquid filled hollow fibers "offers a light weight, low power, and compact system" for generating a multiwavelength laser source for application to Light Detection and Ranging (LIDAR). There is also a greater awareness of the variety of approaches that can be used to create glass - polymer composites to achieve different effects for different device concepts.

The gel silica group has continued to show that while they are in many respects working with the most "mature" of the materials concepts and are demonstrating various device concepts, there remains much basic research to be done in this field. Progress continues to be made in the understanding of the surface chemistry going on at the pore walls in porous gel silica including more information on the parameters that affect the modes in which water is adsorbed. It is now possible to create gel silica monoliths with 40 angstrom pores for uniform impregnation by laser dyes. Advances have been made in demonstration of the flexibility of gel silica based dye lasers and new concepts employing impregnated gel silica are emerging in distributed feedback lasers, edge-illuminated holograms, devices with graded index of refraction, and pattern recognition.

The inorganic multifunctional materials group evolved out of what was an effort focused on high temperature superconductors. Relatively large samples of CdS quantum dot materials with very good optical quality have been prepared using the sol-gel technique. When ORMOSIL matrices are used, these materials can be prepared with excellent quality at firing temperatures of only 300°C. Methodologies have also been developed which have led to a better understanding of the packing modes of molecular salts in coordination and

organometallic chemistry and how these modes influence conductivity and ferromagnetic and NLO properties.

Key Issues

With the development of photorefractive multifunctional polymeric materials, there are new opportunities to realize devices which could not be made with inorganic photorefractive materials because of material quality or sensitivity reasons. However, a key property, response time, must be significantly improved for some of the most interesting applications, e.g., beam steering. Thus a greater effort must be made to understand the dynamics of the multistage photorefractive process.

As more is understood about the molecular basis for NLO and other interesting properties, the focus is shifting somewhat to the dependence of these properties on packing modes and interactions which affect the local order and ultimately bulk structure. The fact that local order can impede poling even when liquid crystalline phases are not evident indicates the need to understand how this local order can be influenced.

The observation of a ferroelectric effect in amorphous lithium niobate thin films points to the need to examine this class of materials in greater depth. It also suggests that more needs to be understood about the fundamental nature of the ferroelectric effect.

Summary

In the past year excellent progress has been made in understanding the influence of molecular structure and surface processes on the NLO, electrooptic, and other properties in a wide range of materials, including impregnated gel silica, multifunctional polymers, polymer blends, and polymer - glass composites. New device concepts and new insights into the role of local order on material processing and properties have also emerged. Greater control of material quality and the ability to predictably combine different functional groups to make truly multifunctional materials were identified as key program objectives at last year's OGAMM meeting. This year it is clear they have been achieved.

Functional Polymers and Guest-Host Polymer Blends for Optical and Electronic Applications

Graham Williams, Professor of Chemistry, University College of Swansea, SA2 8PP, in collaboration with Professor F.E. Karasz, University of Massachusetts, and Dr. G.S. Attard, University of Southampton, U.K.

Introduction

Organic polymer films, 1-100 μm in thickness, comprising functional polymer molecules or guest molecules in a host polymer medium may exhibit a range of useful optical, electrical/dielectric and electro-optical properties. Table 1 indicates some of these, gives their origins in molecular behaviour and their potential applications in optics and electronics. The susceptibility factors for the different functions (e.g., SHG generation) may be varied over a wide range by choice of chemical structure, polymer morphology and the method used for sample preparation. While individual properties are of interest in their own right, special interest is attached to the possibility that a given polymer film may exhibit multi-functionality^{1,2}, leading to a synergism of several functions. This is not possible with conventional inorganic materials, thus polymer materials offer new possibilities for devices.

While it has been demonstrated that the properties of functional polymer films may be optimized to give practical device materials, an important consideration is the possible loss of property with time for a variety of reasons (see Table 1). Molecular motions feature strongly as a mechanism for loss of property. Our research during the past year has involved the study of the electrical/dielectric, optical and electro-optical properties of novel liquid-crystalline (LC) and amorphous polymers and has been aimed at obtaining a fundamental understanding of the motional properties (through the dielectric relaxation behaviour) and the electric-field-induced alignment behaviour so that the physical properties of practical materials may be controlled and be retained without loss of function with time.

Table 1

Physico-chemical Phenomenon	Macroscopic observable	Nature of polymer phase	Potential application	Possible mechanisms for loss of property
Photobleaching, photochromism, photoisomerization	Optical contrast, dichroism and birefringence	A,LC	Data storage (reversible), optical elements, (e.g. diffraction gratings, holograms, waveguides)	Further photobleaching, photoreversal, loss of alignment(LC), molecular motion, diffusion
Laser-induced polarization via higher-order polarizabilities	SHG, THG, four wave mixing	A,LC	Non-Linear optics(NLO), harmonic generation	Loss of poling by molecular motion
Melting of crystalline phase or LC phase	Optical contrast by light scattering	X,LC	Data storage (reversible)	
Dipole alignment, mechanical deformation	Spontaneous polarization	A,X,LC	Piezoelectric devices	Loss of alignment, charge neutralization, molecular motion
Dipole alignment, thermal pulse	Spontaneous polarization	A,X,LC	Piezoelectric devices	ditto
Motion of charges (electrons, holes, ions)	dc and ac conduction	A,X	Semiconducting, conducting and photo-conducting materials	Chemical fatigue, electrode processes
Deposition of charged species	Electrochromism	A	Optical Storage(reversible)	ditto

Key: A = Amorphous, X = Crystalline, LC = Liquid Crystalline.

Experimental

Computer controlled apparatus were used for broad-band dielectric relaxation spectroscopy (10-10⁶Hz) and thermally-stimulated-current measurements. A dielectric/optical cell was devised and was incorporated into a computer-controlled hot-stage attached to an Olympus polarizing microscope, thus allowing simultaneous optical microscope observations and dielectric measurements to be made with samples undergoing thermal/electrical treatments. Optical textures were recorded with a camera or with a CCTV/VCR system, thus allowing time-dependent observations to be made, which are particularly interesting for LC polymer films.

Molecular Motions in Functional Properties

Molecular motions in amorphous, crystalline or liquid crystalline polymers may play a part in creating or destroying a particular physical property of a polymer film. For example, to obtain samples suitable for SHG purposes, a material is 'poled' in the melt using an electric field, leading, through molecular mobility, to a perturbation of the orientational distribution of the polarizable molecules or groupings. The sample is then cooled into the relatively immobile glassy state with the field maintained, giving a 'poled' sample. Loss of the field-perturbed distribution in the glass over a period of time may be due to local reorientational motions (β -process). In order to obtain a better understanding of the roles that molecular motions play in the creation and loss of functional properties, we have carried out^{3,4} detailed surveys and analyses of the dielectric properties of amorphous, crystalline and LC polymers and of small-molecule glass-forming systems. For amorphous polymers the occurrence, nature and mechanisms for α , β and $\alpha\beta$ relaxations have been investigated and the coupling between the α -process (dynamic glass transition) and the β -process (limited motions) is demonstrated even when they are well-resolved in the time or frequency domains. The common observation that the α -process in most glass-forming systems is characterized by the Kohlrausch-Williams-Watts (KWW) stretched exponential function for all types of measurement (dielectric, NMR, quasi-elastic light scattering, volume, enthalpy and specific heat relaxation) is discussed in terms of generic mechanisms for the cooperative motions of molecules. Many of the functional properties indicated in Table 1 exhibit physical aging through motional processes, and those latter processes need to be suppressed in order to maintain the property of a device. In this context it is important to note that molecular reorientational motions are best understood in terms of molecular time-correlation functions $\langle D_{mn}^J(\Omega(t))D_{mn}^{*J}(\Omega(0)) \rangle$ and we should distinguish between the tensorial rank for the functions responsible for dielectric relaxation (rank one), NMR relaxation, quasi-elastic light scattering, fluorescence depolarization (rank two) and the decay of SHG (rank three). The different correlation times may be inter-related using information theory, thus the rate of SHG decay may be predicted from a knowledge of the dielectric properties in suitable cases. Hence, a knowledge of molecular motions in the glassy state and the LC state, and how they are affected by chemical preparation and electrical/thermal treatments provides a basis for optimizing the required property (Table 1) and inhibiting its decay process.

Liquid-Crystalline Side Chain Polymers

The study which was initiated for a number of siloxane-chain and carbon-chain polymers having the mesogenic groups in the side chain (as described in ref. 2), has been continued and extended. Experimental data for the dielectric and optical properties of films in different states of macroscopic alignment, as prepared using electrical/thermal treatments, have been analyzed in detail and several of the results have been published⁵⁻⁷ or are being submitted for publication^{8,9}. The results to date may be summarized as follows:-

(i) Siloxane-chain homopolymers and copolymers were readily aligned homeotropically (H) or planarly (P), or to any extent of intermediate alignment, using the two-frequency addressing principle. The dielectric spectra obeyed the mixture law

$$\epsilon(\omega) = (1 + 2S_d) \cdot \epsilon_{\parallel}(\omega) / 3 + 2(1 - S_d) \cdot \epsilon_{\perp}(\omega) / 3 \quad (1)$$

where S_d is the director order parameter and $\epsilon(\omega)$, $\epsilon_{\parallel}(\omega)$ and $\epsilon_{\perp}(\omega)$ are the complex dielectric permittivities for a sample of intermediate alignment (having a director order parameter S_d), and for the H and P aligned samples, respectively. S_d may be determined from the permittivity curves $\epsilon'(\omega)$ or from the loss curves $\epsilon''(\omega)$, thus the extent of macroscopic alignment was readily determined for samples undergoing realignment in the presence or absence of directing electric fields. The dielectric spectra ($\epsilon''(\omega)$ - vs - $\log f/\text{Hz}$) for H- and P-aligned samples were analyzed in terms of the four orthogonal relaxation modes for the anisotropic motions of the dipolar head groups of the mesogenic side chain. Studies of the kinetics of the realignments $H \leftrightarrow P$ in directing fields at different sample temperatures revealed that lowering the temperature only a few degrees below the clearing temperature T_c reduced the realignment rates dramatically, and clearly demonstrated the practical temperature range in which a sample may be aligned $H \leftrightarrow P$. Figure 1 shows, as one example, the loss spectra for H- and P-aligned polymer I (whose structure is appended) at different temperatures. The difference in spectra is evident and shows that (a) the 00 mode dominates the spectrum of the H-aligned material, (b) the 10 mode is essentially absent for the P-aligned material, (c) that as T_c is approached the decrease in local order parameter S leads to a decrease in height of the 00 mode and to a corresponding increase in the height of the 10 mode, as predicted by molecular theory¹⁰. The optical properties show marked changes during the transformations $H \leftrightarrow P$, and the kinetics of the optical changes complement the kinetics of change of S_d , as determined by the dielectric measurements made simultaneously. It is shown that the values of S_d hardly change as optical transparency for the H-aligned material is gradually achieved at the final stages of the transformation $H \leftrightarrow P$, showing that only slight imperfections in alignment have a marked effect on the optical transparency. Studies of this kind for different siloxane-chain LC polymers give results which are reproducible and are consistent with macroscopic continuum theory for the dielectric properties and for the alignment behaviour and also with molecular theory¹⁰ for the dielectric properties. Of the different siloxane-chain polymers studied, polymer I is identified as a material whose alignment behaviour and optical properties can be closely controlled and it is

particularly well-suited for applications for optical data storage and NLO in its pure and doped states.

(ii) The carbon-chain LC polymers we have studied have significantly higher glass-transition temperatures (T_g) and clearing temperatures (T_c) than the siloxane-chain LC materials. Raising T_g has the advantage that the carbon-chain polymers are in the glassy LC state around room temperature, thus enhancing their properties (Table 1) and reducing physical aging effects. However, high T_g and high T_c means that electric-field-induced alignment is carried out at significantly higher temperatures than those used for the siloxane-chain polymers. This also means that dc conductivity is high at the operating temperatures for E-field-induced alignment, and this may have an adverse effect on the alignment process. Using pure materials, and using an 'electrical cleaning' method we have developed which reduces the conductivity by up to a factor of five, we have succeeded⁸ in obtaining well aligned samples of carbon-chain LC polymers, e.g., of polymers II and III, and have studied their dielectric and optical properties. The relaxation properties of these styrene and acrylate-based polymers resemble those for amorphous solid polymers in contrast to the siloxane-chain polymers whose properties resemble those of low molar mass liquid crystals. A combined dielectric and optical study of NLO polymers supplied by Dr Attard having a structure similar to polymer II with variable spacer length $3 < m < 12$ are presently being investigated.

Electrets from NLO Polymers

We have studied the thermally-stimulated depolarization currents (TSDC) derived from electrets of LC polymers having the structure of polymer II except the spacer group has $m=5$ (polymer IV say). The changes in the TSDC curves obtained when the electret was aged for different periods of time at different fixed temperatures in the glassy LC phase were studied and were consistent with physical aging of the specimen. As one example of the results of different thermal/electrical treatments of the sample, figure 3 shows the changes in the TSDC curves on repeated formation of the electret. Remelting the specimen regenerates the sample but repeated cycling gives again the diminution of the TSDC curve, which reflects a systematic loss of stored charge, and hence of NLO activity. These and related studies of NLO polymers are being pursued in order to identify the mechanisms for the loss of electret property shown in figure 3.

References

- [1] A. Buckley, G. Gallagher-Daggitt, F.E. Karasz and D.R. Ulrich, (Eds.), *Multifunctional Materials*, Mater.Res.Soc.Boston, 1990.
- [2] Proc. 3rd OGGAM Meeting, Keswick, 1990..
- [3] G. Williams, *Molecular motion in glass-forming systems*, J.Non Cryst.Solids, 1991, 131, 1-11.
- [4] G. Williams, *Dielectric relaxation of amorphous, crystalline and liquid crystalline polymers*, in Materials Science and Technology, Vol. 12, E.L. Thomas and E.J. Kremer (Eds.), Ch. 11, 45 pp, VCH Publ. 1991, in press.

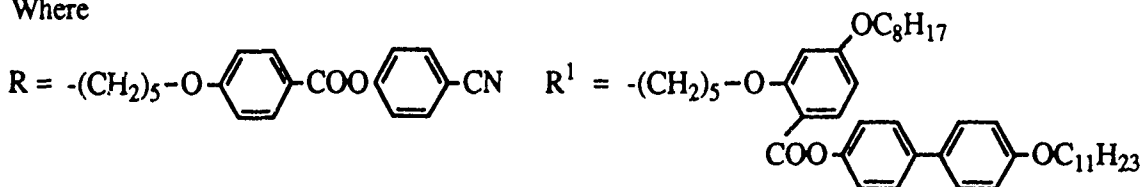
- [5] G. Williams, A. Nazemi and F.E. Karasz, *Dielectric relaxation properties and alignment behaviour of LC side-chain polymers*, in ref. 1, p. 227-237.
- [6] A. Nazemi, E.J.C. Kellar, G. Williams, F.E. Karasz, J.S. Hill, D. Lacey and G.W. Gray, *Electric field induced AC alignment and realignment, a study of a LC polymer having longitudinally and laterally-attached mesogenic groups as side chains, monitored through dielectric spectroscopy and optical thermomicroscopy*, *Liquid Crystals*, 1991, **9**, 307-320.
- [7] G. Williams, A. Nazemi, F.E. Karasz, J.S. Hill, D. Lacey and G.W. Gray, *Dielectric relaxation properties and alignment behaviour of a LC polymer having laterally-attached mesogenic groups*, *Macromolecules*, 1991, in press.
- [8] A. Nazemi, G. Williams, G.S. Attard and F.E. Karasz, *AC alignment behaviour and molecular dynamics of two NLO LC side chain polymers studied by dielectric and optical techniques*, *J.Mater.Chem.*, submitted.
- [9] A. Nazemi, G. Williams and F.E. Karasz, *Molecular dynamics and alignment behaviour of a LC copolymer containing longitudinally and laterally-attached mesogenic groups in the side chain*. Being submitted.
- [10] G.S. Attard, K. Araki and G. Williams, *A simple approach to the dielectric relaxation behaviour of a LC polymer and its application to the determination of the director order parameter for partially-aligned material*, *Brit.Polym.J.*, 1987, **19**, 119-127.

Polymer Structures

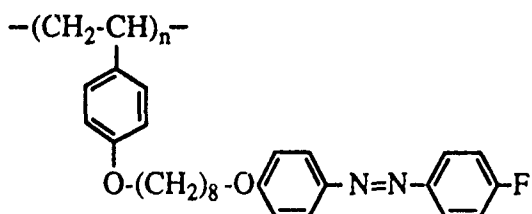
I. JSH. Copolymer with longitudinal and transverse LC groups. $T_g = 6^\circ\text{C}$; $T_c = 120^\circ\text{C}$. Sample provided by Prof.Gray and Dr.Lacey (Hull).



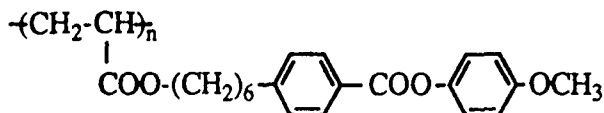
Where



II. JSD2. Photoactive polymer. $T_g = 55^\circ\text{C}$; $T_c = 117^\circ\text{C}$. Sample provided by Dr.Attard (Southampton).



III. PA6. Acrylate Polymer. $T_g = 62^\circ\text{C}$, $T_c = 116^\circ\text{C}$. Sample provided by Dr. F. Kremer (Mainz).



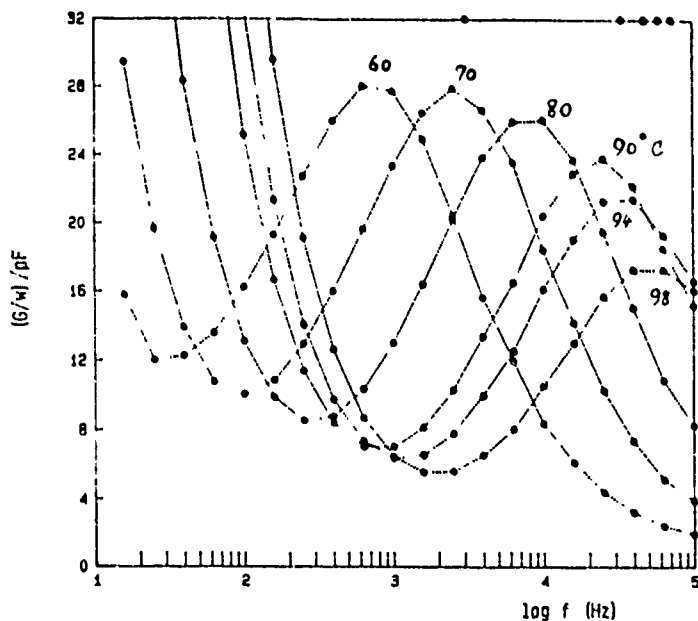


Figure 1. Dielectric loss spectra for homeotropically-aligned polymer I at different temperatures. The rising loss at low frequencies is due to ionic conductivity.

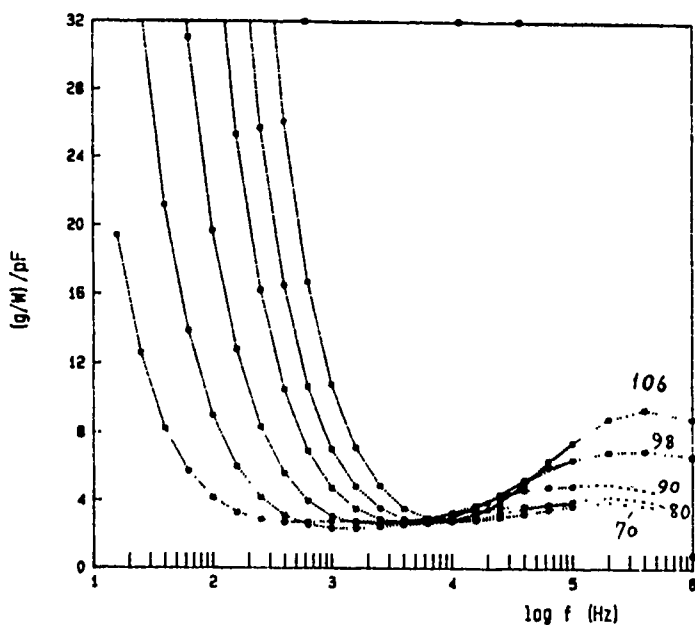


Figure 2. Dielectric loss spectra for planarly-aligned polymer I at different temperatures. The rising loss at low frequencies is due to ionic conductivity.

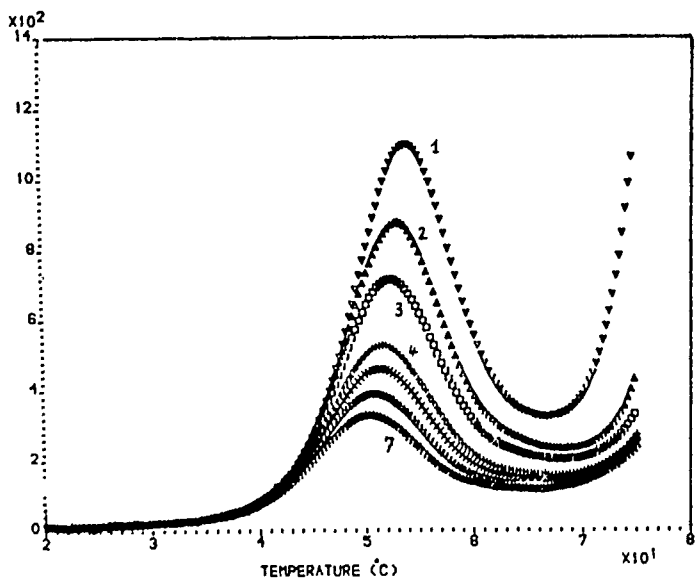


Figure 3. Thermally-stimulated current data for polymer IV. The effect of repeated cycling is a loss of the peak intensity.

CONTROL OF MOLECULAR ORGANISATION IN SIDE-CHAIN POLYMERS AND LOW MOLAR MASS LIQUID CRYSTALS

G.S. ATTARD, Department of Chemistry, The University, Southampton SO9 5NH.

In 1982 Meredith et al. described the second order non linear optical (n.l.o) properties of liquid crystalline (L.C.) side-chain polymers. Since then considerable effort has been directed at the design, synthesis, and characterisation of n.l.o. active L.C. side-chain polymers. The main motivation underlying much of this work can be traced to theoretical predictions of hypersusceptibility enhancement resulting from the orientational order which is a characteristic of L.C. materials. In addition, it was recognised that side-chain polymers offer considerable scope for a "molecular engineering" approach to materials design. However, in spite of the potential importance of orientational ultrastructure in enhancing n.l.o. behaviour, much of the effort in elaborating design criteria for n.l.o. active materials has concentrated on understanding the relationships between the electronic structures of n.l.o. chromophores and their optical properties. In 1987 we began a systematic programme of research aimed at developing a detailed understanding of how changes in the basic structural elements of side-chain LCPs affect the ultrastructure, phase behaviour, molecular dynamics, and ultimately, the optical and dielectric performance of these materials. The magnitude and complexity of the task is highlighted by Figure 1, which shows in schematic form, the various basic structural elements that make up a side-chain LCP.

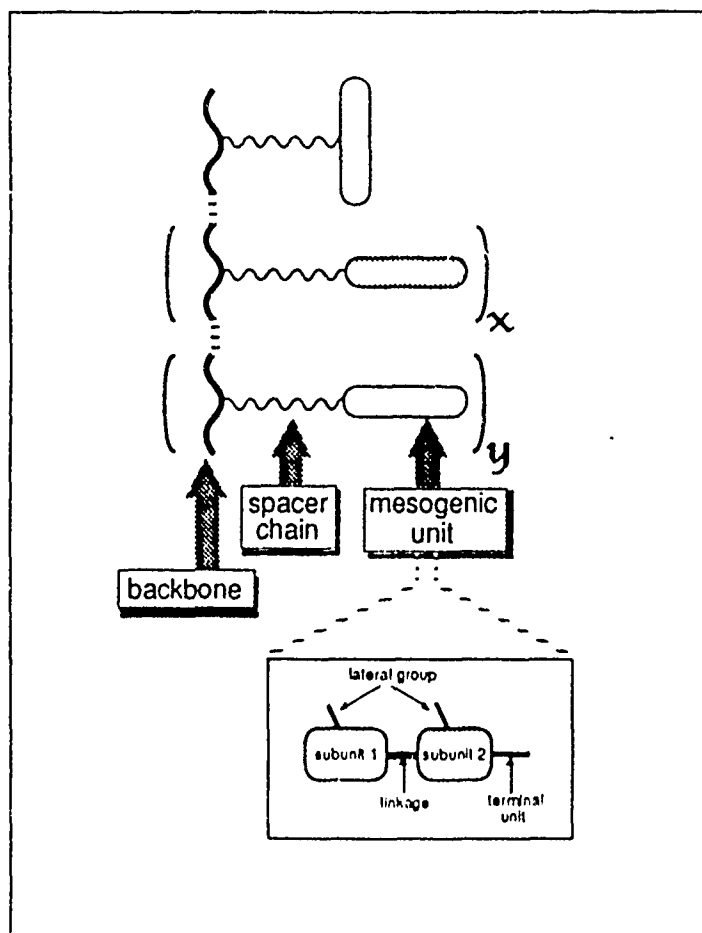


FIGURE 1

The first phase of the programme concentrated on the development of synthetic protocols which resulted in batch reproducibility and high material purity. As a consequence of our ability to achieve reproducible syntheses we could be confident that any observed changes in material properties were not artefacts of the synthetic procedure; a problem which had been evident in many previous reports concerning side-chain LCPs. The second phase of the programme consisted the synthesis of homopolymer based on poly(styrene) in which (i) the spacer chain lengths, (ii) the terminal groups, (iii) the lateral groups, and (iv) the linking groups were varied in a systematic fashion. The choice of poly(styrene) as backbone was dictated by the preception that a high T_g would be an important factor in determining the long-term n.l.o. performance of the materials. The main structure-property relationships which emerged from a detailed study of the LCPs we synthesised can be summarised as follows:

- with only two exceptions, all the LCPs showed smectic mesophases
- all the homologous series exhibited an oscillation in their smectic to isotropic transition temperatures as a function of the parity of the spacer chains; a behaviour which is analogous to that observed in low molar mass materials
- for a given length of spacer chain, the clearing temperatures were found to depend on the nature of the terminal group and followed the sequence $-OMe > -CN > -NO_2 > -F$; the sequence also applies to low molar mass mesogens
- the glass transition temperature, T_g , for materials with strongly dipolar mesogens is consistently lower than that for materials with relatively non polar mesogens
- both T_g and the clearing temperatures were found to depend on the molecular weight of the polymer.

In order to establish a formal framework for the interpretation of the thermal properties of the homopolymers we developed a molecular field theory suitable for side-chain polymers. This mathematical theory combines the approach adopted in the modelling of orientational interactions in rod-like molecules with the Flory rotational isomeric state (RIS) model. One of the main features of the theory is that it demonstrates that the coupling of the backbone and side-chain conformations (and their dynamics) with the orientational interactions (and anisotropic dynamics) of the mesogenic units is a crucial aspect of the thermal behaviour of these materials irrespective of spacer chain length. This contrasts with previous, intuitive, rationalisations of transitional behaviour in side-chain LCPs.

From the point of view of second order n.l.o. performance, one of the most important design aspects is the role of dipole moments in determining thermal properties and poling behaviour. As has already been mentioned, the homopolymer series studied showed that strong dipoles in the mesogenic unit lead to a plasticisation effect on T_g . This aspect is not covered by the molecular field theory we developed since it involves specific interactions (dipole-dipole) between pairs of molecules (molecular field theories are based on single particle orientational distribution functions). However, dipole-dipole interactions are expected to have major effects on the poling behaviour of materials. In order to obtain insights into the effects of dipole-dipole interactions on poling behaviour we developed a statistical thermodynamic theory which relates $\chi^{(2)}$ to long-range orientational order and to dipole-dipole correlations. The theory shows that for typical values of the order parameters $\langle P_2 \rangle$ and $\langle P_4 \rangle$, a 70% reduction in the magnitude of $\chi^{(2)}$ is to be expected for typical dipole correlations (as quantified by the Kirkwood

g-factors). This prediction provides an explanation for the observation that the enhancement of $\chi^{(2)}$ in mesogenic systems is consistently smaller than predicted by molecular field theories. The theory also has profound design implications since to date the principal n.l.o chromophore design criterion has been to maximise the product ($\mu\beta$).

Guided by the insights obtained from our theory of dipole-dipole effects we have recently begun to investigate methods of frustrating dipole-dipole correlations in L.C. phases. Unfortunately, the traditional way of achieving this (i.e. by the use of bulky lateral groups in the mesogenic unit) leads to significantly lower β values. Our approach has been to design copolymers in which charge-transfer type interactions overcome the dipole-dipole correlations. In order to establish the design criteria required to achieve such effects we have conducted, in phase three of the programme, a systematic study of structure-property relationships in binary copolymers. The homologous series of statistical binary copolymers shown in Figure 2 were synthesised, and their thermal properties and phase ultrastructures were investigated.

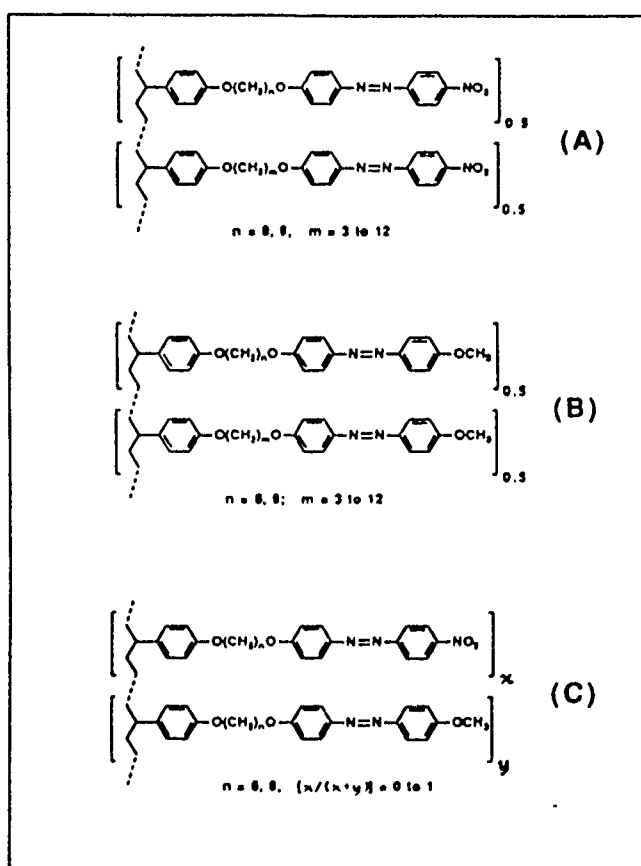


FIGURE 2

The main structure-property relationships that have been determined to date are summarised as follows:

- when the two components of the copolymer have the same mesogenic unit but differ in the length of their spacer chains small but significant deviations from predicted behaviour are observed, these deviations can lead to either an increase or a lowering of the clearing temperature (see Figures 3 and 4)

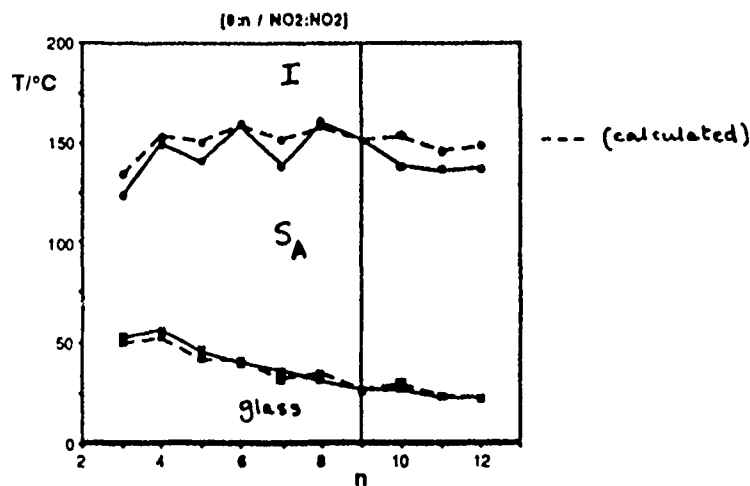


FIGURE 3

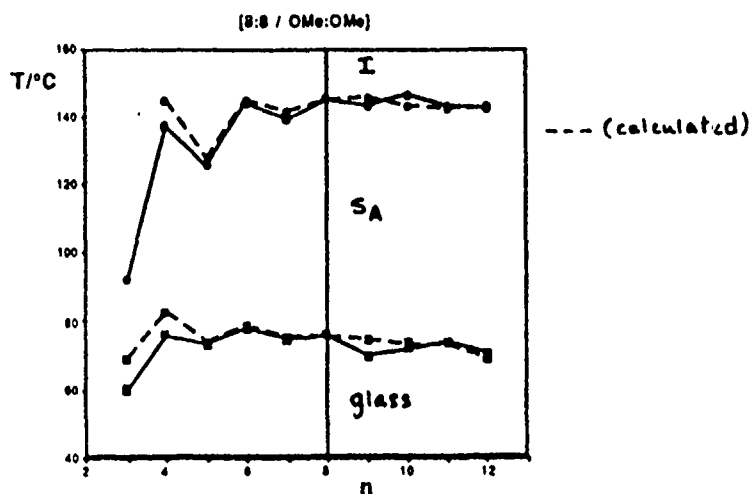


FIGURE 4

- in accord with expectations, deviations from ideal behaviour are more pronounced for copolymers with strongly dipolar mesogenic units
- when the two components of the copolymer have the same length of spacer chain but have different mesogenic units which are capable of participating in charge-transfer type interactions, dramatic deviations from predicted behaviour are observed (see Figures 5 and 6)

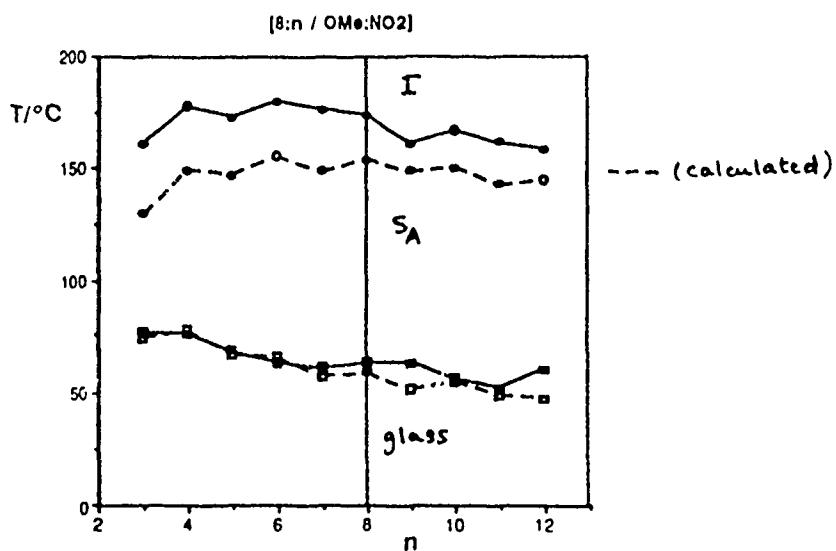


FIGURE 5

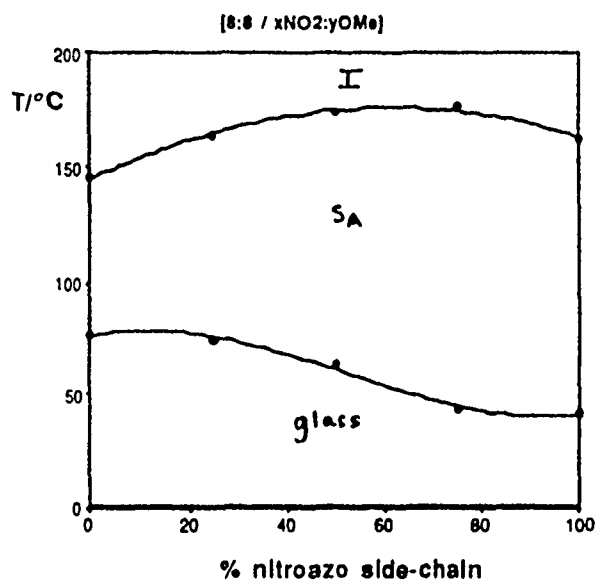


FIGURE 6

The way in which dipole-dipole interactions, charge-transfer interactions, and differing lengths of spacer chains can be exploited to control the L.C. ultrastructure are illustrated schematically in Figure 7. The most recent work in this phase of the programme has built on the structure property relationships outlined above and has been targetted at copolymers in which the transition into the L.C. phase lies just below the glass transition. Systems such as those illustrated in Figure 8 exhibit a significant build-up of long-range order without actually being liquid crystalline. We are currently investigating whether this type of behaviour provides significant improvement of optical losses compared with aligned L.C. systems

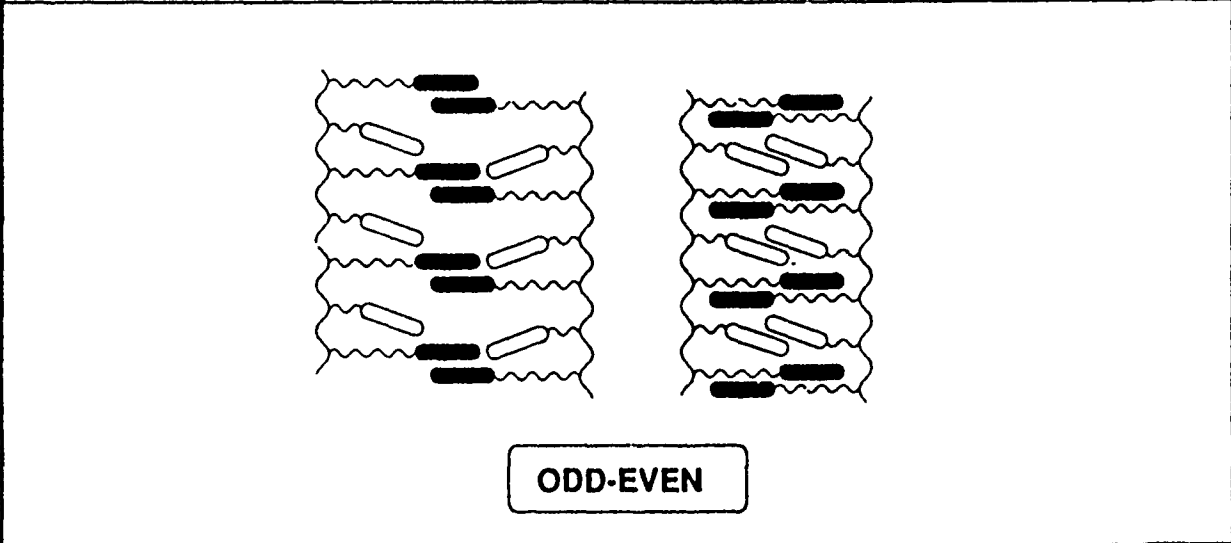
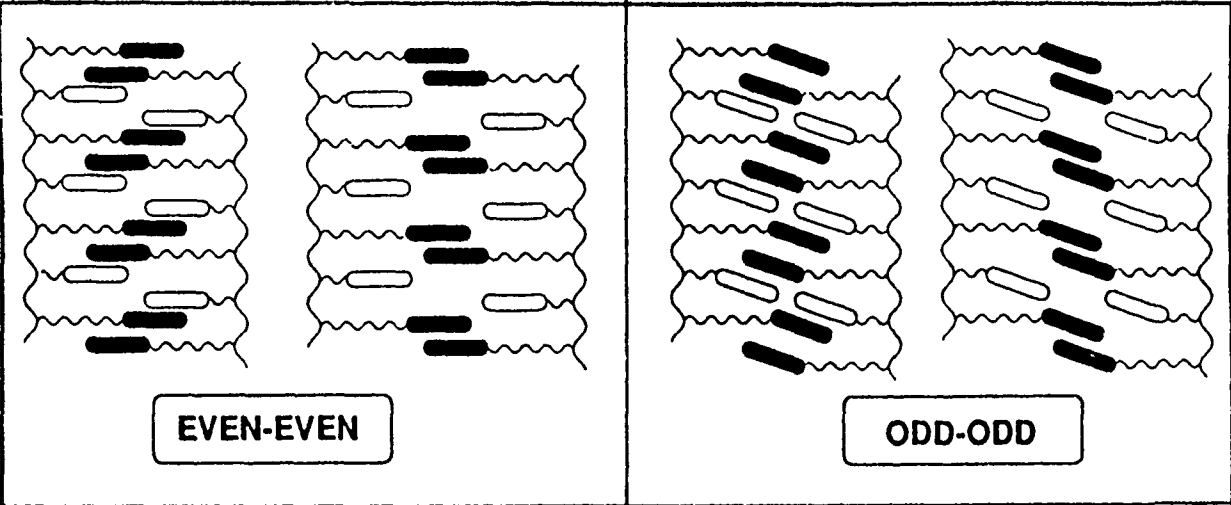
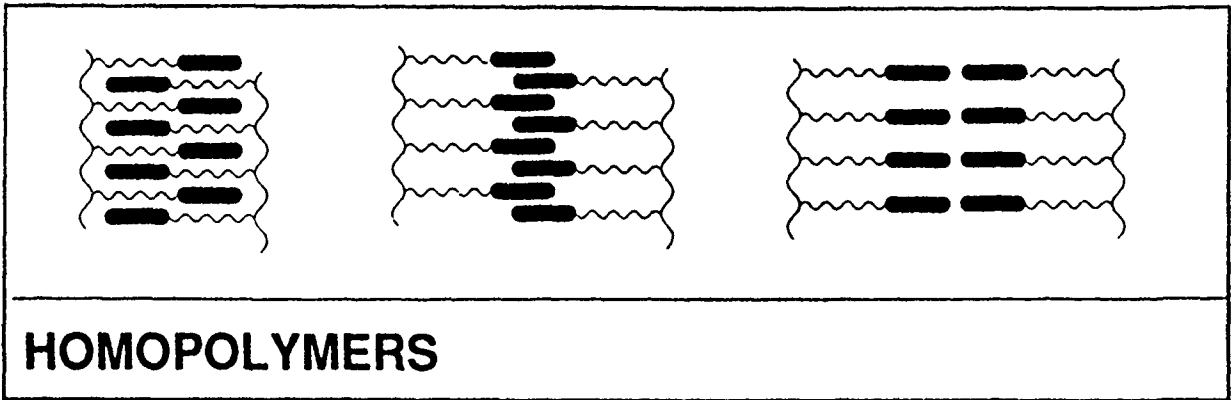


Fig 7

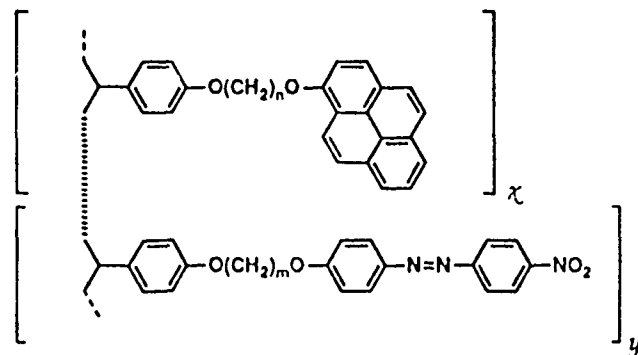


FIGURE 8

In phase four of the programme we have adopted an alternative strategy to the engineering of n.l.o. materials. This alternative approach is based on the concept that the rich diversity of orientational and spatial ultrastructures which is encountered in low molar mass liquid crystals can be exploited in the processing of highly ordered polymers or bulk single crystals. The first demonstration of "proof of concept" was achieved with a discotic material which was modified so that it contained diacetylenic units in the side-chains. We found that this material could be processed from its liquid crystalline phase into continuous highly ordered fibres. The fibres could be polymerised by uv radiation to give highly ordered polydiacetylene networks. Detailed X-ray diffraction studies of the polymerised and unpolymerised fibres showed them to be virtually single-crystal fibres.

We are currently working to extend this approach to the processing of $\chi^{(2)}$ materials while also making use of the insights obtained from our theory of dipole-dipole interactions. In addition, as part of a separate research programme we had developed a detailed understanding of structure-property relationships in symmetric and asymmetric dimeric mesogens. The principal features which are of relevance to phase four of the current programme are summarised as follows:

- certain asymmetric dimeric mesogens consisting of mesogenic units capable of participating in charge-transfer interactions (see Figure 9) form smectic phases with an unusual type of locally polar ultrastructure

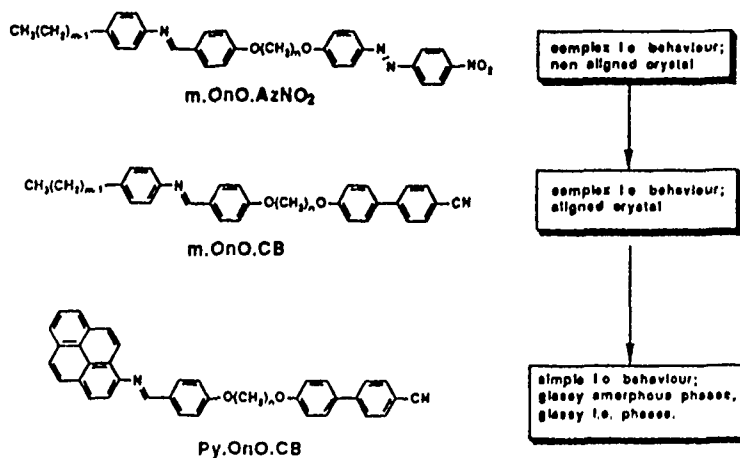


FIGURE 9

- some of the asymmetric dimeric mesogens form net-shape defect free single crystals when cooled in the presence of a modest magnetic field (1.2 Tesla)
- symmetric dimers which contain pyrene units form glassy phases above room temperature (T_g between 65°C and 30°C); the glassy phases can be amorphous, nematic, or smectic depending on the length and parity of the chain linking the two mesogenic units.

The unusual ultrastructure of the smectic A phases of the asymmetric mesogens suggests that it should be possible to achieve highly non centrosymmetric structures. This is because in these materials the poling process would involve the realignment of microdomains rather than the biasing of a molecular Boltzmann distribution. It is also possible that non centrosymmetric structures could be achieved through the action of surface forces in a manner analogous to the mechanism which underlies the formation of Langmuir-Blodgett films (see Figure 10).

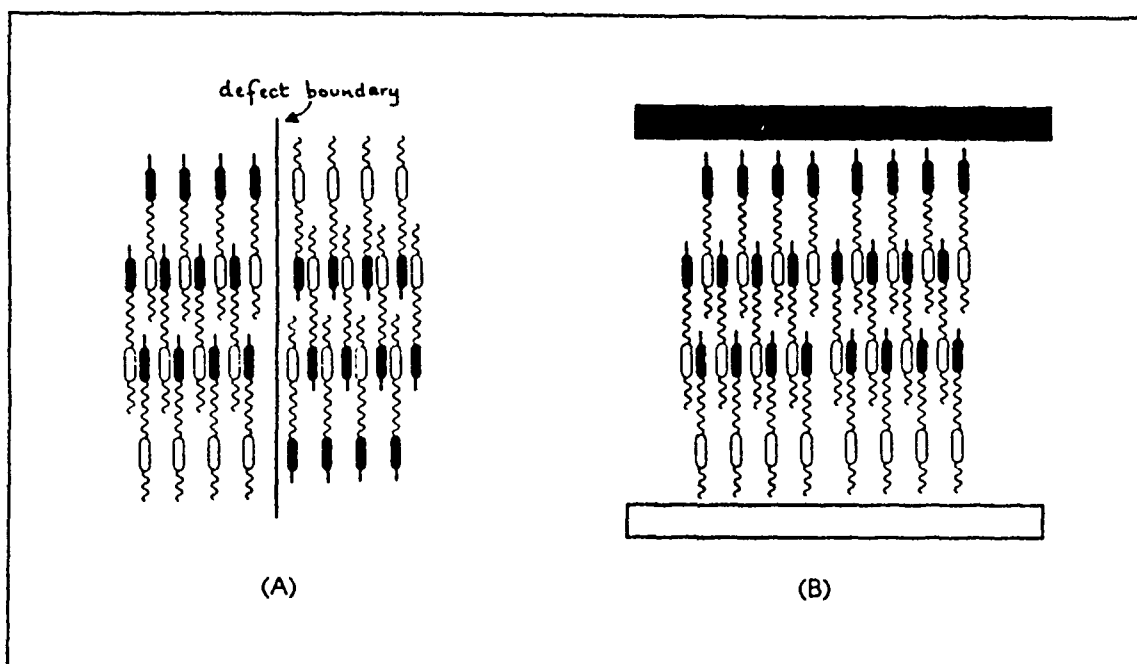


FIGURE 10

Such non centrosymmetric structures could be preserved either as glassy phases or as net shape single crystals. In our first attempt to demonstrate that this type of behaviour can be exploited for $\chi^{(2)}$ n.l.o. materials we synthesised a homologous series of asymmetric dimers as model compounds. The thermal properties of these materials (see Figure 11) are summarised below:

- all homologues form nematic phases; the N-I transition temperature exhibits a dramatic alternation as a function of the parity of the central chain
- apart from the propyl and undecyl compounds, all materials form smectic phases
- all materials form glassy L.C. phases with T_g ranging from 58°C to 35°C.

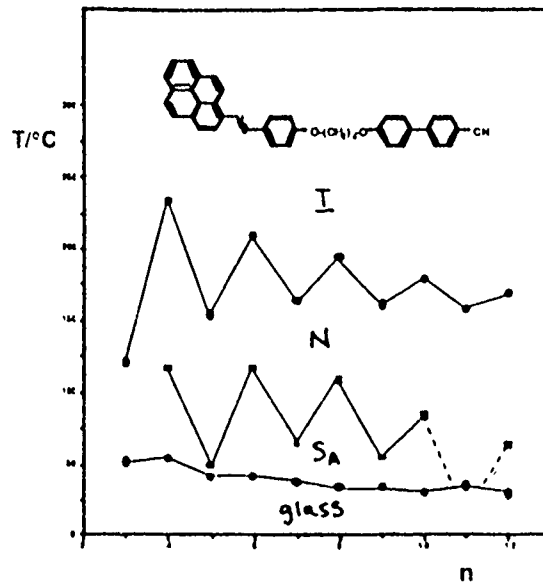
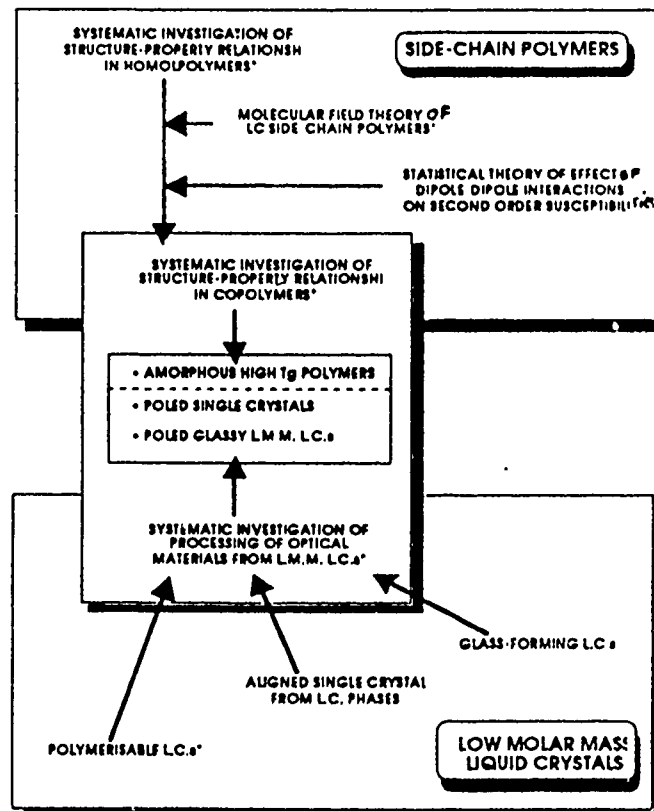


FIGURE 11

As can be seen the materials exhibit the required combination of thermal properties; studies of the poling behaviour, $\chi^{(2)}$ properties, and optical losses of these materials are currently in progress.

A schematic overview of the principal technical elements of the research programme to date is shown in Figure 12.



(*) # F49620-87-C-011

POLYARYLENE VINYLENE COPOLYMERS

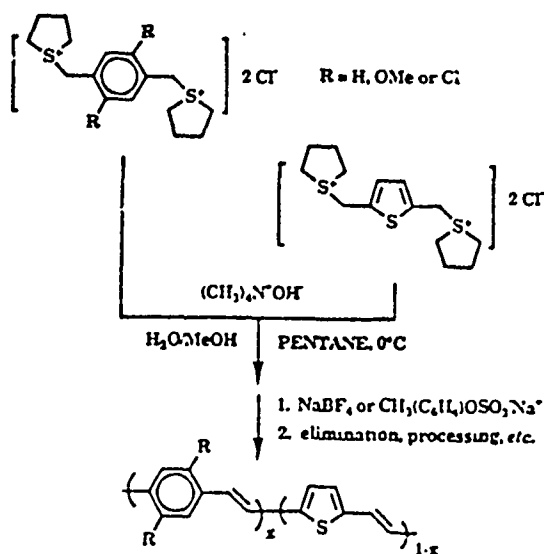
F. E. Karasz

University of Massachusetts

We present data and results concerning the synthesis of poly(*p*-phenylene vinylene-co-2,5-thienylene vinylene) (PPV-co-PTV) and other related copolymers. The studies of the molar-equivalent homopolymer blends (denoted by PPV/PTV) are also included.

1. Synthesis

The reaction scheme used for the synthesis of PPV-co-PTV (scheme 1) is a combination of the procedures reported earlier for poly(*p*-phenylene vinylene) (PPV), poly(2,5-thienylene vinylene) (PTV) and poly(2,5-dimethoxy-1,4-phenylene vinylene) (PdMeOPV) which were designed to improve the preparation of polyarylene vinylenes. The standard procedure which involved the addition of an equimolar amount of base to the bis(methylene-dialkylsulfide)-arylene monomers dissolved in water and cooled to 0°C was modified to produce better yields, higher molecular weights and organic solubility. Thus sodium tetrafluoroborate (NaBF₄) was used to exchange the halide counter-ion (usually Cl) of the PPV precursor polymer to a fluoroborate (BF₄) and produce an organically soluble PPV precursor polymer.



Scheme 1. The Synthetic Pathway to PPV-co-PTV and Other Related Copolymers.

The molar-equivalent homopolymer blends used for the purpose of comparing physical properties with those of the copolymers were prepared. The homopolymer blends were prepared in the same solvent systems and treated with the same counter-ion exchange compounds as those used in the copolymer reactions. The PTV homopolymer precursor was treated with NaBF_4 or $(\text{CH}_3)\text{-}p\text{-C}_6\text{H}_4\text{-(SO}_3\text{Na}^+)$, depending on whether they were to be codissolved with the PPV precursor or the PdMeOPV precursor, even though there was no apparent effect of these compounds on the PTV precursor.

2. The Copolymeric Nature of PPV-co-PTV

In any copolymer synthesis it is essential to confirm that the product is a true copolymer and not a homopolymeric blend. Kossmehl *et al.* showed that PPV has a C-H out-of-plane bending *trans*-vinylene infrared (IR) absorption maximum at 970 cm^{-1} and that the equivalent absorption maximum of PTV was at 930 cm^{-1} . Model compounds of known repeat-unit sequence were prepared *via* Wittig reactions, and they showed that insertion of PTV units into a PPV chain caused the *trans*-vinylene absorbance maximum of the compound to shift from 970 cm^{-1} to 930 cm^{-1} as more PTV units replaced the PPV units in the chain. It was, therefore, expected that the PPV-co-PTV prepared *via* the Wessling method, if it were not composed of large blocks of PPV and PTV, should show the same shift in maxima.

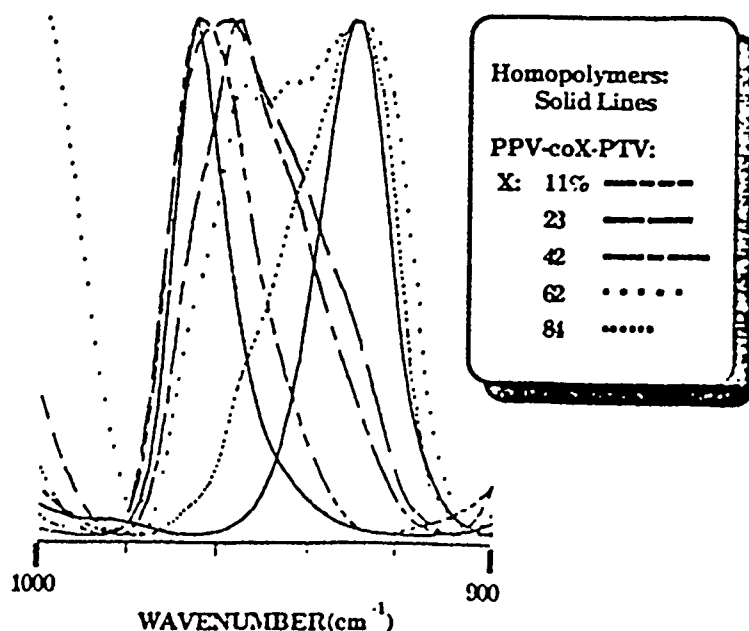


Fig. 1. *Trans*-vinylene IR Absorption for PPV, PTV and PPV-co-PTV of Varying Composition.

The studies in this copolymerization of the FTIR absorbance for this region indeed show a shift of absorbance maxima for the PPV-co-PTV as those observed in the oligomers (fig. 1). Moreover, there was no evidence for contiguous repeat units greater than five, except in the extreme ratios of monomer feed where it was expected. This indicated that there was very little "blockiness" to the copolymer, that is, the PPV-co-PTV existed as a random copolymer. The fact that the absorbance pattern showed discrete maxima rather than a smooth curve suggested that the measurement discriminated between different pentads or even smaller units.

A comparison with the IR absorbance patterns (fig. 2) of the molar equivalent blends of PPV and PTV emphasized the distinction of the copolymers from blends. There was no shift of the IR maxima from the 970 cm^{-1} maximum of PPV to the maximum at 930 cm^{-1} of PTV, rather, both maxima at 970 cm^{-1} and 930 cm^{-1} were observed throughout the whole range of blend composition.

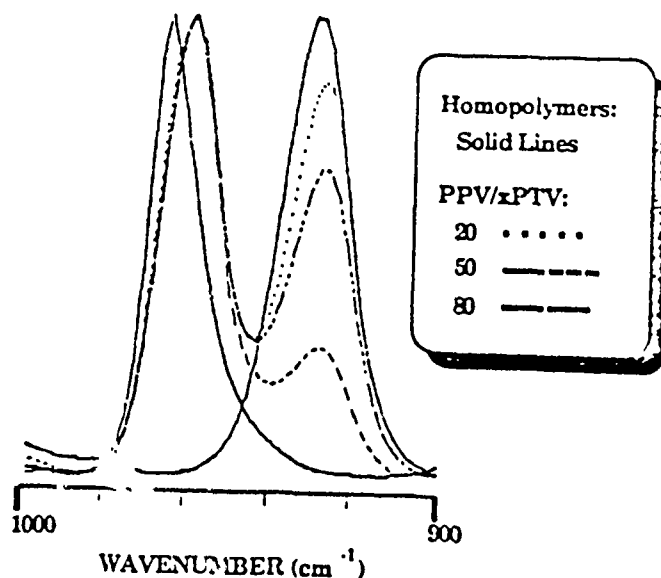


Fig. 2. *Trans*-vinylene IR Absorption for PPV, PTV and PPV/PTV of Varying Composition.

3. Conductivity of Unoriented PAV Copolymers and Blends

PPV has been shown not to form redox products with iodine, its oxidation

potential being slightly too high (0.76 V *vs.* standard calomel electrode (SCE)). PTV on the other hand, has been shown to be oxidized by iodine to give high (as much as 200 Scm⁻¹) conductivities. The conductivity experiment on PPV-*co*-PTV is, therefore, an indication of the susceptibility of varying lengths of PTV segments to iodine doping, the intramolecular correlation of PTV repeat units, the intermolecular proximity of the PTV charge-carriers and the charge-density or charge-transport capacity of PTV within a random copolymeric system.

This dramatic increase in conductivity (fig. 3) suggested that the conductivity for the PPV-*co*-PTV system was strongly dependent on the intramolecular correlation of the PTV repeat units, that is, each increment of contiguous PTV repeat units successively lowered the oxidation energy until the point where iodine was able to oxidize the material. The previously described IR results suggested that PPV-*co*-PTV was a random copolymer, in which case, at 80% PTV copolymer composition, there would be four contiguous PTV repeat units on average. It was therefore postulated that the threshold for PTV ionization by iodine must be four repeat units.

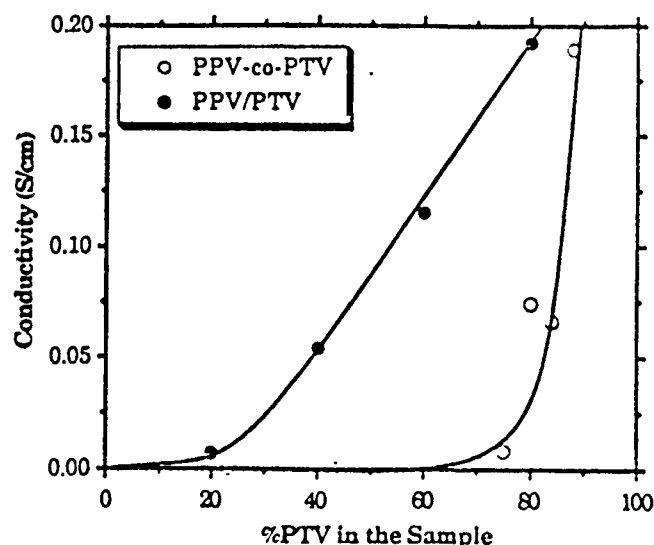


Fig. 3. Conductivities of the Iodine-doped Samples in the PPV-PTV System.

Similar conductivity measurements obtained for PPV/PTV blend samples showed a markedly different trend (fig. 3). The blends showed a transition at

approximately 20% PTV composition. The first section - from 0-20% PTV - showed conductivities that were independent of the change in the PTV content of the blend, that is, the conductivity was constant within this range of compositions. This was followed by a linear dependence on the PTV content for compositions greater than 20% in PTV.

In the homopolymer blends of PPV/PTV, the average number of PTV repeat units per chain remained constant and uninterrupted by PPV segments so that the inherent charge-transport capacity of the PTV chain remained constant with varying PTV content in the blend. The only limiting factors in the measured conductivities of the blends were the charge-density of the bulk sample and the intermolecular proximity of the PTV chains. The charge-density of the bulk sample is linearly proportional to the PTV content within the sample. The chain-proximity of PTV chains should manifest itself as a critical limit of concentration below which the conductivity of the sample would be negligible having no mechanism to transfer electrons from chain to chain.

THIN FILMS OF FUNCTIONAL POLYMERS

Naoya Ogata

Department of Chemistry, Sophia University

7-1 Kioi-Cho, Chiyoda-Ku, Tokyo 102, Japan

INTRODUCTION

Novel types of non-linear optical (NLO) polymers are currently focused on high intensities of second and third harmonic generations (SHG or THG) and also on the retention of their activities in a prolonged period to prevent the relaxation behaviors.

In order to achieve these requirements it is expected that rigid structures of high temperature polymers may retain the high NLO activities because of their high glass transition temperatures. Thin films of high temperature polymers can be prepared at air/water interface by the Langmuir-Blodgett (LB) method which provides well-aligned molecular architectures. Therefore, various high temperature polymers have been synthesized as thin films by using the LB method.

It is also expected that hydrogen-bondings among polymers may prevent the relaxation behaviors of NLO activities and yet may keep a good processability to form thin films. So, various acetylated derivatives of poly(vinylalcohol) (PVA) which contained NLO active moieties were synthesized and their NLO activities were evaluated.

THIN FILMS OF HIGH TEMPERATURE POLYMERS

Various types of high temperature polymers were prepared as thin films at air/water interface by using the LB method. Particularly, poly(benzothiazole) (PBT) is known as a stable and very rigid polymer which cannot be processed as thin films because of dissolution problems for common solvents. However, the synthetic route as shown in Fig. 1 made it possible to prepare thin films of PBT with well-ordered structures.

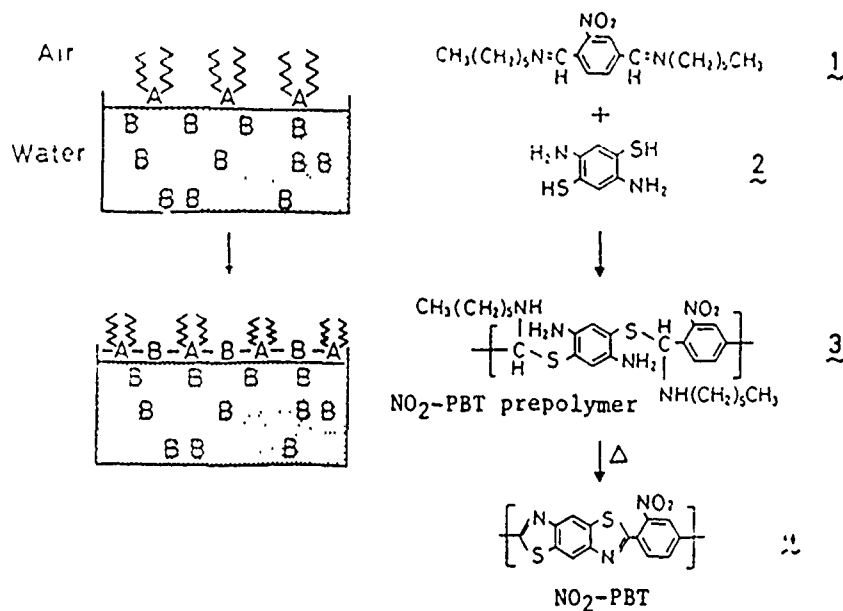


Fig. 1 Reaction scheme to prepare thin films of NLO active PBT at air/water interface

The SHG intensity of the NO_2 -PBT prepolymer was evaluated as $\chi_2 = 21 \text{ pm/V}$. However, the SHG intensity decreased remarkably with increasing heat-treatment temperatures to prepare NO_2 -PBT, as shown in Fig. 2, in which the SHG intensities were compared with the absorption peak ratios between CH_2 and NO_2 , which represented the structural change from the prepolymer to NO_2 -PBT.

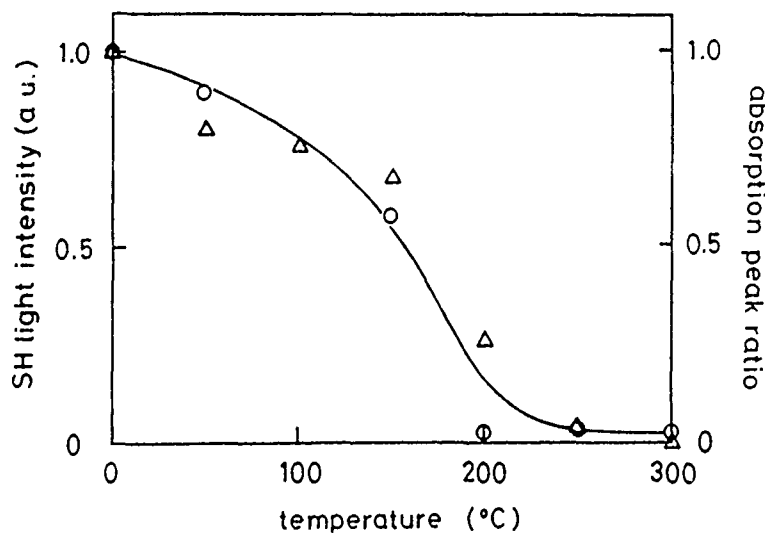


Fig. 2 Relationship between the SH light intensity (○) and heat-treatment temperatures (Δ) absorption peak ratio of CH_2/NO_2

The decrease in the SH light intensity might be due to the radamization of the well-ordered structure of the NO₂-PBT prepolymer which might be caused by the heat-treatment at high temperatures. In order to improve the SHG intensity, Corona poling method was applied to the thin film of NO₂-PBT after the heat-treatment. Conditions for the Corona poling was as follows: distance from cathode=1 cm, voltage= 9 kV, temperature = 110°C, time= 1 hr. Fig. 3 indicates the SHG intensity of the poled NO₂-PBT in comparison with the NO₂-PBT after the heat-treatment at 300°C for 30 min.

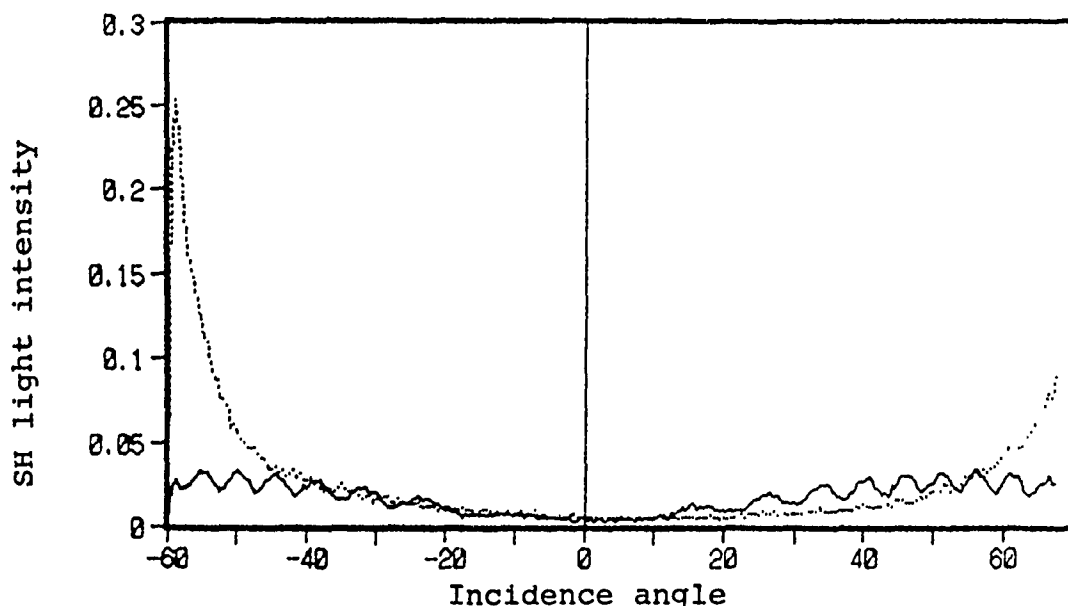


Fig. 3 SHG intensities of NO₂-PBT before and after Corona poling
 — : before, : after

It is seen in Fig. 3 that the SHG intensity increased by the Corona poling method and the χ_2 value was evaluated as 25 pm/V. The relaxation behavior of the SHG intensity of the poled NO₂-PBT was very stable and no change of the SH light intensity was observed after one month at room temperature. Perhaps, the rigid structure of NO₂-PBT might prevent the relaxation, as was expected before. This result was a notable achievement for the novel type NLO polymers.

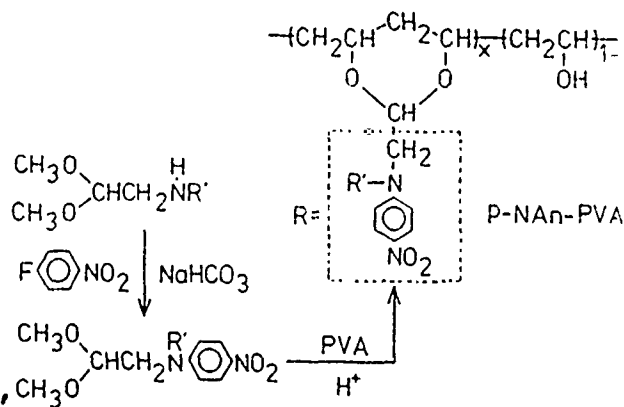
THIN FILMS OF ACETALYZED PVA

Acetylated PVA containing p-nitroaniline moiety as a NLO active site was synthesized by the following reaction route:

The p-NAn-PVA was soluble in DMF or DMAc and could be spin-coated on quartz plate as a thin film.

The Corona poling method was applied to the thin film of p-NAn-PVA to achieve molecular orientations of the NLO moiety.

Conditions for the Corona poling was as follows: Temp.=75°C, V=10 KV, time = 30 min.



The SHG intensity of the Corona-poled thin film of p-NAn-PVA was evaluated as shown in Fig. 4.

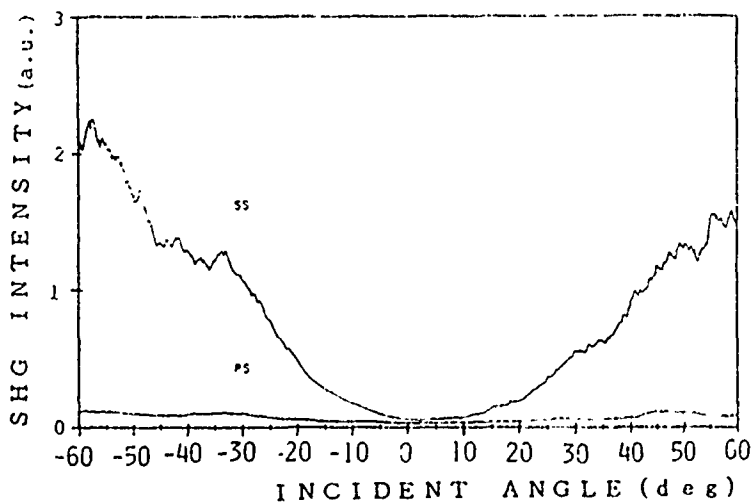


Fig. 4 SHG intensity of the Corona-poled p-NAn-PVA thin film

The calculated χ_2 (d_{33} constant) of the poled p-NAn-PVA was 40.8 pm/V and the relaxation of the SHG intensity was less than 10% after one month at room temperature. This stable NLO activity of p-NAn-PVA might be caused by hydrogen-bondings through OH groups in main chains.

THIN FILMS OF NLO ACTIVE POLY(ACROLEIN)'s

Poly(acrolein) with high molecular weights was easily obtained by a conventional radical polymerization of acrolein and it reacted with p-nitroaniline to prepare NLO active polymers as side chain types. Table I summarizes synthesized poly(acrolein)'s having NLO active moieties as pendant Schiff bases. They were soluble in DMF and spin-coatable as thin films.

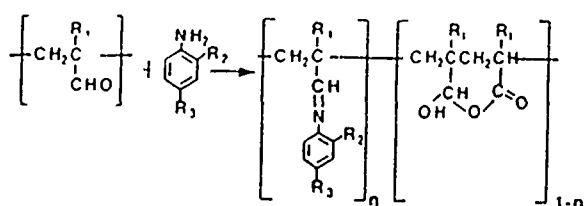



Table I Synthesis of poly(acrolein) derivatives

R ₁	R ₂	R ₃	n	Cut-off length/nm
H	H	NO ₂	0.4	520
CH ₃	H	NO ₂	0.3-0.4	510
CH ₃	H	 NO ₂	0.3	—
CH ₃	NH ₂	NO ₂	0.3	—

The SHG intensity of the planary-poled poly(acrolein) which contained p-nitroaniline was measured as shown in Fig. 5. The calculated SHG value χ_2 was 15 pm/V. Since the amount of the incorporated NLO active moiety was in the range of 30-40 mol%, the χ_2 value was not satisfactorily high. The relaxation behavior of the poly(acrolein)'s after poling was 40% loss after one month at room temperature.

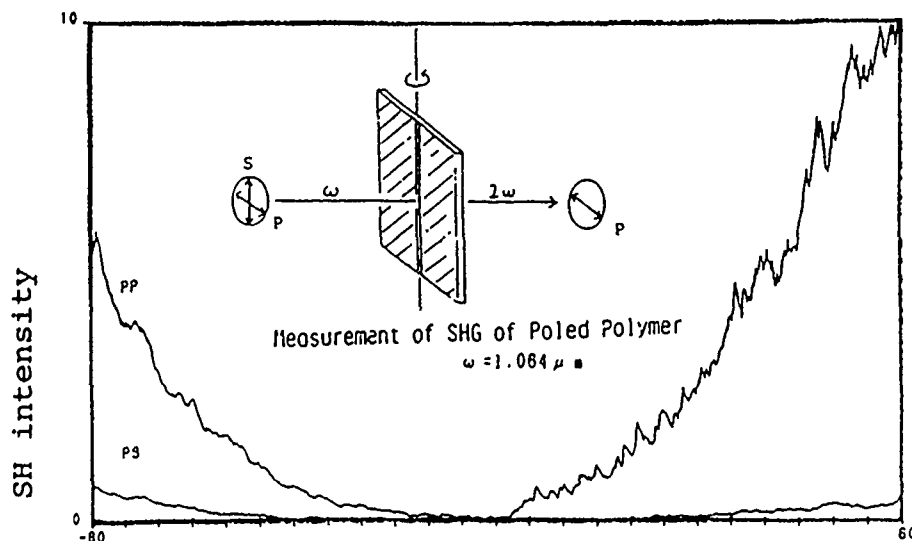


Fig 5 SHG measurement of poly(acrolein) derivative

CONCLUSION

Various types of novel NLO active polymers were designed and synthesized as thin films to prepare SH active polymers. PBT thin film which was formed at air/water interface by the LB method could maintain the stable SHG activity by the Corona poling, presumably due to the rigid structure of PBT.

NLO active polymers derived from PVA and poly(acrolein) were synthesized and evaluated in terms of SHG activities and it was found that the hydrogen-bondings among polymers were effective to prevent the relaxation behavior after electric poling.

NOVEL ELECTROACTIVE AND NONLINEAR OPTICAL COMPOSITES

Paras N. Prasad
Photonics Research Laboratory
State University of New York at Buffalo
Buffalo, NY 14214

I. NONLINEAR OPTICS AND DEFENSE TECHNOLOGIES OF SDI INTEREST

Nonlinear optical processes will play a key role in development of many defense technologies of significant value to SDI. It will be critical to the development of defense technology for sensor protection. Here the use of light-intensity-dependent transmission properties of materials can protect human eyes or optoelectronic sensors from unwanted or stray sources of laser radiation. Rapid optical beam steering for target detection and sensing is another technology which requires nonlinear optical function. A third area would involve frequency shifting to generate multiwavelength laser sources and modulators for space-based communication and sensing. The possibility of multiwavelength usage minimizes the threat of counter measures (interference) against a single wavelength. Optical processing and optical storage of information is also of great importance to defense technology, where high-speed modulators and demodulators are needed. These methods will allow parallel processing with greatly enhanced speed. Yet other areas of interest to SDE are use of nonlinear processes for laser pulse shaping and correction of beam distortion for laser targetting.

II. TECHNOLOGICALLY RELEVANT ISSUES

Technologically relevant issues differ somewhat for different applications, although some material issues from defense technology perspectives are common. The need for reliable performance under large fluctuations in ambient conditions as well as for higher optical damage thresholds and high optical throughput of the device are essential to all defense applications.

Crystalline materials have been used for second harmonic generation, parametric oscillation and amplification. There is a need to employ highly efficient crystals which can be used with low power and lightweight diode lasers. Naturally, this application will require a large $\chi^{(2)}$ value, the second-order nonlinear bulk susceptibility. Two additional requirements that must be met for efficient frequency conversion are phase-matching and broad band transparency.

For electro-optic applications such as electro-optic modulation, optical beam steering, and spatial light modulation, an electric field is used to affect the light signal. These are also second-order processes.¹ For optical beam steering utilizing electro-optic effect there is a need for stable poled polymeric materials with electro-optic coefficients in the range of $10^2 - 10^3$ pm/v. In addition, it is also imperative that the material has a low dc dielectric constant. A low dielectric constant helps in two ways: it enhances the field across the sample for a given applied voltage, and it enables a faster time response because of a reduced RC time constant.

Most third-order nonlinear optical devices are based on the intensity dependence of the refractive index which provides a mechanism for all optical processing and control.¹ In order for a device to operate at low optical power, the corresponding nonlinear susceptibility $\chi^{(3)}$ must again be large. For broad band response and femtosecond operation, non-resonant purely electronic nonlinearity is needed. Since the major attractive feature of all optical processing is the tremendous gain in speed, the fastest nonlinear optical response is provided by nonresonant nonlinearity. Nonresonant nonlinearity is also desirable because no optical loss from absorption and subsequent thermal effects are present. An especially complicating thermal effect is thermal nonlinearity (thermally-induced refractive index) which can build up because of its extremely slow relaxation. All these processes point to polymeric nonlinear materials as being the materials of choice. However, for device applications the $\chi^{(3)}$ value must be increased by at least two-orders of magnitude over the currently achieved value.

III. OBJECTIVES OF OUR SDI-SPONSORED RESEARCH

The specific objectives of the research are as follows:

A. MATERIALS DEVELOPMENT:

(i) To produce molecular, polymeric and composite materials with enhanced $\chi^{(2)}$ by a combination of theoretical modeling, synthesis and processing, that meet other material requirements for applications in second harmonic generation, parametric processes and high band width electro-optic modulation. (ii) To produce polymeric and composite materials with significantly enhanced $\chi^{(3)}$, very low optical losses (less than 1 dB/cm) for applications in wave guide optical switching, laser pulse shaping, and sensor protection. (iii) To develop molecular and polymeric photorefractive materials for correction of beam distortion in laser targeting applications and in holographic imaging.

B. DEVICE DEVELOPMENT:

Study some important specific device processes such as electro-optic modulation, waveguide optical nonlinearity, frequency shifting, broad band amplification and laser pulse shaping.

IV. AN EFFECTIVE MECHANISM OF TECHNOLOGY TRANSFER

At Buffalo a very effective mechanism exists for technology transfer whereby conceptual and fundamental work on novel materials and devices conducted at the university can be transferred for applications into new technology and eventual commercialization. Our Photonics Research Laboratory at the State University of New York has a special relation with the Laser Photonics Technology, Inc., which is located in the Western New York Technology Development Center, an incubator facility of the University aimed at stimulating the transfer of basic knowledge to high technology. A good example is the novel nonlinear optical process in a hollow fiber filled with organic liquids which was developed at the Photonics Research Laboratory under the SDI support. Now under an SBIR support from SDI, Laser Photonics Technology is conducting technology oriented development of this novel process to produce a compact lightweight multiwavelength source for application in space based optical communication and sensing systems.

V. OUR APPROACH AND ACCOMPLISHMENTS

We have a comprehensive and multidisciplinary approach to develop novel classes of molecular nonlinear optical materials. This integrated approach consists of the following steps: (i) Theoretical modeling and a systematic study of the structure - property relation in sequentially built or substituted structures to identify chemical units and bonding structures which enhance nonlinear optical response. (ii) Development of new $\chi^{(2)}$ and $\chi^{(3)}$ materials through composite microscopic and bulk structures, simultaneously exhibiting large nonlinearities and high optical and materials qualities. (iii) Careful characterization of the linear and nonlinear optical properties using a variety of experimental techniques including ultrashort laser pulses of approximately 50 femtoseconds width. (iv) Investigation of processes leading to device failure, involving optical damage or device lifetime limitation. (v) Study of useful device processes using composite structures and configurations.

MATERIALS DEVELOPMENT

Theoretical Modeling. We have developed a new semi-empirical procedure based time-dependent coupled perturbed Hartree-Fock method (TDCPHF) to compute all the tensor components of various nonlinear optical coefficients as a function of frequency for a given molecular structure. In particular, we use the intermediate neglect of diatomic differential overlap (INDO) approximation² of molecular orbital theory, as recently modified by Lipinski and coworkers.³ The present formulation does not involve any arbitrary parameterization procedure that often limits the predictive capability of most of the existing semi-empirical approaches. From the *ab initio* calculations we have found that one has to use an improved basis set with diffuse and polarization functions in order to properly account for the nonlinear effects which involve anharmonic displacement of electrons (described by the tail portion of the wave function). We improved our INDO-TDCPHF method by including double zeta functions augmented by diffuse and polarization functions. To develop confidence in the predictive ability of this semi-empirical method our strategy is to compare the results of the semi-empirical calculations of small molecules

with that of the ab-initio as well as with the experimentally measured values. The initial results are very encouraging.

Novel Inorganic-Organic Crystalline Composite Materials for Second Harmonic Generation and Parametric Processes. In our photonics research laboratory we have investigated⁴ the following crystalline complexes which exhibit large $\chi^{(2)}$:^{5,6}

CHI₃:3C₉H₇N
(Iodoform: 3 quinoline)

CHI₃:3S₈
(Iodoform: 3 sulfur)

SbI₃:3S₈
(Antimony triiodide: 3 sulfur)

These are binary crystalline complexes between two molecular units, but there is no evidence of any significant charge transfer from one component to another. A very interesting feature illustrated by the above set of examples is that one can substitute either component with an organic or an inorganic molecular unit to optimize the nonlinear optical response. The last complex consisting of antimony tri-iodide and sulfur has an advantage over organic crystals in that it is not soft or highly volatile. Furthermore, it does not introduce the complication of CH-overtone absorption in the near IR. These particular binary complexes represent a class of materials that have a broad transparency range. Recently, we have developed several crystalline complexes of p-nitroaniline (which by itself shows no second harmonic due to centrosymmetric crystallization) that exhibit strong second harmonic generation.

Langmuir-Blodgett Films for Second-Order Effect. Langmuir-Blodgett (L-B) films offer another important approach to create bulk order and noncentrosymmetry with monomolecular thickness control and microstructures. We are synthesizing a novel class of polymeric polyelectrolytes containing side-chain organic molecular salt units which have been shown to exhibit large $\chi^{(2)}$. Important issues in relation to the L-B films include the maintenance of structural correlation from one layer to another in order to produce a highly ordered multilayer film, the stability of these multilayers and the transfer of the films^{7,8} to the solid substrate. We used a combination of various spectroscopic techniques coupled with the quartz-crystal microbalance method used in our laboratory^{7,8} to investigate these multilayer films and explore the use of mixed layers producing highly ordered and stable multilayer films.

Synthetic approach. We have synthesized a large number of sequentially built and systematically derivatized organic and organometallic structures and investigated their nonlinear optical response. These studies have yielded some very valuable information on functional groups which may enhance nonlinear optical response and also improve processibility.

Recently, a joint effort of Polymer Branch at Wright Laboratory and our Photonics Research Laboratory at SUNY at Buffalo has resulted in a comprehensive study of structure-nonlinear optical properties of a large number of systematically varied aromatic heterocyclic compounds involving fused ring benzimidazole and benzthiazole structures.⁹ This study has provided many useful insights some of which are as follows: (a) a sulfur ring in a conjugated structure is much more effective than a phenyl ring or other heteroaromatic ring such as furan or pyridine in increasing optical nonlinearity, (b) an olefinic double bond provides a highly effective π -delocalization and consequent increase of the third-order nonlinearity, and (c) grafting of pendent aromatic groups through attachment to a nitrogen atom in a fused benzimidazole ring provides a means for producing two-dimensional π -conjugation leading to an enhancement of γ and also improved solubility.

The search of third-order materials should not just be limited to conjugated structures. But only with an improved microscopic understanding of optical nonlinearities, can the scope, in any useful way, be broadened to include other classes of molecular materials. Incorporation of polarizable heavy atoms may be a viable route to increase γ . A suitable example is iodoform (CHI₃) which has no π -electron but has a $\chi^{(3)}$ value comparable to that of bithiophene. Organometallic structures represent another vast class of molecular materials which are largely unexplored. We have synthesized and investigated a large number of systematically derivatized monomeric and oligomeric structures involving ferrocene units.

Optimization at the Bulk Level. Here our goal is to optimize for necessary multifunctionality by control of design at the bulk level. We have focused on designs which would enhance nonlinear optical response, produce low optical loss, and introduce other necessary bulk properties such as mechanical strength, environmental and thermal stability and high optical damage threshold. The two broad approaches taken are: (a) orientation

control for enhanced response. For this purpose we have used successive monomolecular layer deposition of Langmuir-Blodgett film heterostructures and electric field poling of bulk structures for second-order nonlinear material; and stretch orientation of polymeric structures for third-order nonlinear optical material. (b) Composite heterostructures. We have developed several new classes of composites structures which are extremely promising. Another significant development by optimization of bulk properties is the successful achievement of photorefractive effect in polymers. Some selected examples are provided below.

Sol-gel Processed Novel Multicomponent Inorganic Oxide:Organic Polymer Composites for Nonlinear Optics. Sol-gel processing has been used to prepare a new class of multicomponent inorganic oxide:organic polymer composites of very high concentrations which show great promise for both second- and third-order nonlinear optics.^{10,11} A special processing technique has permitted the preparation of $\text{SiO}_2/\text{TiO}_2$ /organic polymer composites in which the relative composition can be judiciously varied to select the linear refractive index for applications in integrated optics. Furthermore, this composite has been doped with both inorganic and organic dopants. The composite film doped with molecules with large second-order nonlinearity has successfully been electrically poled to produce stable align structures.^{10,11} Both second-harmonic generation and electrooptic modulation have been achieved in such poled $\text{SiO}_2/\text{TiO}_2$ /polymer composite.^{10,11} For third-order nonlinear optics, composites of SiO_2 and V_2O_5 with poly-p-phenylene vinylene and the various derivatives up to 50% by weight have been prepared.¹² Simultaneous study of femtosecond degenerate four-wave mixing, optical Kerr gate and transient absorption have been conducted to understand the mechanisms of third-order optical nonlinearity.¹³ In these polymer:glass composites, optical gate action on femtosecond time scale has been observed.

Novel Photorefractive Polymers. Photorefractive materials have emerged¹⁴ as an important class of nonlinear optical materials which show large optically induced refractive index changes. Even though the overall manifestation is like a third-order nonlinear optical effect (light induced refractive index change), the mechanism involves a photo-induced charge separation which sets up an electric field to produce a refractive index change by the $\chi^{(2)}$ electro-optic mechanism.¹⁴ Therefore, a photorefractive material is actually a $\chi^{(2)}$ medium which also contains centers to produce photo-induced carriers. Furthermore, the carriers must have sufficient mobility to separate and set up a strong electric field. Inorganic ionic crystals such as LiNbO_3 , BaTiO_3 and SBN have been used in the past for photorefractive effects.¹⁴ Polymeric materials are very attractive for a photorefractive effect because they exhibit the largest $\chi^{(2)}$. Also, they offer the flexibility to tailor their structure and composition to control other properties necessary for photorefractive effects. Therefore, it is possible to decrease the response time, which traditionally is very slow in the inorganic ionic photorefractive crystals. Poled polymeric structures have many desirable materials quality including the ease of fabrication of various device structures (wave guides). Photoconductivity in polymeric structures has been widely studied.¹⁵ It can result from the intrinsic structure of the polymer or be derived from various dopants.

In collaboration with the Corporate Research Laboratory at the Eastman Kodak Company, we have successfully studied the photorefractive behavior in electrically poled photoconductive polymers containing second-order nonlinear chromophores. Photoconductivity, electro optic modulation, and degenerate four wave mixing in the phase conjugate geometry have successfully been documented to confirm the photorefractive behavior.

DEVICE DEVELOPMENT

Many device concepts have been developed at our Photonics Research Laboratory. Some of these concepts are already being investigated for technology applications and commercialization by Laser Photonics Technology, Inc. We have utilized the sol-gel processed composites materials containing a saturable absorber for laser pulse shaping by Q-switching and mode-locking utilizing both single cavity and coupled cavity configurations.

The sol-gel processed inorganic oxide:poly-p-phenylene vinylene (PPV) composites films have excellent optical quality and excellent surface finish for application in optical recording. Using a 1 μm thick film of the silica:PPV composite on a glass substrate we have successfully fabricated a two-dimensional grating by crossing femtosecond pulses at 602 nm. The silica:PPV or V_2O_5 :PPV films have also successfully been used to develop light emitting diodes for applications in electro-luminescent display panels. Because of the flexibility to change the inorganic oxide or organic polymer component, the sol-gel processed composite films are also being examined for applications in acoustic impedance matching and surface acoustic wave devices.

Using an optical waveguide configuration with several $\chi^{(3)}$ polymer and composite materials power limiter behavior has been obtained in the optical output-input relation. Femtosecond optical Kerr-gate action has been demonstrated.

Kerr-Scattering in Liquid Filled Hollow Fiber as a Multiwavelength Laser Source. Laser Photonics Technology, Inc. (LPT) has recently been expanding the scope of the stimulated Rayleigh-Kerr scattering work accomplished in the Photonics Research Laboratory where generation of broad band coherent radiation from a Kerr liquid filled hollow fiber was demonstrated.¹⁶ The thrust of the LPT, Inc. effort has been to optimize the operational parameters such that this technology could be applied to Light Detection and Ranging (LIDAR) systems.

The advantage of this approach over existing methods of multiwavelength coherent light generation is that it offers a light weight, low power, and compact system to generate comparatively large operational frequency ranges exceeding 3000 cm^{-1} . The goal of the LPT, Inc. work is to optimize several critical properties in order that the range of the generated frequencies is maximized and that sufficient intensities are obtained. Equally important is the stability of the output; the system should perform so as not to cause significant fluctuations over and above that which are created by the driving laser.

Those parameters that are perceived as being most important to the overall efficiency of the process are the: (1) choice of Kerr medium, (2) fiber geometry (length and diameter), and (3) driving laser characteristics including the pulse width and pulse power.

Accomplishments thus far have indicated that CS_2 is the most effective liquid. In addition, the importance of solvent purity was demonstrated by the production of small bubbles at high powers in liquids that were not as highly purified. The lack of any significant absorption at this frequency indicates that any bubble formation is the likely consequence of impurities. The inevitable scattering from these bubbles is catastrophic for any intended applications.

It has been established that the length of the fiber significantly improves the generation efficiency of the coherent radiation. For 1.5 m long fiber with $50 \mu\text{m}$ diameter, conversion efficiency with respect to the incoupled power is greater than 50%. Furthermore, device operation at pump power densities approximately ten times above the threshold power density, i.e. 30 MW/cm^2 , yields broadband coherent output whose intensity fluctuations do not significantly exceed those of the pump radiation.

The driving beam pulse width, along with the device length, has a definite impact on the range of generated frequencies. If adequately chosen, both stimulated Rayleigh-Kerr and Raman-Kerr scattering contribute to the generation of about 4000 cm^{-1} wide range of coherent visible frequencies when 532 nm pump beams are used. It has been established that upwards to 50 percent of the coupled input energy is converted to red shifted frequencies. It is expected that further optimization of these critical parameters will result in the device capable of generating broadband coherent radiation whose working intensity is close to 40% of pump intensity.

REFERENCES

1. P. N. Prasad and D. J. Williams, "Introduction to Nonlinear Optical Effects in Molecules and Polymers", Wiley, New York (1991).
2. J. A. Pople, B. L. Beveridge and P. A. Dobosh, *J. Chem. Phys.* **47**, 2026 (1967).
3. J. Lipinski and J. Leszczynski, *Int. J. Quantum Chem.*, **22**, 253 (1982), J. Leszczynski and J. Lipinski, *Z. Naturforsch.* **42a**, 160 (1987), J. Lipinski, *Int. J. Quantum Chem.* **34**, 423 (1988).
4. A. Samoc, A. Krajewska-Cizio and P. N. Prasad, submitted for publication.
5. A. Samoc, M. Samoc, J. Funfschilling, I. Zschokke-Granacher, *Chem. Phys. Letters*, **114**, 423 (1985).
6. T. Bjorvatten, O. Hassel and A. Lindheim, *Acta Chem. Scand.*, **17**, 689 (1963).
7. P. B. Logsdon, J. Pflieger and P. N. Prasad, *Synth. Metals*, **26**, 369 (1988).
8. P. N. Prasad, M. Casstevens and M. Samoc, *SPIE Proceedings*, **1056**, 117 (1989).
9. P. N. Prasad and B. A. Reinhardt, *Chem. Mater.* **2**:660 (1990).
10. P. N. Prasad, Y. Zhang, and R. Burzynski in "Proceedings of Ultrastructure Conference on Sol-gel Processing", Orlando, Florida, 1991, Ed. L. L. Hench, Wiley (in Press).
11. Y. Zhang, Y. P. Cui, C. J. Wung, P. N. Prasad, and R. Burzynski, *SPIE Proceedings*, Vol. 1560 (1991).
12. C. J. Wung, Y. Pang, P. N. Prasad, and F. E. Karasz, *Polymer* **32**, 605 (1991).
13. Y. Pang, M. Samoc, and P. N. Prasad, *J. Chem. Phys.* **94**, 5282 (1991).
14. "Photorefractive Materials and their Applications", Vols. I and II, Eds. P. Gunther and J.-P. Huign, Springer-Verlag, Berlin (1989).
15. "Electrical Properties of Polymers", Eds. D. A. Seanor, Academic Press, New York (1982).
16. G. S. He, R. Burzynski, and P. N. Prasad, *J. Chem. Phys.* **93**, 7647 (1990).

DEVELOPMENT OF NONLINEAR OPTICAL DEVICES BY IMPROVEMENT OF MOLECULAR HYPERPOLARIZABILITIES AND VIA PHOTOPROCESSING

L. R. DALTON, DEPARTMENT OF CHEMISTRY, UNIVERSITY OF SOUTHERN CALIFORNIA, LOS ANGELES, CA 90089-1062

PHOTO-INDUCED CHEMICAL AND CONFORMATIONAL CHANGES FOR DEVELOPMENT OF OPTICAL STRUCTURES

Photo-induced conformational changes are well-known in chemistry. For example, lasers have been used to initiate addition to multiple bonds, e.g., photo-induced crosslinking and polymerization reactions involving polyalkenes and polyalkynes. Also, conformational changes such as cis-trans isomerization about double bonds are well-known photo-processes. Other conformational changes include ring opening-closing reactions and photo-induced keto-enol tautomerism. Finally, it can be observed that changes of state (solid-liquid-gas and between various liquid crystalline phases) can be driven by laser irradiation and local heating effects. We have undertaken the systematic exploitation of these processes to control ultrastructure for the development of precise patterns or circuits for optical signal transport and processing.

In a recent article¹, we demonstrated the use of photo-induced isomerization and cross-linking reactions to develop integrated optical circuits (e.g., channel waveguides). In that work, an index of refraction change on the order of 0.3 is induced by a photo-stimulated isomerization about an azo linkage which is locked in place by a simultaneous photo-stimulated cross-linking reaction involving either double or triple bonds. This work involved synthesizing polymers containing three functional segments (see Fig. 1 below).

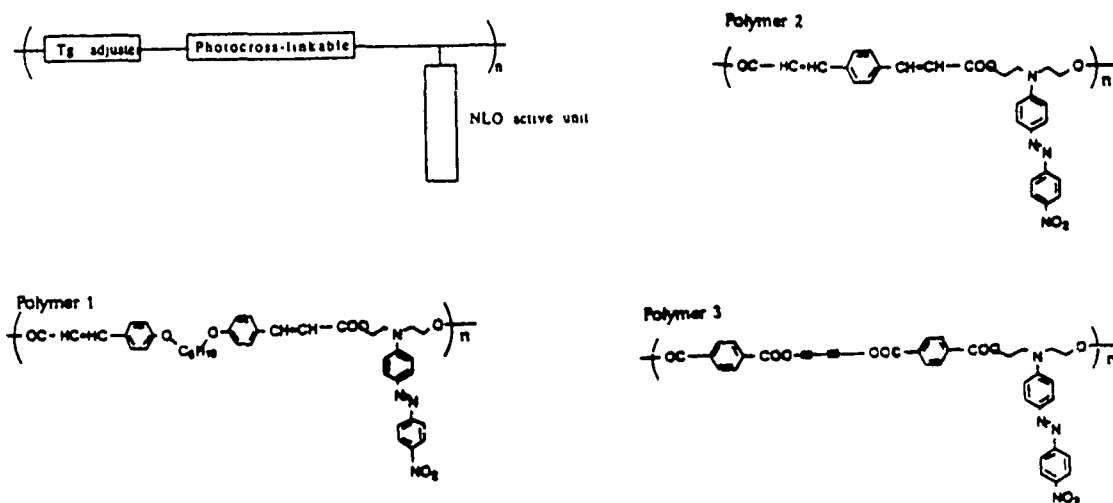


Figure 1. Structure of Photoactive Azobenzene Polymers

In addition to development of integrated optical circuits, this particular polymeric structure is convenient for realizing polymers with large second harmonic generation efficiencies. Second harmonic generation requires the material to exhibit macroscopic as well as molecular non-centrosymmetric symmetry. For polymeric materials containing a noncentrosymmetric electroactive moiety as a side chain pendant, the required macroscopic order is typically achieved by electric field poling of the material in a liquid or fluid state

followed by cooling the materials to lock-in poling-induced order. We, and many other groups, have endeavored to stabilize the poling induced macroscopic order by crosslinking the material exploiting either photo-initiated or thermally-initiated processes. Very stable material is possible with the crosslinking approach since the resultant film is tough, solvent resistant, and maintains its alignment reasonably well. We² have reported on a polyester NLO material which retains 90% of its initial NLO activity for over 3000 hrs after poling. The NLO coefficient is large ($d_{33} = 56 \text{ pm/V}$, $r_{33} = 26 \text{ pm/V}$) in this material because of the NLO side chain pendant accounts for approximately 65% of the weight of the material. Using corona poling (voltage approximately 200 V/mm) it was possible to achieve 41% effective alignment of the disperse red molecules.

A very promising new approach is a two-component thermal-setting polymer host which results in a two dimensional mesh-like polymer structure with the NLO moiety as a high density side-chain pendant (see Fig. 2).

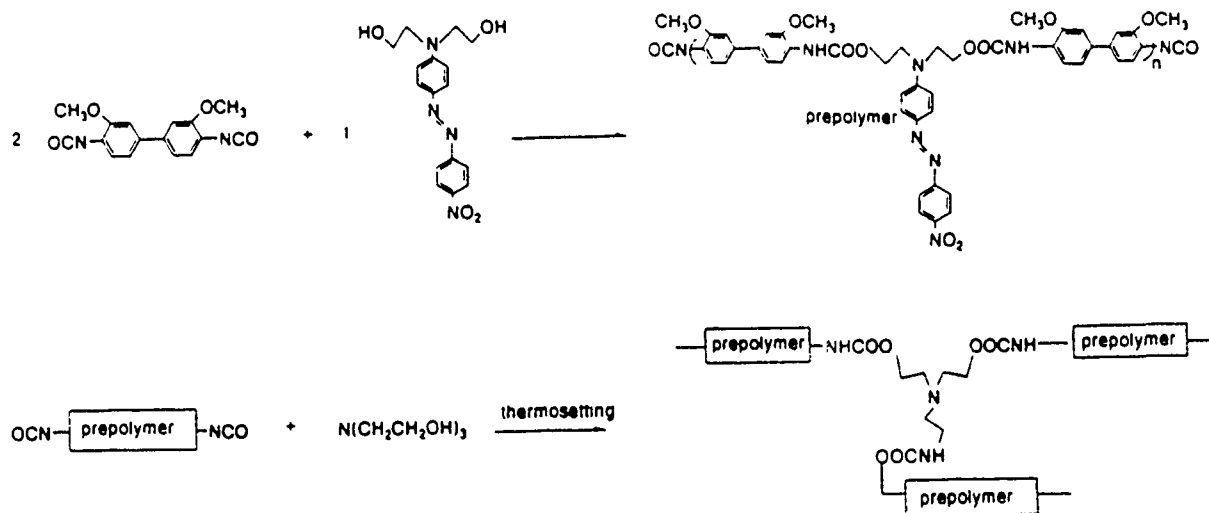


Figure 2. Synthesis and Processing of Thermosetting NLO Polymer

This mesh is an almost completely crosslinked and results in an extremely stable, tough and chemically inert film. Our initial studies showed no observable decay in NLO activity after several hundred hours and even more important, these films can be used at temperatures up to 365 K without observable loss of alignment. Using a two solvent approach, high optical quality films of up to 10 μm thickness can be spin-casted prior to thermal setting. Our initial measurements of the infrared absorption using patterned waveguides show very low loss; less than we are able to measure by our conventional techniques. These thermal setting polymers are extremely chemically inert and can be removed only by plasma oxygen etching. They, therefore, look very promising for hybrid semiconductor devices since they may withstand some portion of the normally used semiconductor device processing. An intriguing and potentially important observation is the possibility of using lift-off techniques to transfer a fully poled NLO organic film to a second substrate which may contain other organic and semiconducting devices. We have some preliminary indications that this is possible and work on integration is proceeding at the Photonics Institute at USC.

One of the requirements for successful exploitation of second harmonic generation in non-centrosymmetric materials is phase matching of the first and second harmonic signals. Materials with NLO and micropatterning properties offer an elegant solution to this problem exploiting what has been called "quasi-phase-matching". This approach can lead to a very efficient conversion since the harmonic and fundamental are in the same order waveguide mode and the mode spatial overlap is large. For typical organic NLO materials for doubling from the infrared to the visible, the required periodicities are in the 5-15 μm range and hence micro-patterning is the key to this approach. We have recently reported micropatterning to sub-micron resolution in both index of refraction ($\Delta n = 0.3$) and birefringence ($\Delta(n_e - n_o) = 0.2$) using 488 nm radiation. In addition, after poling, second harmonic and electrooptic coefficients can be selectively erased to sub-micron resolution by UV radiation.

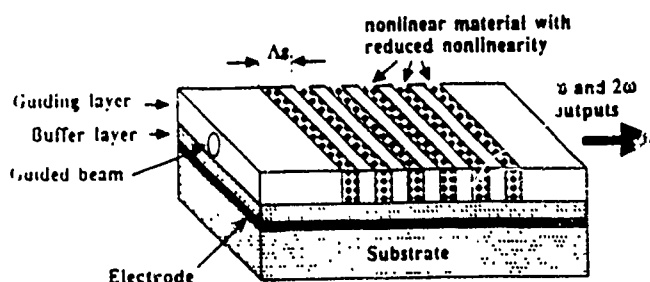


Figure 3. Quasi-Phase Matched Second Harmonic Generation Using Patterned Nonlinear Materials.

Linearly polarized short wavelength visible or ultraviolet light can also be used to write birefringent diffraction gratings. As an example of the various applications, we have written birefringent gratings of up to 2000 lines/mm; the resolution was limited by the laser wavelength and recording geometry. The diffraction efficiency of a $1\mu\text{m}$ periodicity thin grating was measured with a 775 nm Ti:Sapphire laser probe beam at different polarization angles with respect to the exposure beam polarization as is shown in Fig. 4. The diffraction efficiency curve has the familiar cosine square form (the excitation transition rate is proportion to the square of the overlap integral of the Hamiltonian, $H_1 = \mu E \cos \phi$). A 9:1 diffraction efficiency ratio of the two polarization eigenmodes was measured; this ratio is in good agreement with the theoretical prediction using a simple three level model. The effect of exposure energy on the phase delay between the two eigen-polarization modes is shown in Fig. 5a and the corresponding photoinduced birefringence is shown in Fig. 5b. The photoinduced birefringence-exposure energy curve resembles a typical Hurter-Driffield curve for photographic materials except for a decrease of Δn at high exposure levels. Maximum measured n values are summarized in Table 1.

Thin film waveplates of $<1\mu\text{m}$ thickness showed $>\pi/4$ phase delay and good temporal stability.

Figure 4. The Diffraction Efficiency of a Birefringent Grating as a Function of Different Probe Polarizations

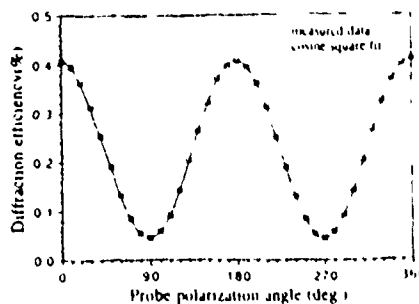


Figure 5. Dependence on Exposure Energy Density

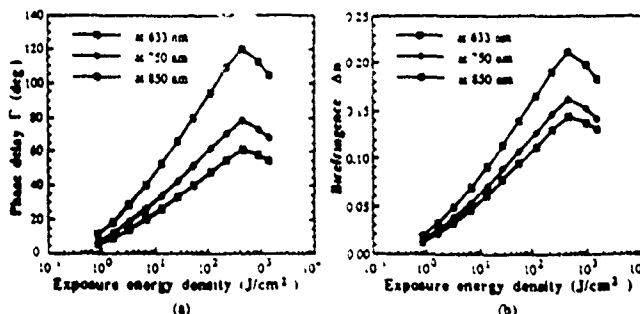


Table 1: The measured maximum refractive index changes and birefringence data at several wavelengths

Wavelength	@ 633 nm	@ 750 nm	@ 800 nm	@ 850 nm
Refractive index	1.950	1.848	1.830	1.816
Maximum index change under unpolarized light exposure	0.32	0.26	0.25	0.24
Maximum birefringence Δn	0.21	0.16	NA	0.14

CHARACTERIZATION OF OPTICAL NONLINEARITIES

Unfortunately space does not permit a comprehensive view of materials synthesized and characterized during the past year, thus this discussion focuses upon selected examples of particular interest.

A new technique, analogous to biological staining procedures, has been developed for incorporating charged electroactive moieties into polymer films³. This has been used to obtain preliminary susceptibility measurements for several dye systems including ruthenium red. Metallomacrocyclic materials continue to be of interest as NLO materials because of the contribution of metal-ligand and ligand metal charge transfer transitions to optical nonlinearity⁴. In recent, multi-color experiments, we have demonstrated by pumping the metal-ligand CT transition that this contributes dramatically to measured optical nonlinearities. Recently, we have undertaken investigation of the photosynthetic reaction center (supplied by J. R. Norris of Argonne Natl. Lab.) and associated chlorophyll model compounds. Optical nonlinearities were observed to be somewhat greater for the reaction center than for model compounds; however, the picosecond decays for both degenerate four wave mixing and pump-probe experiments require consideration of both electronic and nuclear motion. A typical result is the pump-probe data shown in Fig. 6. DFWM temporal responses are characterized by both exponential electronic components and an oscillatory component associated with nuclear motion. The period of the oscillatory component (<2 psec) is extremely short for nuclear motion. One conceivable explanation is photoinduced keto-enol tautomerism which can exist for chlorophyll but not for other porphyrins. A femtosecond

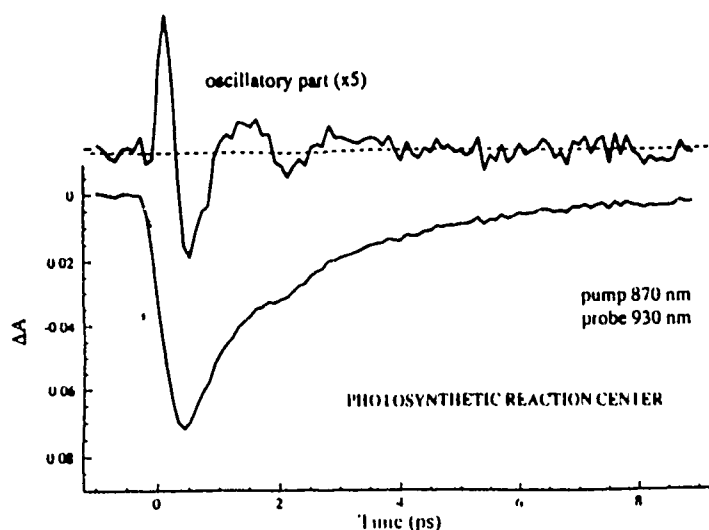


Figure 6. Pump-Probe Experiment on Photosynthetic Reaction Center laser system based upon a pumped and amplified Coherent MIRA Ti:Sapphire has recently been activated at USC and is being used to investigate the fundamental excitation and charge separation processes of the reaction center.

Another novel system that we have studied during the past year is C60 (footballen; reg. no. 99685-96-8) and the related C70 ([5,6]fullerene-C70; 115383-22-7). Preliminary DFWM measurements indicate moderately large optical nonlinearities with picosecond lifetimes even though the optical gap is much larger than in analogous sp^2 polyenes (see Fig. 7).

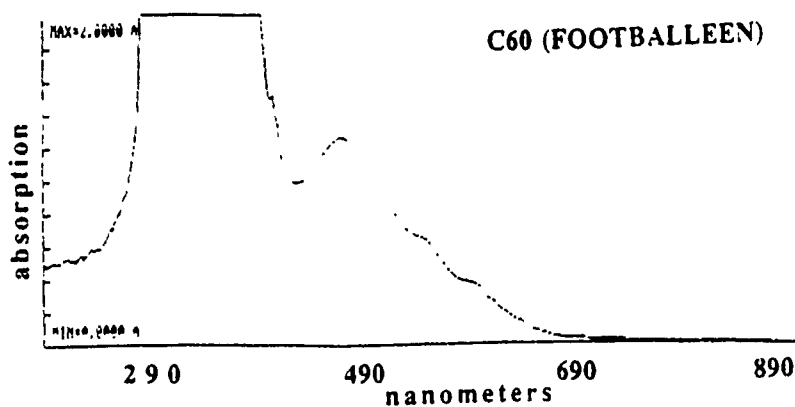


Figure 7. Optical Spectrum of C60

REFERENCES

1. Y. Shi, W. Steier, L. P. Yu, M. Chen and L. Dalton, *Appl. Phys. Lett.*, **58**, 1131 (1991); see also, K. Beeson, et. al., *Appl. Phys. Lett.*, **58**, 1955 (1991).
2. Y. Shi, W. Steier, L. Yu, M. Chen and L. Dalton, *Proc. SPIE*, **1559** (1991).
3. R. Montgomery, Ph.D. Thesis, Univ. of S. Cal., Los Angeles, 1991.
4. L. Yu, D. Polis, L. Sapochak and L. Dalton, in *Organic Molecules for Nonlinear Optics and Photonics*, NATO ASI Vol. 194, eds. Messier, Kajzar and Prasad, (Kluwer Academic Press, 1991) pp. 273-99; S. Yang, Q. Qian, L. Zhang, P. Qui and Z. Wang, *Opt. Lett.*, **16**, 348 (1991); D. Rao, F. Aranda, J. Roach and D. Remy, *Appl. Phys. Lett.*, **58**, 1241 (1991); H. Sakaguchi, T. Nagamura and T. Matsuo, *Jap. J. Appl. Phys.*, **30**, L377 (1991).

Multifunctional Macromolecules: Combining photoconductivity and electro-optic activity to create photorefractive polymers.

M. J. Sansone, K. Blatter, G. J. Breckenridge, A. J. East, H. A. Goldberg, M. S. Kwiatek, C. F. Shu

**Hoechst Celanese Corporation
86 Morris Avenue
Summit, N.J. 07901**

A summary of a presentation made at the Fourth Annual OGAMMs review in Ilkley, UK on August 21, 1991.

Introduction

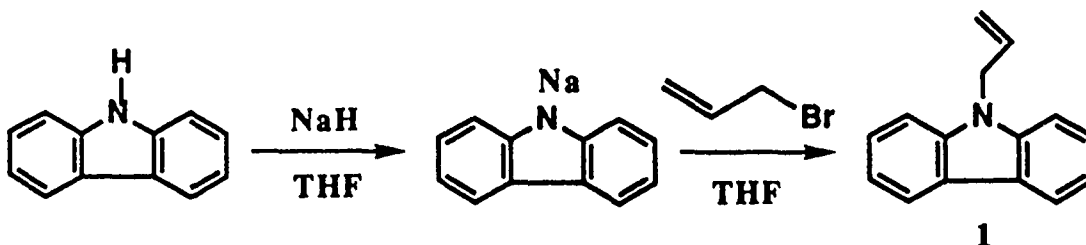
During the course of the M3 program, the concept of multifunctionality has evolved. In its most general terms, a multifunctional polymer is a material which can perform more than one function e.g. electro-optic and pyroelectric functions. A more restricted and perhaps more interesting definition of a multifunctional macromolecule is a polymeric material in which two or more functionalities are incorporated into its structure and, as a direct consequence, a new functionality is created which otherwise would not exist. In this paper, we describe our efforts to create and characterize a photorefractive polymer by grafting electrooptic and photoconducting units onto a polysiloxane backbone.

Photorefractive materials are defined as electro-optic materials in which refractive indices are changed by photo-induced space-charge fields via the electro-optic effect.¹ The photorefractive effect has been observed in a number of inorganic, electro-optic systems such as LiNbO₃, BaTiO₃, CdS, GaAs to name just a few. Recently, several research efforts in the area of organic photorefraction have been reported in the literature. The photorefractive properties of a single crystal of cyclooctylaminonitropyridine doped with TCNQ was disclosed.² IBM³ and Kodak⁴ have also reported results in which an electro-optic polymeric host was mixed with photoconductors and sensitizers to create a guest/host photorefracting system.

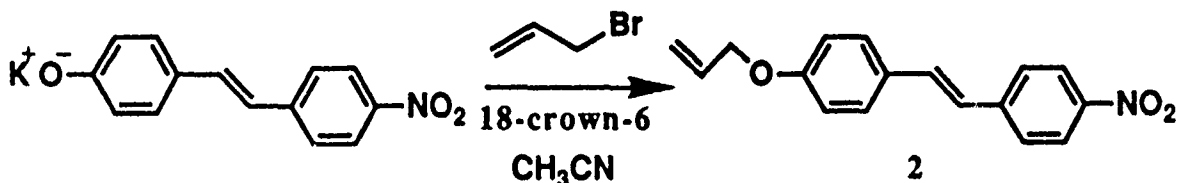
To achieve the photorefractive effect in a single polymeric material would require the presence of at least two major functionalities - photoconductivity and electroactivity. Basically, the material would function as follows: an incident light beam creates an exciton (an electron-hole pair) in the photorefractive material. This pair separates via diffusion, drift (external electric field), or the photovoltaic effect setting up a space charge field. This space charge field modulates the refractive index through the linear electrooptic effect. The potential applications of such materials are numerous and depend on, among other things, the speed, sensitivity, and maximum refractive index change of the material. Areas of application include optical interconnects, dynamic holography, phase conjugate mirrors, spatial light modulators, beam steerers, wavefront amplifiers, and oscillators.⁵ It is expected that polymeric photorefractors will offer improvements in sensitivity due to their larger electro-optic figures of merit, n^3r/ϵ , while also enabling the fabrication of low cost, large area devices. Such devices are practically unattainable with crystalline materials. We report here the first successful combination of photoconductivity and electro-optic activity in a covalently bonded system.

Synthesis

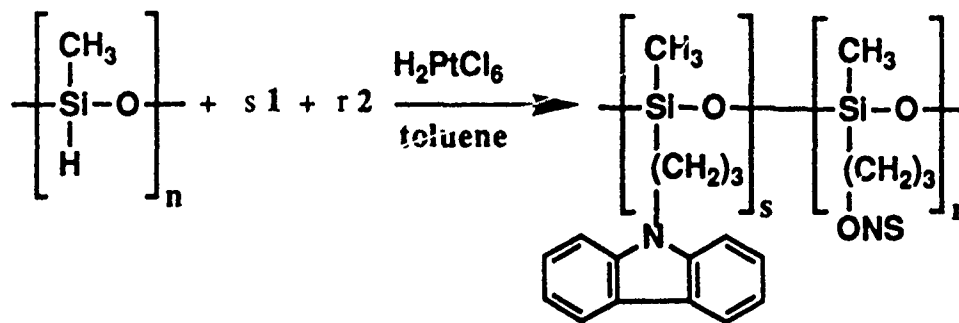
Polymethylhydrosiloxane is an easily functionalized polymer. Substitution via hydrosilylation across a terminal alkenyl group is a well known reaction that offers wide flexibility in the choice of side chain substituents⁶. Side chain polysiloxanes containing carbazole units isolated from the backbone by different length alkyl spacer groups have been studied for their photoconductive properties by Haarer.⁷ Because of our previous efforts in the M3 program, oxynitrostilbene was selected to provide the electrooptic function. Carbazole was chosen for obvious reasons to provide the photoconductivity function. Preparation of N-propenyl carbazole was accomplished by first reacting carbazole with sodium hydride in THF to form the anion. This is subsequently reacted with allyl bromide to afford the desired carbazole with a terminal alkenyl group.



The propenyl oxynitrostilbene is prepared by reacting the potassium salt of oxynitrostilbene with allyl bromide in acetonitrile using 18-crown-6 to sequester potassium.



These two substituents are then mixed together in the desired ratio and reacted with the polymethylhydrosiloxane in toluene. The reaction is catalyzed by chloroplatinic acid.



Addition of the side groups was better than 99%. The ratio of carbazole units to ONS units in the first polymer prepared was 9/1. The T_g was found to be 57°C by DSC. A second polymer with a 3/1 ratio was also prepared. Confirmation of the degree of substitution and the relative ratio of the substituents was obtained by NMR. Most of the results reported herein are on the first polymer.

Characterization

There are two principal methods for measuring the photoconductive behavior of materials: the photoinduced discharge (PID) method and the time of flight method. The latter method is preferred because it is easier to analyze mathematically and yields carrier mobilities and transit times. The PID method simulates the xerographic process and is experimentally easier to implement but not readily analyzed. We have used a Monroe Static Charge Analyzer model 276A to test materials by the PID method. This instrument is widely used for characterization of photoconductors in the photocopier industry. The material to be measured is coated onto two 1 inch diameter discs which are placed into a revolving turntable. The samples are spun at 600 rpm over two corona charging stations 120 degrees apart. The corona charging can be positive or negative. The samples are charged in the corona field. An ac electrometer consisting of three electrodes, placed 120 degrees apart, measures and averages an ac voltage on the samples proportional to the charge on the samples.

After the samples are corona charged, photocharge generation can be induced with a broadband light source. The tungsten filament lamp peaks at about 1 μm . The instrument has a filter holder which can accommodate 2" x 2" filters. The change of sample voltage with time, dV/dt , both without and with illumination is output to a computer via an IEEE board.

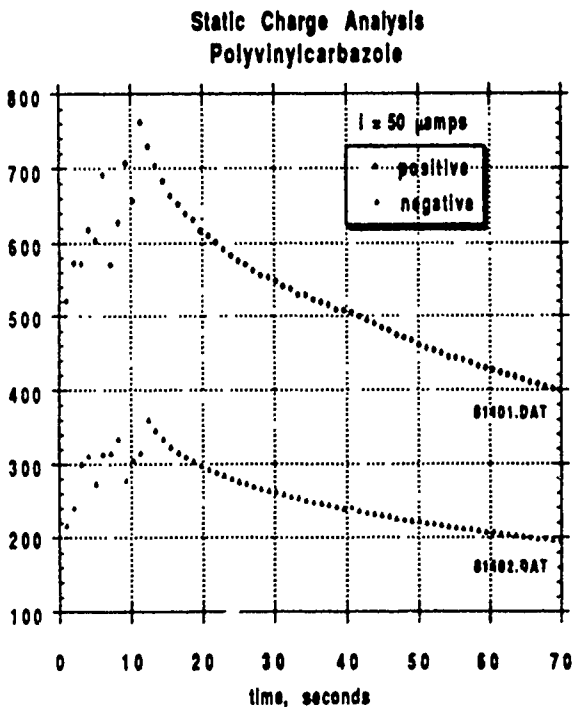


Figure 1

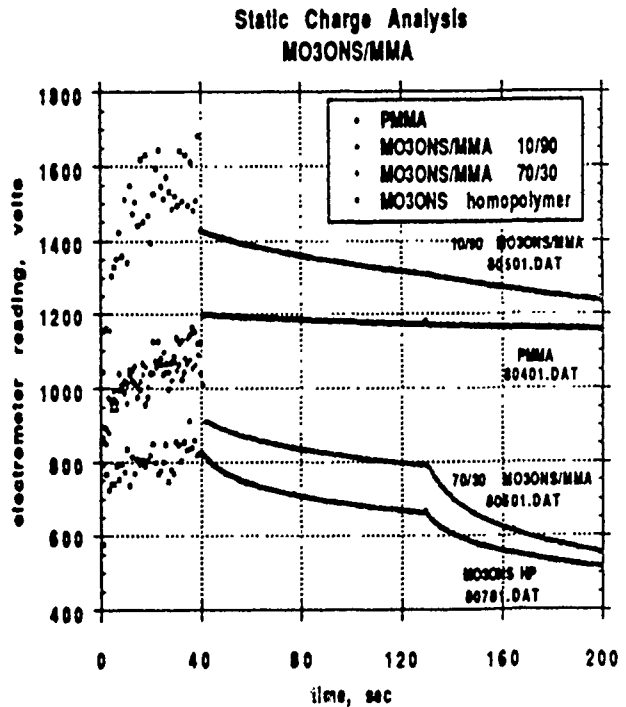


Figure 2

A PID curve is shown in figure 1 for PVK (polyvinylcarbazole). No photodecay was observed because the tungsten lamp cannot initiate charge generation in PVK. Both positive and negative corona was applied at 50 μamps current. The surface charge and dark decay were higher with

the positive corona than with the negative corona which is consistent with the fact that the predominant charge carriers in PVK are holes.

The PID curves for some MO3ONS/MMA compositions and PMMA are shown in figure 2. PMMA shows no dark or photo decay as expected. The 10/90 MO3ONS/MMA exhibits increased dark decay and little, if any, photo decay. At the higher concentrations of oxynitrostilbene, there is clear indication of photo-induced decay which indicates that ONS is generating and moving charge, although not effectively. Attempts to isolate the spectral region using bandpass filters was not successful, presumably because of signal loss in the filters.

The 90/10 carbazole/ONS/polymethylsiloxane polymer (K/ONS/PMS) was dissolved in cyclohexanone and spincoated on ITO coated glass cut to fit the static charge analyzer. A positive corona current of 50 mamps was used to charge the surface to 540 V for 10 seconds. This was followed by a 30 second dark decay period and then 30 seconds of photo-induced decay (figure 3). It is clear that the oxynitrostilbene is responsible for charge generation. The strong photo decay is due to the presence of the carbazole which, although not generating charge, is a good organic photoconductor.

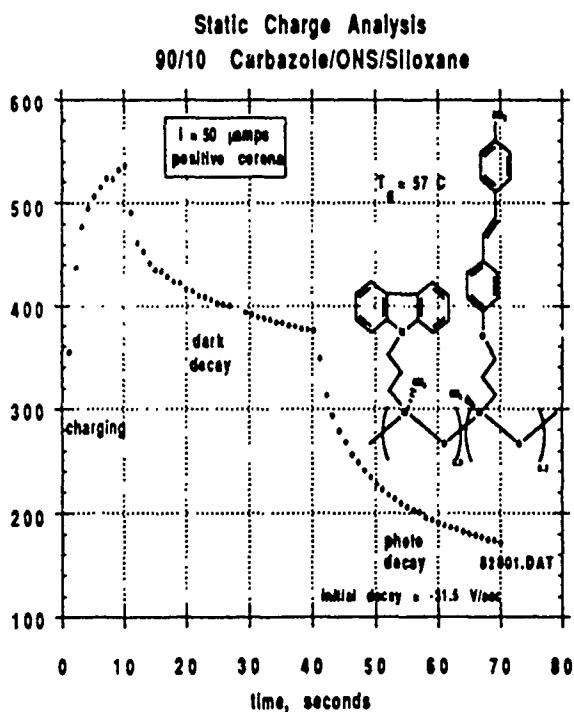


Figure 3

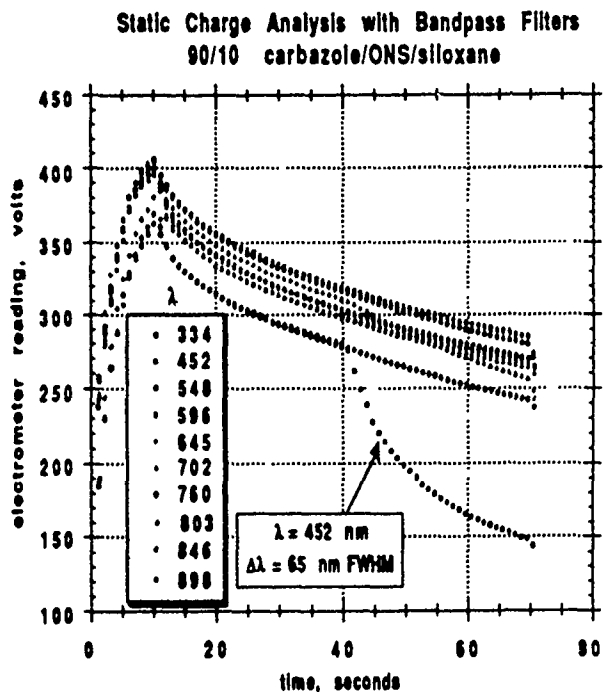


Figure 4

Figure 4 shows the PID curves generated by filtering the output of the tungsten lamp on the static charge analyzer. The 452 nm filter with a 65 nm pass band gave the only photo response. It should be remembered that the spectral output of the tungsten lamp peaks at about $1 \mu\text{m}$ so that the 334 nm filter, which has a passband of only 2 nm, is receiving too little radiation to observe a photoresponse. In fact, a very strong photo response is expected in the UV due to

charge generation by carbazole. In our system, charge is being generated by the oxynitrostilbene and transported by carbazole.

Samples of 90/10 K/ONS/PMS were spincoated on ITO glass, baked for 19 hours at 155°C, electroded with gold, and poled at 60°C, three degrees above T_g . The results are summarized in table 1. The maximum poling voltage was 63 V/ μm . Samples were held in the dark for various periods of time as shown in the table. However, the dark currents are still appreciable and this may be the reason for the poling voltage being limited to 63 V/ μm . The best pyroelectric coefficient obtained was 1.45 $\mu\text{Cm}^{-2}\text{K}^{-1}$. This is somewhat higher than might have been expected from our earlier work on PMMA based polymers, but this might be due to the significantly lower T_g and higher backbone flexibility in siloxane polymers.

Sample	Poling Voltage V/ μm	Pyro Coeff $\mu\text{Cm}^{-2}\text{K}^{-1}$	Comments
B-1	75		breakdown at 63 V/ μm
A-1	50	0.70	dark chamber-1 hr
B-2	60	0.96	dark chamber-4 hrs
A-1R	62	1.45 1.38 1.13 1.10	dark chamber-16.5 hrs day 2 day 4 day 5

Table 1

The refractive index on sample A-1R was measured on the Metricon 2010 prism coupler at two wavelengths, 0.633 and 1.3 μm and found to be 1.642 and 1.612 respectively. The electro-optic coefficients were measured using a reflection technique and found to be 1.0 and 0.7 pm/V at 0.632 and 1.3 μm respectively. Table 2 compares this new data with some earlier data on MO3/ONS and MO6/ONS obtained in the first phase of this program.

Sample	vol % ONS	pyro coeff $\mu\text{Cm}^{-2}\text{K}^{-2}$	pyro vol% x 100	EO coeff pm/V	EO vol% x 100
10/90 MO3ONS	17.8	2.23	125	286	16.1
5/95 MO6ONS	9.7	1.75	18.0	1.8	18.6
10/90 MO6ONS	17.1	2.00	11.7	2.6	15.2
10/90 ONS/K/PMS	7.9	1.45	18.4 (29.3)*	1.0	13 (20)*

* corrected for poling voltage.

Table 2

The EO coefficients were all measured at 0.632 μm , and the ONS/K/PMS polymer has the electro-optic activity expected from our earlier work on PMMA based polymers.

Summary of Results

Polymethylhydrosiloxane has been successfully functionalized with a photoconductive carbazole side chain and an electro-optic oxynitrostilbene side chain at mole ratios of 9/1 and 3/1 K/ONS. The hydrosilylation reaction proceeds essentially to completion and the substitution ratio is close to the initial reactant ratio. The 90/10 composition has been characterized by a photo-induced decay technique. It was determined that the oxynitrostilbene was generating charge which appears to be transported by the carbazole units. Polymer absorption occurred at 450 nm and below. The tungsten lamp on the static charge analyzer provides little UV radiation where carbazole absorbs. The material was poled at 63 V/ μm . The pyroelectric coefficient was 1.45 $\mu\text{Cm}^{-2}\text{K}^{-1}$ and the electro-optic coefficient was 1.0 pm/V at 0.632 μm . Both are reasonable values. In fact, when corrected for volume percent ONS and poling voltage, the pyroelectric coefficient is unexpectedly high. This material represents the first demonstration of photoconduction and electro-optic activity in a single polymer. Photorefraction should result from this combination of properties, and will be demonstrated. Future material variants will also be synthesized in order to optimize the photorefracting properties.

-
- ¹ P. Günter and J.-P. Huignard, Photorefractive Materials and Their Applications I, Springer-Verlag 61, 1988
 - ² K. Sutter and P. Günter, "Photorefractive gratings in the organic crystal 2-cyclooctylamino-5-nitropyridine doped with 7,7,8,8-tetracyanoquinodimethane", *J.Opt.Soc.Am.*, 7 (12), p2274-78 (1990)
 - ³ S. Ducharme, J. C. Scott, R. J. Twieg, and W. E. Moerner, "Observation of the photorefractive effect in a polymer", *Phys. Rev. Lett.*, 66 (14), p 1846-49 (1991)
 - ⁴ J. S. Schildkraut, "Photoconducting electro-optic polymer films", *Appl. Phys. Lett.* 58 (4), p340-342 (1991)
 - ⁵ P. Günter and J.-P. Huignard, Photorefractive Materials and Their Applications II, Springer-Verlag 62, 1988
 - ⁶ P. Strohrig, "Polymers with pendant carbazole groups", *Makromol. Chem., Rapid Commun.* 7, 771-775 (1986)
 - ⁷ H. Domes, R. Fischer, D. Haarer, P. Strohrig, "Polymers with pendant carbazolyl groups, 4", *Makromol. Chem.* 190, p. 165-174 (1989)

Applications of Photorefractive Polymers

M.R. Worboys and S.C. Gratzke

GEC-Marconi Research Centre,
West Hanningfield Road,
Chelmsford, Essex, CM2 8HN.

Abstract

The photorefractive effect has been widely studied in inorganic materials such as BSO, SBN and GaAs, and a large number of possible applications are discussed in the literature. However, none of these have been widely implemented. Photorefractive materials are either extremely difficult to prepare, or require very high optical power densities for efficient operation. Polymers (of suitable composition) represent a new class of photorefractive materials which could overcome many of the problems associated with the more traditional inorganic materials. In this paper we examine the origins of the photorefractive effect, the selection of suitable figures of merit to enable different materials to be compared, and the approach to be used in selecting suitable applications to take advantage of the polymer properties.

Introduction

Inorganic photorefractive materials have been known for just over twenty years and their applications have been considered in some detail [1]. There are two main classes of inorganic photorefractives, electro optic oxides and semiconductors. The properties of materials within each of these classes varies considerably and, as different applications require different material properties, it is normally the case that each material is best suited to a given application. For example, some applications require fast material response times, some require high diffraction efficiency. The performance of these materials in many of the applications is generally acceptable but the widescale exploitation of the photorefractive effect has been limited due to the difficulty of obtaining and processing samples into the correct form.

Several publications have recently appeared in the literature [2,3,4,5] which have reported initial measurements on the photorefractive properties of organic crystals and polymers. In some respects these reports may be considered as a natural progression from inorganic materials since the basic requirements for a photorefractive material are a high electro optic coefficient and photoconduction, both of which are achievable in organic materials [6,7]. Polymers, in particular, have the attractive advantage of being readily processible into either thin film or bulk samples using simple, well characterised techniques such as spinning, dipping, casting, injection moulding or thermal compression. Such processibility, combined with other attractive features of organic materials (such as a low dielectric constant), could result in these materials becoming an important third class of photorefractives and enable the widespread implementation of many of the applications which have been studied.

The Marconi Research Centre has just started a study of photorefractive applications in the context of the properties of organic materials. Our aim is to identify the applications to which organic materials are best suited and perhaps identify those which can uniquely be implemented using organics, for example, those perhaps requiring large area conformal coatings. Such an approach requires an understanding of the basic photorefractive effect (and how it occurs in organics) and the identification of suitable figures of merit (FOM) so that

meaningful comparisons can be made. This work will be carried out over the next year but an initial explanation of the approach to be taken is given here. The results of this study will be fed back to the Hoechst Celanese Corporation which is actively involved in developing organic photorefractives. The materials which are produced will be evaluated at MRC for the applications identified as most suitable in this study.

The Photorefractive Effect

The photorefractive effect is widely documented [1] and the principle is shown below in Figure 1. When two incident coherent light beams interfere in the crystal, photons in the bright parts of the interference fringes are absorbed and create free carriers. These free carriers move within the crystal by diffusion (or drift under the influence of an external applied field) until they are trapped in the dark parts of the interference fringes. The net result is a periodic spatial charge pattern. This charge pattern generates an electric field which, via the Pockels effect, causes a change in the refractive index which has the same spatial frequency Λ as the optical interference pattern. The induced refractive index pattern can exhibit a spatial phase shift ϕ relative to the interference fringes, where ϕ can be of the order of $\pi/2$. The phase shift is due to the fact that the charge distribution moves, and also due to the fact that the electric field distribution is dependent on the derivative of charge distribution.

The photorefractive effect is essentially a combination of four separate physical processes. These are;

- (i) Photogeneration - photons are absorbed and free carriers generated.
- (ii) Photoconduction - the free carriers move through the material under action of the photo-induced (or applied) electric field.
- (iii) Trapping - the free carriers are trapped to produce a static charge distribution.
- (iv) Electro optic effect - the electric field generated by the trapped charge produces a variation in the refractive index of the material.

In considering the overall efficiency of the photorefractive effect it is important to consider the efficiencies of all of the above processes. Similarly, the photorefractive effect is a combination of the response times of all the above processes.

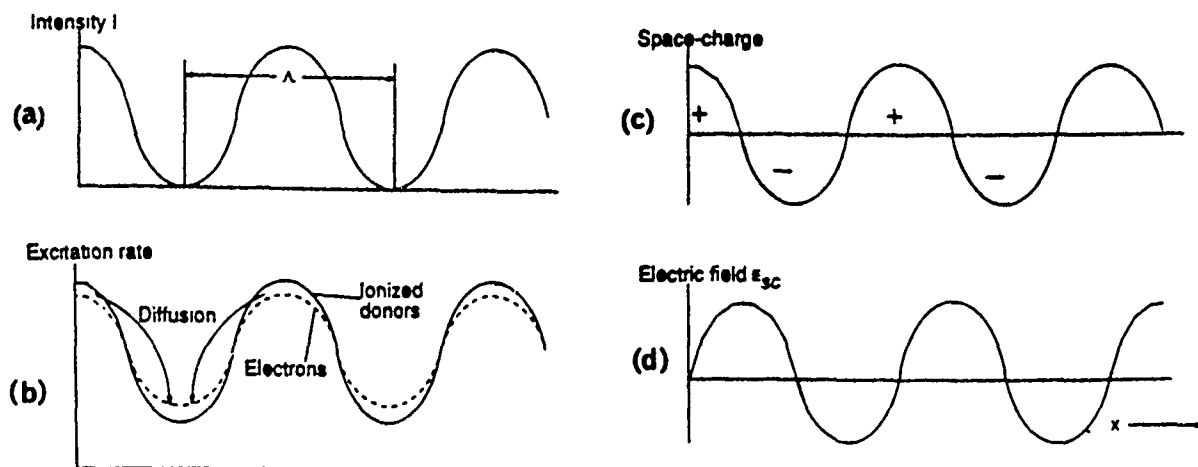


Figure 1: The principle of the photorefractive effect.

It is worth noting that there is a distinction between the photorefractive effect discussed in this paper, where photogenerated charge moves and is trapped by defects in the material, and the references to photorefractive effects made in the literature which are often used to describe effects which are photochemical or photothermal in origin.

Figures of Merit

A number of figures of merit (FOM) are commonly used in the discussion of photorefractive materials [8].

One of the most important of these, the photorefractive sensitivity S , is defined as the refractive index change Δn per unit absorbed energy density

$$S = \frac{\Delta n}{\alpha I_0 \tau} \quad \dots (1)$$

where α is the crystal absorption coefficient at recording wavelength λ , τ is the crystal response time and I_0 the incident power density. Since the grating response time of a photorefractive crystal is the dielectric relaxation time multiplied by a function of different parameters such as the applied field E_0 , the recording wavelength λ , the drift length r_E and the diffusion length r_D of the photo-carrier, we can write

$$S = \frac{1 n_o^3 r}{2 \epsilon \epsilon_0} F(E_0 \lambda r_E r_D) \quad \text{or,} \quad S \propto \frac{n_o^3 r}{\epsilon} \quad \dots (2)$$

where r is the electro optic coefficient and ϵ is the dielectric constant.

The steady state diffraction efficiency η of a thick phase transmission grating, although not a true FOM, is an important parameter and is given by [9]

$$\eta = \exp\left(\frac{-\alpha d}{\cos \theta}\right) \cdot \sin^2\left(\frac{\pi d \Delta n}{\lambda \cos \theta}\right) \quad \dots (3)$$

where θ is Bragg angle inside the crystal and d is the thickness of the crystal. High diffraction efficiencies are achieved by using materials with high ($\sim 10^3 \text{ pm} \cdot \text{V}^{-1}$) electro optic coefficients or by using very thick gratings. The major disadvantage of using a thick grating is that it has a very small acceptance angle - i.e. efficient diffraction would only occur over a very small range of incident beam angles which would significantly reduce the practical usefulness of the interaction. Diffraction efficiencies of close to 100% can be achieved in some inorganic materials such as BaTiO₃, SBN and BGO but usually only at the expense of reduced sensitivity and speed.

The time τ taken for the refractive index grating to build up is an important FOM. The changes in refractive index occur as a result of the build up in the space-charge field (via the electro optic effect) and so depends on the efficiency and timescales of both the charge generation and transport process. Unlike other nonlinear effects where the process is electronic in origin and so virtually instantaneous, the photorefractive nonlinearity can be very slow and has time responses ranging from 10^{-9} s to 10^3 s.

In addition to the FOMs discussed above there are other useful FOMs which are commonly used. One such example, which enables a comparison to be made between fast and slow materials illuminated with the same incident beam intensity, is the energy per unit area to write a grating having a 1% efficiency in a 1 mm thick crystal. Another is the energy required to reach the steady state diffraction efficiency, a FOM which often determines the

crystal chosen for a particular application. One of the tasks which will be undertaken as part of our study is to identify the relevant materials parameters for the organic materials so that FOMs such as these can be calculated. The key FOMs for any applications of interest will be established.

A few comparative figures are shown in Table 1 for the common inorganic photorefractives and some of the organic materials which have recently appeared in the literature. It can be seen that whilst the electro optic coefficients of the organic materials reported here are lower than those of the inorganics, this is more than compensated in the FOM n^3r/ϵ by the lower dielectric coefficients. The two polymers listed in Table 1 were guest/host materials, i.e. EO polymers made photoconductive by the presence of a guest dopant.

Material	n	ϵ	$N_{pr}(cm^{-3})$	$r_{ij}(pm.V^{-1})$	Δn_{max}	$n^3r/\epsilon (pm.V^{-1})$
LiNbO ₃	2.259	29	-	31	10 ⁻⁴	12.3
BaTiO ₃	2.365	168	10 ¹⁶	80	5x10 ⁻⁵	6.3
Ba _{0.39} Sr _{0.61} Nb ₂ O ₆	2.3	750	10 ¹⁶	216	-	3.5
Bi ₁₂ GeO ₂₀	2.55	47	-	3.4	-	1.2
IBM polymer [5]	1.63	2.9	1.9x10 ¹⁵	-	-	
Kodak polymer [4]	~1.7	3.9	-	~2	-	2.5
COANP:TCNQ[2,3]	1.7	~3-4	-	~10	~2x10 ⁻⁶	12.3-16.4

Table 1: Comparison of some basic materials parameters for photorefractive materials (N_{pr} is the photorefractive trap density).

The approach to be taken in this programme is to combine the EO and the photogeneration/transport properties within a single polymer (or copolymer) which is expected to produce even higher FOMs. The COANP crystal doped with TCNQ has the highest FOM of all the materials listed. However, it would be naive to consider a single FOM as an indication of photorefractive efficiency. For example, the diffraction grating in the COANP:TCNQ material took between 20 and 100 minutes to reach peak diffraction efficiency. It should be noted that polymers with EO coefficients higher than those reported above have already been developed by both the Hoechst Celanese Corporation and MRC (with n^3r/ϵ of 160 pm V⁻¹ and 110 pm V⁻¹ respectively).

Applications

A very large number of applications of photorefractive materials have been studied since they were first reported in the literature. Clearly there is not room to detail them here but a representative selection includes two and four wave mixing, phase conjugation, laser beam steering and optical interconnect, optical logic gates, image subtraction, novelty filters, image convolution and correlation, and optical memories (optical image storage and associative memories). The requirements of each of these will be evaluated by MRC to determine which are best suited to implementation using organic materials. Clearly a small

number, such as laser beam steering, phase conjugation and image correlation, will be of particular interest and will be studied in greater depth with a view to implementation using organic materials as they become available.

Summary

The photorefractive effect is well documented and has been widely studied using inorganic crystals. However, these materials are difficult to grow and process so that they are expensive and only available for very specialised applications. Photorefractive polymers are a new class of materials which, as yet, have not been widely studied for photorefractive applications. We have outlined here the advantages offered by the use of these materials and, as our study progresses, will be able to identify the applications to which these materials are best suited. As well as existing applications it is likely that new uses will be found for these materials which exploit the unique properties of polymers.

References

- [1] See, for example, "Photorefractive Materials and their Applications", Eds P. Günter and J.P. Huignard, Volumes I and II, Springer Verlag, 1988 and 1989 respectively.
- [2] Sutter, K., Hulliger, J. and Günter, P., "Photorefractive Effects Observed in the Organic Crystal 2-Cyclooctylamino-5-Nitropyridine doped with 7,7,8,8 - Tetracyanoquinodimethane", *Solid State Comms.*, **74**(8), 867-870 (1990).
- [3] Sutter, K. and Günter, P., "Photorefractive Gratings in the Organic Crystal 2-Cyclooctylamino-5-Nitropyridine doped with 7,7,8,8 - Tetracyanoquinodimethane", *J. Opt. Soc. Am. B*, **7**(12), 2274 (1990).
- [4] Schildkraut, J.S., "Photoconducting Electro-Optic Polymer Films", *Appl. Phys. Lett.*, **58**(4), 340 (1991).
- [5] Ducharme, S., Scott, J.C., Twieg, R.J. and Moerner, W.E., "Observation of the Photorefractive Effect in a Polymer", *Phys. Rev. Letts.*, **66**(14), 1846 (1991).
- [6] See, for example, "Nonlinear Optical and Electroactive Polymers", Eds. P.N. Prasad and D.R. Ulrich, Plenum Press, 1988.
- [7] Haarer, D., "Photoconductive Polymers: Structure, Mechanisms and Properties", *Die Ang. Makromol. Chemie*, **183**, 197-220 (1990).
- [8] Rajbenbach, H., Huignard, J.-P. and Günter, P., "Optical Processing with Nonlinear Photorefractive Crystals", Chapter 5 in *Nonlinear Photonics*, Eds. H.M. Gibbs, G. Khitrova and N. Peyghambarian, Springer Verlag.
- [9] Kogelnik, H., *Bell Syst. Tech. J.*, **48**, 2909 (1969).

Acknowledgements

This work was funded by SDIO/IST through AFOSR under subcontract from the Hoechst Celanese Corporation (F49620-91-C-0062DEF).

Local Electric Fields in Poled Polymers as probed by Photoconduction Experiments

D. Haarer, University of Bayreuth, Physics Institute

Introduction

Recently 'photorefractive materials' have attracted attention as materials for creating instant erasable holograms /1, 2/. Such materials are characterized by having both, photoconductive and electro-optic groups. Through the photoconductive groups one can create light-induced charge carriers; these, in turn, will create space charge fields which modulate the refractive index of the polymeric material. A holographic grating can, hence, be stored in the material until the charge carriers, which form a grating, will be redistributed to provide an uniform material.

Photoconductive Experiments

In order to characterize the photoconductive properties of the presently used NLO-materials we investigated co-polymers with oxynitrostilbene groups, as shown in Fig. 1, co-polymerized with methyl methacrylate in various concentrations.

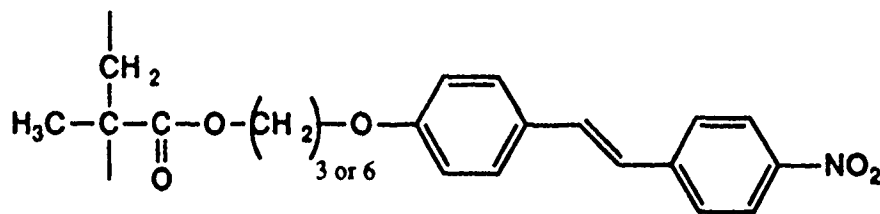


Fig. 1 NLO active side groups used for the photoconduction experiments

For determining the quantum yield of the charge carrier production and the mobility of the charge carriers we performed time of flight (TOF) experiments in which charges are produced on the surface of the sample by irradiation into the main absorption of the NLO-chromophore. In an applied field the charges give rise to a displacement current as shown in Fig. 2 in a symbolic fashion.

Here the charge carriers to be investigated are holes; one assumes that the electrons have already tunneled back to the positive electrode.

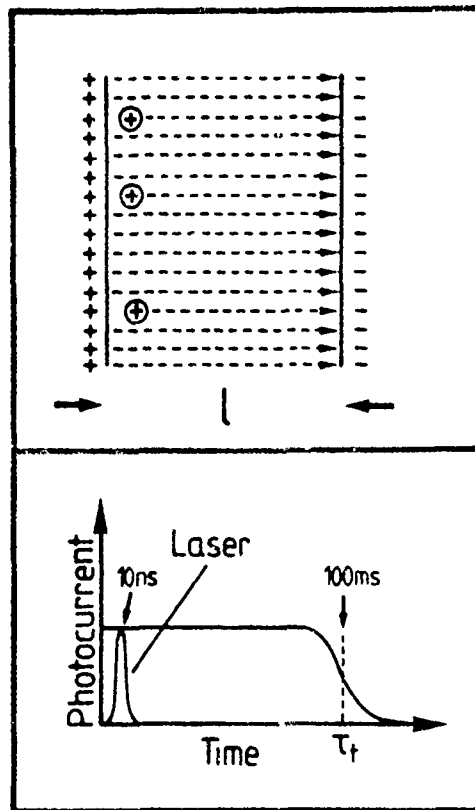


Fig. 2 Symbolic description of a typical TOF-experiment. The laser pulse and the induced photocurrent for nondispersive transport (see text) are given in the lower part of the figure.

The high electric field which is applied to the sample causes the charges to traverse the sample (the thickness is typically 10μ ; the penetration depth of the light is typically $0.1 - 0.3 \mu$). The break in the photocurrent as τ_t marks the time at which the bulk of the charge carriers arrives at the counter electrode. The mobility μ of the material is then given by

$$\mu = \frac{l}{E \cdot \tau_t} \quad (1)$$

where E is the applied electric field and τ_t is the transit time as defined above and l is the thickness of the sample. For details see ref. /3/.

A typical cross section through a sample is given in Fig. 3. The sample is illuminated through a semi-transparent electrode at the top. The substrate is an aluminized mylar film or a NESA-coated glass electrode.

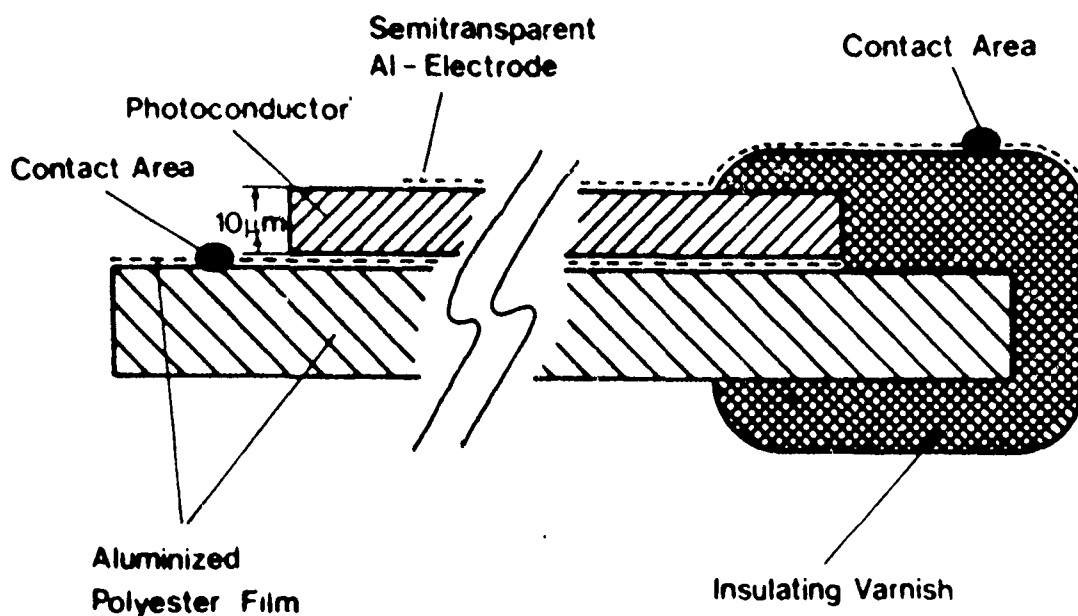


Fig. 3 Cross section through a typical sample. The insulating varnish on which the top electrode is mounted prevents electrical breakdown at the edges.

Unfortunately, simple TOF-experiments can, in most cases, not be interpreted as straight forward as has been done in equ. (1). In most cases polymeric materials are characterized by a 'dispersive transport' rather than by 'Gaussian transport' which characterizes crystalline materials with 'well defined' mobilities (see ref. /3/). In the case of polymers, the dynamic parameters, characterizing the charge carrier propagation vary over many orders of magnitude and, hence, the photocurrent can better be analyzed mathematically by evaluating the Laplace-transformed observable (see for instance ref. /4/). In doing so it can be shown that, for simple cases, a double-logarithmic plot of the current versus time yields two straight lines, whose slopes are different and show a noticeable break at the 'effective transit time' τ_t /5/. This transit time can then be related to the mobility in the usual way as given in equ. 1.

Fig. 4 shows a photoconduction experiment using a conventional photoconductive polymer, namely a carbazole substituted polysiloxane polymer. This material (upper curve) shows a transit time at about 10^{-3} s. Note, that the two slopes before and after the transit time τ_t should - in theory - add up to a numerical value of minus two. This is rather well fulfilled for the siloxane photoconductor. Here the effective mobility is on the order of $2 \cdot 10^{-6}$ cm²/Vs. Such a value can be considered as being typical for amorphous polymers (amorphous silicon has a mobility on the order of unity) (see references in /3/).

It can be shown in mathematically that the more dispersive a material behaves, the closer the slope of the photocurrent approaches unity. A slope of unity means that the charge carrier distribution only smears out in field direction due to heavy trapping of charge carriers in the bulk of the sample (see ref. /3/). Such a behavior can be considered as extremely dispersive; it means that the mobility cannot be defined through a straight forward TOF-experiment, since the effective transit time τ_t does not show up as an abrupt change in the slope. Fig. 4 (lower curve) shows the photocurrent of a 50% NLO-copolymer on the same scale. The slope is, within experimental error, close to one and, thus, does not allow the determination of an effective mobility μ_{eff} . Also, the effective quantum yield for charge carrier production is about 10^{-5} and, thus, three order of magnitude lower than the yield in a typical 'good' photoconductive polymer (at comparable field values; see ref. /3/).

What is interesting is the fact that the poor NLO-photoconductor shows comparable quantum yields for both, electrons and holes. This is shown in Fig. 5; here a positive electric field corresponds to hole-conduction and a negative electric field corresponds to electron conduction. Most organic materials are hole conductors (the best known example is PVK = polyvinyl carbazole). Fig. 5 also shows a uniform decay of the photocurrents of slope on for both, electrons and holes. This holds even for elevated temperatures (+ 73° C). There is also no marked difference between the 30% copolymer and the 50% copolymer.

In summary, by NLO materials which were investigated in the study can be looked upon as photoconductors with low quantum yields (1000 times lower as

compared to good materials). Also, the mobilities cannot be measured due to the totally dispersive nature of the observed photocurrents.

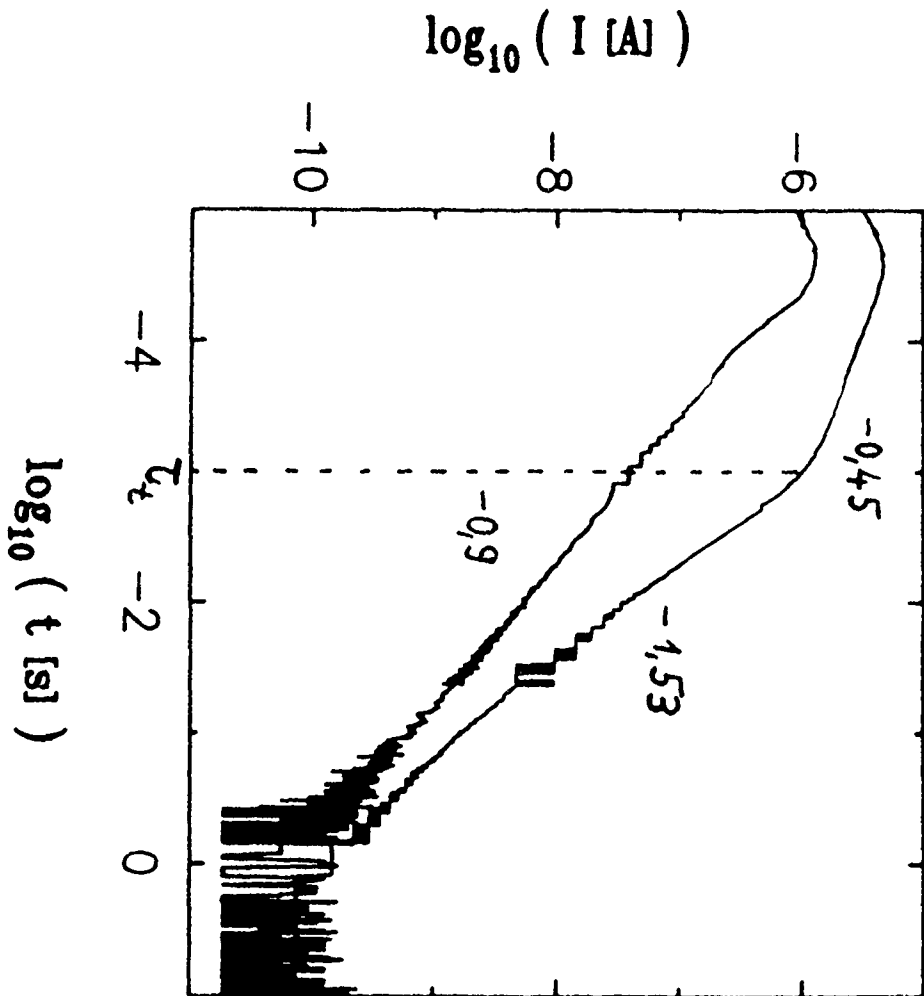
Outlook

At the present time there is a need to develop NLO-materials with higher quantum yields and with less dispersive transport properties. At the present time the highly dispersive nature of the few investigated NLO-materials is not well understood. More experiments on systems which have both, carbazole groups and NLO-groups are in progress.

References

- /1/ J.S. Schildkraut, *Appl.Phys.Lett.* 58, 340 (1991)
- /2/ S. Ducharme, J.C. Scott, H.J. Twing and W.E. Moerner, *Press.Rev.Lett.* 66, 1896 (1991)
- /3/ *Angew. Makromol. Chem.*, 183, (1990) 197 - 220 (3243)
- /4/ E. Müller-Horsche, D. Haarer and H. Scher, *Phys.Rev.* B35, 1273 (1987)
- /5/ H. Scher and E.W. Montroll, *Phys.Rev.* B12, 2455 (1975)

$E = +4 \cdot 10^5 \text{ V/cm}, T = RT$



— copolymer with

50 % chromophore units

quantum yield: 10^{-5}

— Polysiloxane:

$\mu_{\text{eff}} = 2 \cdot 10^{-6} \text{ cm}^2/\text{Vs}$

quantum yield: 10^{-2}

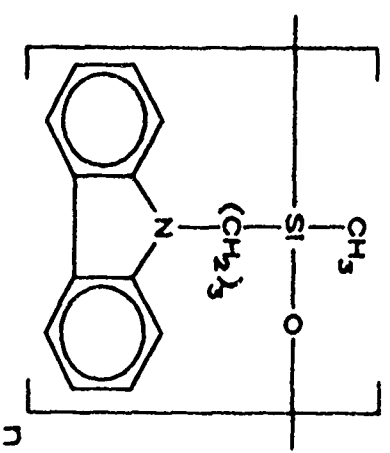


Fig. 4 Photocurrents for a typical organic photoconductor (upper curve) and for the NLO-polymer (lower curve) details see text.

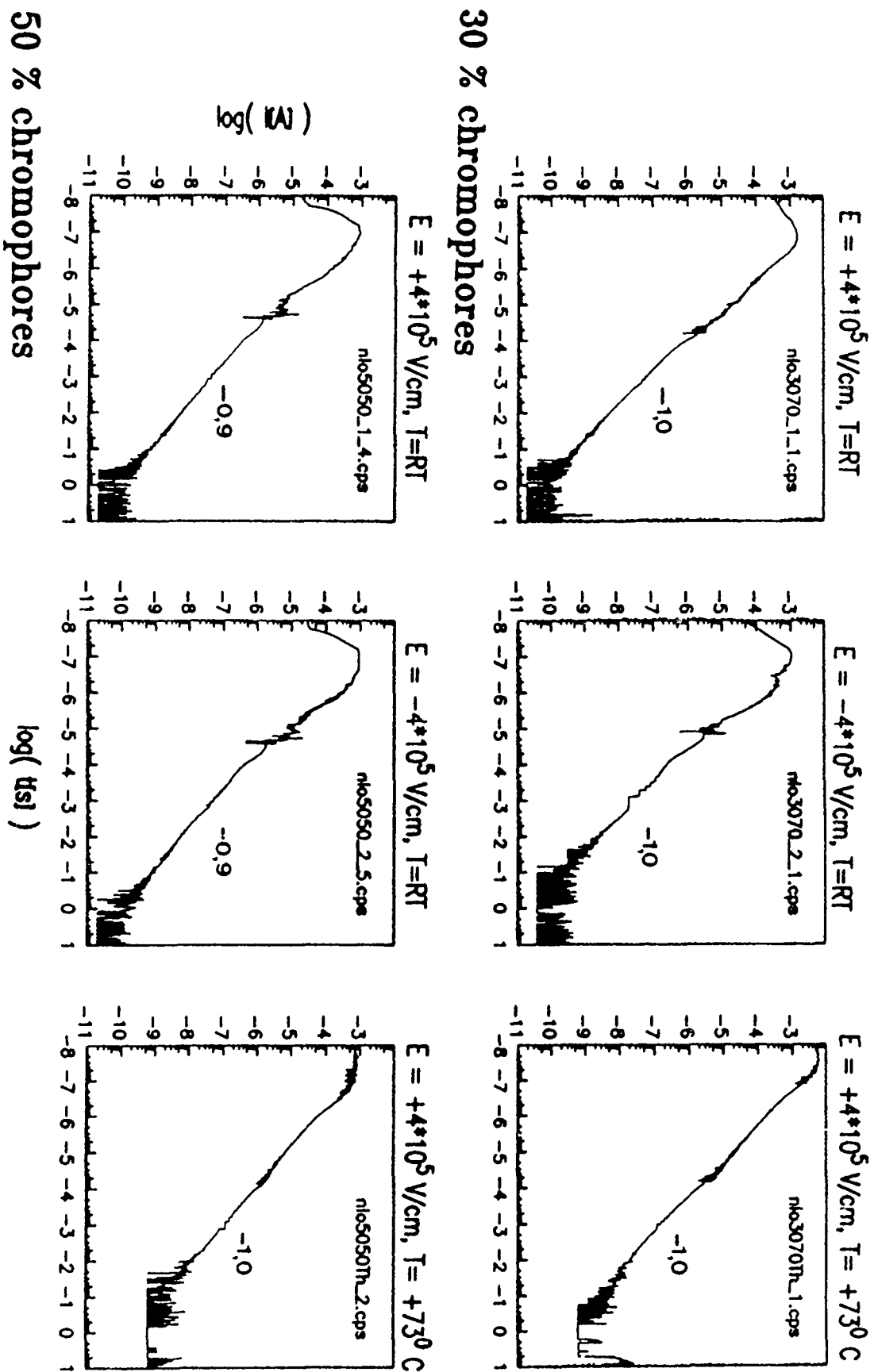


Fig. 5 TOF-curves for electrons and holes respectively, for two NLO-polymers and for two temperatures (see text).

THE EFFECT OF MESOGEN CONCENTRATION ON PYROELECTRIC ACTIVITY AND ON DIELECTRIC AND T.S.C. RELAXATION PHENOMENA

Mr.P.L.Carr, Dr.G.R.Davies & Professor I.M.Ward.

IRC in Polymer Science and Technology
University of Leeds, Leeds LS2 9JT, UK.

At the last meeting in 1990 we presented initial data from IR spectroscopy which suggested that the 10% MO6ONS copolymer films which could be corona poled to give a pyroelectric coefficient of order $3 \mu\text{C}/\text{m}^2/\text{K}$ gave a $\langle P_2(\cos\theta) \rangle$ of approximately 0.15 where θ is the angle between the mesogen long axis and the normal to the film plane. Assuming that the mesogens in the 10% material behave like a dipolar gas this would correspond to a $\langle P_1(\cos\theta) \rangle$ value of approximately 0.5. We have now performed additional experiments and refined our analysis, only to confirm this conclusion.

Surprisingly, corona poled samples of the 100% MO6ONS homopolymer do not display much higher pyroelectric coefficients. Pyroelectric, dielectric and TSC experiments have therefore been performed on a range of copolymers with different mesogen concentrations and spacer lengths in order to determine the reason for the lower than expected activity of the homopolymer.

IR Tilted Film Experiments and Analysis of the IR Data

Tilted film experiments on unpoled samples show that they are not isotropic and the mesogens are preferentially aligned perpendicular to the film giving a $\langle P_2(\cos\theta) \rangle$ of 0.033. Though calculated, corrections due to refraction and refractive index anisotropy were found to be insignificant. Since the poled $\langle P_2(\cos\theta) \rangle$ are calculated with respect to the unpoled, the final poled values are all slightly increased as seen in Fig. 1.

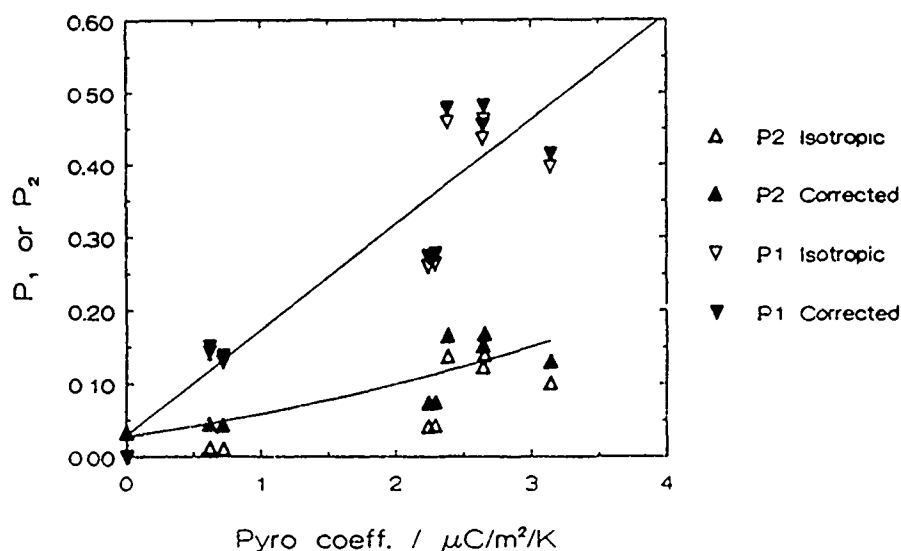


Figure 1. Mesogen Orientation of 10% MO6ONS from IR data

A further correction due to anisotropy of local field effects was also investigated. Unfortunately, refractive indices of the poled films are not available. We have, however,

measured the refractive index of the unpoled film and have tested the effect of allowing the refractive indices of the poled films to take various values, following the theory given by Jarvis and Ward¹. As the in-plane refractive index is reduced, a maximum occurs in the correction factor when $n_2 = n_3 = 1.4$ (when $n_1 \approx 1.9$). Even at this high birefringence, the effect of this correction would be to reduce the highest $\langle P_2(\cos\theta) \rangle$ values by about 2%. We have not, therefore, pursued the experimentally difficult task of measuring the refractive indices of the poled films.

The calculation of $\langle P_1(\cos\theta) \rangle$ from $\langle P_2(\cos\theta) \rangle$ was made on the basis of a Langevin type model in which the energy of a dipole is given by $-\mu E \cos\theta - B \cos^2\theta$ where the term in $\cos^2\theta$ produces a tendency for the dipoles to align perpendicular to the plane of the unpoled film. The constant B was chosen to give $\langle P_2(\cos\theta) \rangle = 0.033$ at zero poling field and the relationship between $\langle P_2(\cos\theta) \rangle$ and $\langle P_1(\cos\theta) \rangle$ was obtained by numeric integration. The $\langle P_1(\cos\theta) \rangle$ obtained in this way are shown in Figure 1.

It is clear that our previous conclusion remains unchanged. The 10% MO6ONS/MMA copolymer can be poled to give quite high mesogen orientation. As will be seen below, however, the homopolymer behaviour cannot be predicted by simple extrapolation of the data for this low copolymer.

Pyroelectric Results

At poling fields up to 100 MV/m the pyroelectric coefficient γ is a linear function of the poling field. We therefore use $d\gamma/dE$ as the measure of the pyroelectric activity shown as a function of mesogen concentration in Figure 2. Each point is the mean of at least three different film samples, poled at five or more poling fields.

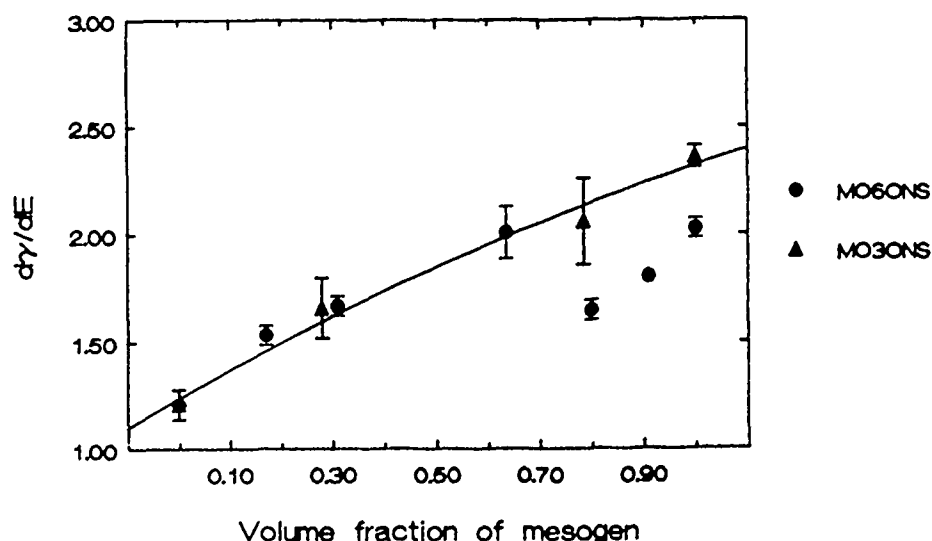


Figure 2. The Pyroelectric activity of MO3ONS and MO6ONS Copolymers

The results for the MO3ONS copolymers are slightly depressed at high concentrations but the MO6ONS data show a sharp fall at 80% (50 mole%) and above. It is significant that this is the onset of liquid crystalline behaviour² and the result suggests that the interactions which promote liquid crystalline behaviour somehow suppress the pyroelectric activity. These data are not sufficient to determine whether it is the pyroelectric mechanism which is affected or merely the degree of orientation. We have therefore measured the polarisation of the samples by integrating their TSC curves.

Total Polarisation from TSC Experiments.

One sample of each copolymer was poled at 12 MV/m and a TSC curve obtained by heating at 10°C/min to a temperature 20°C above T_g . The area under the TSC curve was then used to calculate the polarisations shown in Figure 3.

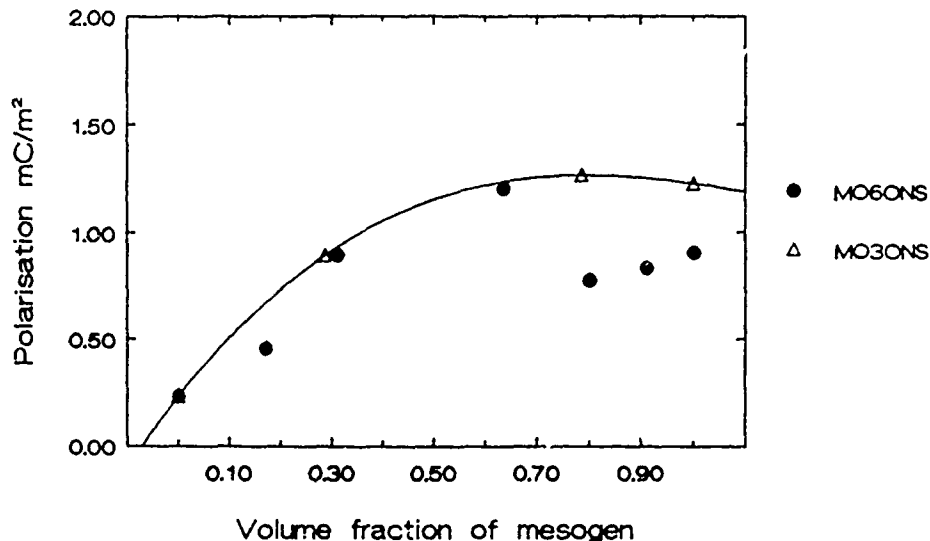


Figure 3. Polarisation at constant Poling Field for MO3ONS and MO6ONS Copolymers.

Although these are single results and probably less accurate than those shown in Figure 1 they are similar in character. The same drop in response is shown beginning at a mesogen concentration of 80% for the MO6ONS copolymer. This would suggest that the reduced pyroelectric activity seen in these samples is due to a reduction in the degree of orientation of the mesogens, rather than a change in the mechanism of pyroelectricity.

Measuring the polarisation produced by low poling fields is effectively a measurement of the low frequency dipolar susceptibility and the data should therefore correlated with the dipolar contribution to the dielectric permittivity as discussed below.

Dielectric Measurements.

We have measured the dipole contribution to the permittivity under conditions approximating to the poling conditions, i.e. at T_g and at very low frequency. Unfortunately ionic conductivity leads to error at these temperatures and frequencies and Cole/Cole plots were not reliable because of the poor data at the lower frequencies. We have therefore estimated the dielectric increment by measuring the permittivity at a temperature corresponding to the loss peak at a frequency of 0.1 Hz and then doubling the difference between this value and the high frequency permittivity. These results are shown in Figure 4.

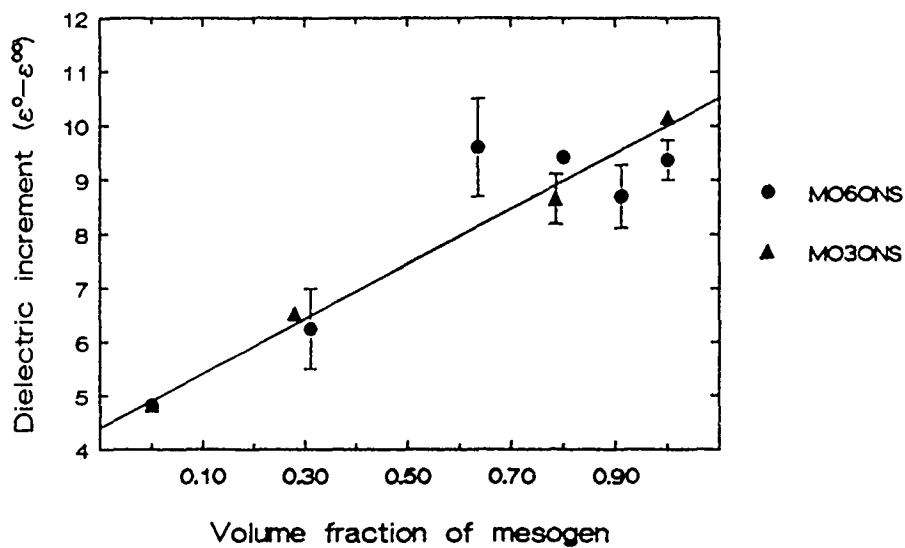


Figure 4. The Dielectric Increment for MO3ONS and MO6ONS Copolymers.

It can be seen that, though scattered, the results follow a similar pattern to that seen in figures 1 and 2. The TSC method would appear to be the better way of obtaining the data, however.

As initially reported last year, a progressive reduction in the β relaxation peak with increased mesogen concentration (not shown) is found. The anti-parallel pairing of the mesogens would appear to suppress the motions involved in this relaxation and thus cause the brittle nature of all but the 10% copolymer films. The previously reported decay of the pyroelectric coefficient with time, also correlated with the β relaxation, has been shown by direct measurement to be caused by the decay of polarisation. Again the homopolymer decays more slowly than PMMA.

IR Spectra

Additional evidence of a concentration dependent interaction between the mesogens is found when the NO_2 symmetric stretch absorption peak at 1340 cm^{-1} is compared for the 10% and 30% MO6ONS copolymers. A shoulder in this absorption peak is seen to increase with dipole concentration, a finding reported by Hoechst-Celanese³ who interpret it as a splitting of the NO_2 symmetric stretching band by interactions between paired mesogens.

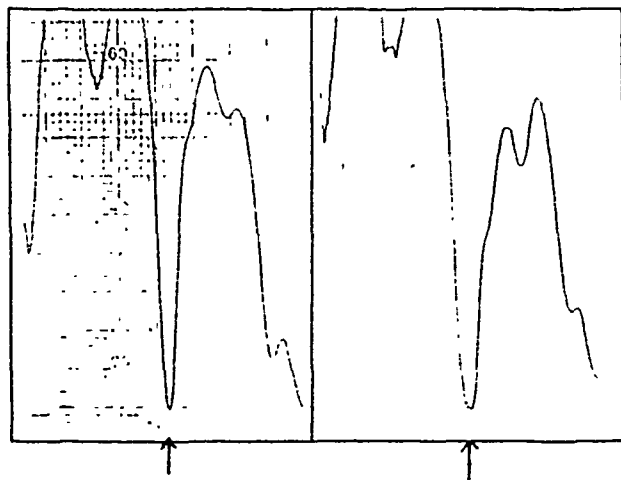


Figure 5. IR Transmission spectra showing the symmetric stretch at 1340 cm^{-1} . Left, 10% MO6ONS, Right, 30% MO6ONS

CONCLUSIONS

The subject of dipole interactions in side chain polymers has been extensively discussed. We believe that these three independent experiments show data which, for the first time, indicates a discontinuity in properties of the MO6ONS copolymers which coincides with the appearance of liquid crystal behaviour. Two of these experiments also show the tendency towards saturation exhibited by both the MO3ONS and the MO6ONS copolymers at volume dipole concentrations above 50%. This finding has in fact been reported by Amano⁴ in measurements of NLO properties in similar side chain polymers.

Clearly, it would be desirable to discover NLO moieties which do not tend to align in this anti-polar fashion. The donor-acceptor structure automatically leads to highly dipolar entities, however, which will always tend to anti-parallel alignment in the absence of specific steric interactions. Liquid-crystalline behaviour does not appear to be necessary or even desirable since it has not proved possible to exploit the theoretically better alignment obtainable in the LC phase.

References

1. Jarvis, Hutchinson, Bower and Ward. *Polymer*, (1980), 21, p41
2. Windle. Private Communication.
3. Refalko. Multifunctional Materials Report. Hoechst-Celanese.
4. Amano and Kaino. *Mol.Cryst.Liq.Cryst.* (1990), 182A, p81

CHARACTERISATION AND KINETICS OF ELECTRIC FIELD ALIGNMENT OF POLY(MO_xONS-CO-MMA)

R.B. FINDLAY and A H WINDLE

Department of Materials Science and Metallurgy, University of Cambridge,
Pembroke Street, Cambridge CB2 3QZ, UK

INTRODUCTION

Last year we reported that poly(MO6ONS) can be aligned by alternating electric fields, and characterised the aligned texture. We have extended our study to monitor alignment in a c/d.c. fields using a new optical technique, both during cooling and at constant temperature.

New materials, poly(MO5ONS) and poly(MO4ONS), were recently synthesised at Hoechst-Celanese, and we have successfully aligned them in alternating electric fields and characterised them using several techniques. Poly(MO5ONS) has some unexpected properties, and may be of interest in the quest for a NLC device material.

Wide angle X-ray diffraction data from unoriented samples of the poly(MO6ONS-co-MMA) copolymer series indicate that the side groups are segregated in compositions richer in side groups than 70/30. Although perhaps not surprising for these smectic samples, the possibility of segregation in the 50/50 material, which showed no a.c. alignment, is of particular interest.

KINETICS OF ALIGNMENT OF POLY(MO6ONS)

An optical technique (see Figure 1) has been used to study the kinetics of alignment of the homopolymer poly(MO6ONS) in electric fields, and to investigate the possibility of pretransitional effects. The technique measures the intensity of light transmitted at an angle to the normal by the sample (the *clarity*) and the intensity transmitted between crossed polars at an equal angle to each polar (the *recorded interference intensity*); the recorded interference intensity is then corrected for scattering by dividing it by the clarity to calculate the *normalised interference intensity*. A series of interference fringes is seen during constant-cooling alignment, which corresponds well, but not exactly, with the number of fringes seen on the conoscopic image of the resulting cold sample. The onset of alignment is accompanied by a fast change in the clarity, so it is possible that fringes may be obscured by this. The number of fringes (often difficult to count) is found to be broadly proportional to the sample thickness.

The previously reported threshold voltage was confirmed, and it is found that all voltages above the threshold cause similar degrees of alignment. Clarity is a crucial issue, and there are several ways to improve it. First, it is noted by Coates *et. al.*¹ that when the Balzers ITO glass is baked to fully oxidise the coating, the surface becomes much smoother. We have noted informally that the clearest samples used baked ITO, suggesting that much of the opacity is due to surface undulations. Second, the sample is only fully clear in those regions in which there was flow during melt pressing, implying that backbone prealignment is important for good smectic A monodomain formation. Finally, annealing the aligned texture a few degrees below the clearing point reduces the defect density, markedly improving the clarity (by eye). This may be due to crystal growth: an unaligned sample annealed in the biphasic region displays contains needle-shaped birefringent entities which have extinction angles at 30° to their long axes.

The biphasic region appears to be thermodynamically stable, and the interference fringes are seen over the same temperature interval regardless of the cooling rate (Figure 2). The fringe pattern repeats itself in reverse on reheating, regardless of whether an electric field is applied or not (Figure 3).

Most work has concentrated on a.c. alignment while cooling from the isotropic to the smectic phase, although alignment at constant temperature in the biphasic region has also been studied. In strong a.c. fields there is some evidence of a small pretransitional effect, visible by eye as a faint birefringent area where the field bulges at the edge of the ITO coating, however, direct measurements in uniform fields using the optical technique have not revealed any evidence of pretransitional effects.

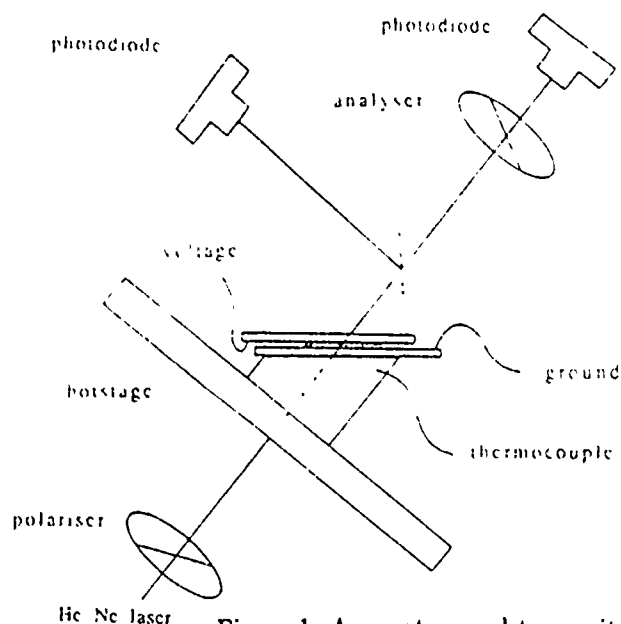


Figure 1: Apparatus used to monitor alignment kinetics.

In d.c. fields there is a pretransitional electrohydrodynamic instability which is detected close to the smectic-isotropic transition (Figure 4). When d.c. and a c. fields are applied together (Figure 5), the d.c. field has the effect of reducing the clarity of the final sample, but apparently without otherwise affecting the alignment process; these results are complicated because the effects of scattering on the measurements are not well understood. The d.c. field does induce some polar alignment in the material despite the stirring, and a small (70 fm/V - 300 times weaker than lithium niobate) second order non-linear optical coefficient was measured.²

OTHER POLY(MO_xONS-CO-MMA) MATERIALS

Poly(MO5ONS), recently synthesised at Hoechst-Celanese, is a smectic A with a layer spacing of 30 \AA , and a large, broad lower angle X-ray peak corresponding to a spacing of 49 \AA (Figure 6). DSC confirms optical observations of a clearing point at 166.9°C on heating and 161.1°C on cooling (extrapolated to zero heating/cooling rate), with an enthalpy of transition of 3.05 J/g . T_g is at 63.1°C (on heating at 20°C/min). It is an interesting material, as it has a large supercooling, a wide biphasic region and a very high threshold field for alignment in alternating electric fields ($17.6 \text{ V}/\mu\text{m}$ on cooling at 1°C/min , compared with $2.8 \text{ V}/\mu\text{m}$ for poly(MO6ONS)). The broad low-angle X-ray peak may indicate that much of the sample is not interdigitated.

Poly(MO4ONS), also recently synthesised, is a liquid crystal of unknown phase type. It is rubbery, and could not be melt-pressed into thin, parallel-sided samples. It aligns in alternating electric fields to form a clear texture, but shows no sharp X-ray peaks due to smectic layers (on either meridional scans or flat-film photographs).

Conoscopy was not possible due to the high level of birefringence (probably due to stress in the rubbery sample). DSC confirms optical observation of a clearing point of 151.8°C on heating and 151.6°C on cooling (extrapolated to zero scanning rate), with an enthalpy of 0.57 J/g . T_g is at 92.9°C (on heating at 20°C/min). It was not possible to measure the threshold voltage because of the sample preparation problem, but it seems to be far easier to align than poly(MO5ONS).

A sample of poly(MO6ONS_{0.7}MMA_{0.3}) which had been aligned in an alternating electric field showed no smectic layer peaks (on meridional scans or flat-film photographs), although conoscopy confirmed strong positive uniaxial alignment. The threshold field at 1°C/min is $8.5 \text{ V}/\mu\text{m}$.

0 °C/min

1 °C/min

10 °C/min

Figure 2: Cooling at different rates. 85 μm sample, 800 V, 3.33 kHz.

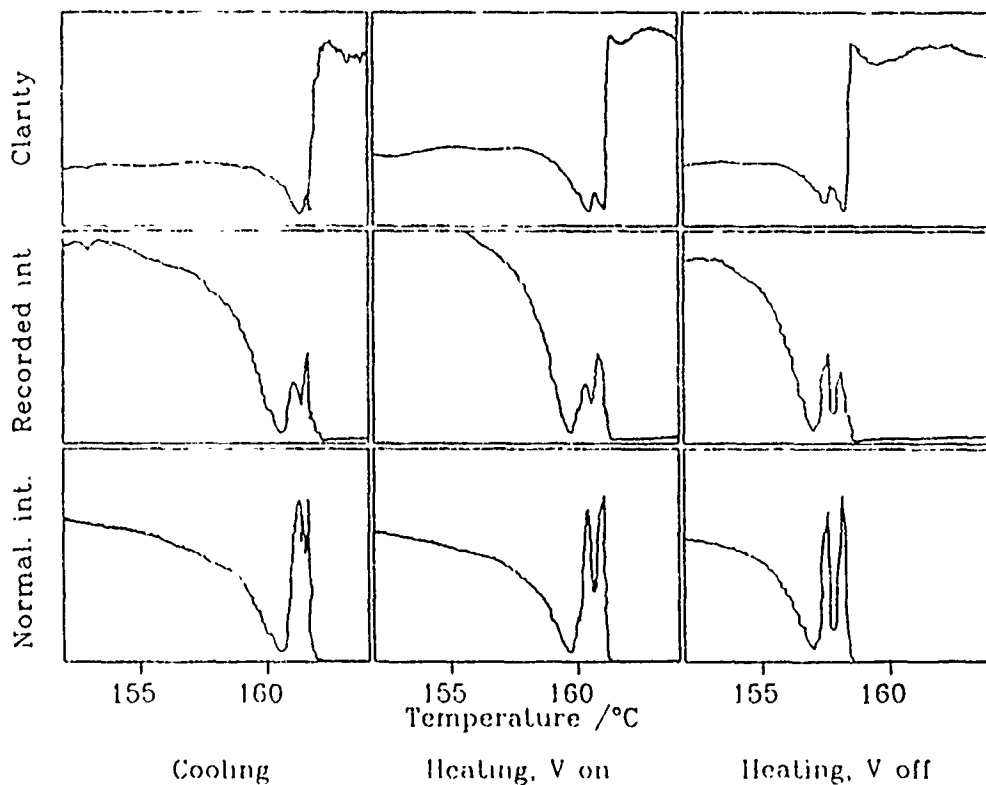
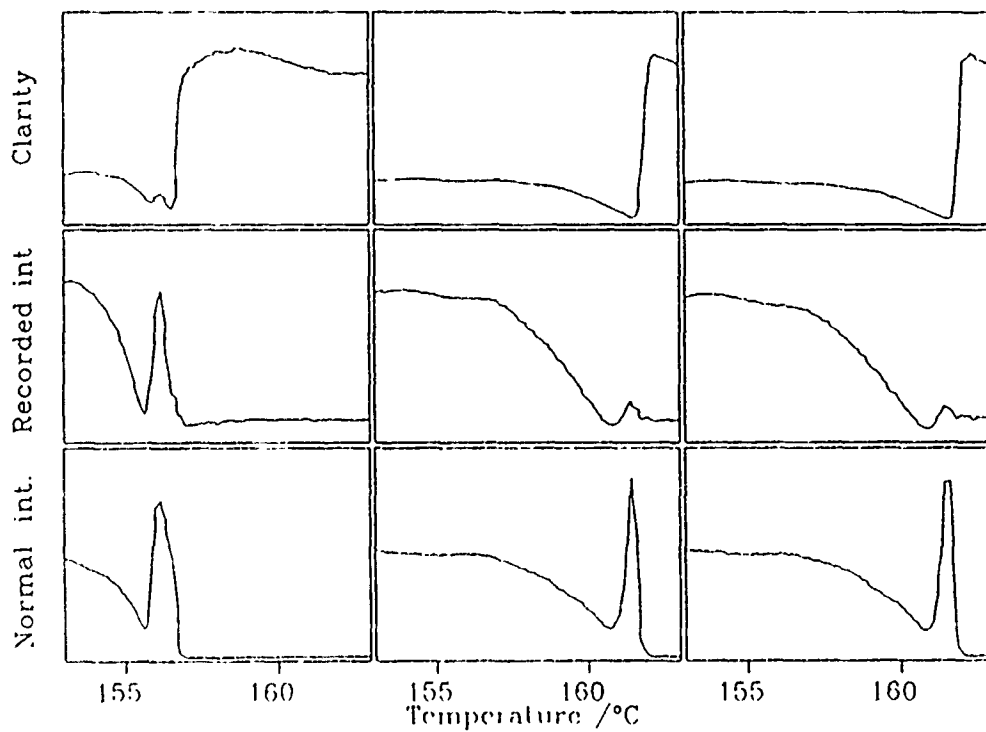


Figure 3: Reversibility of the alignment 77 μm sample, 800 V, 3.33 kHz, 10 $^{\circ}\text{C}/\text{min}$.



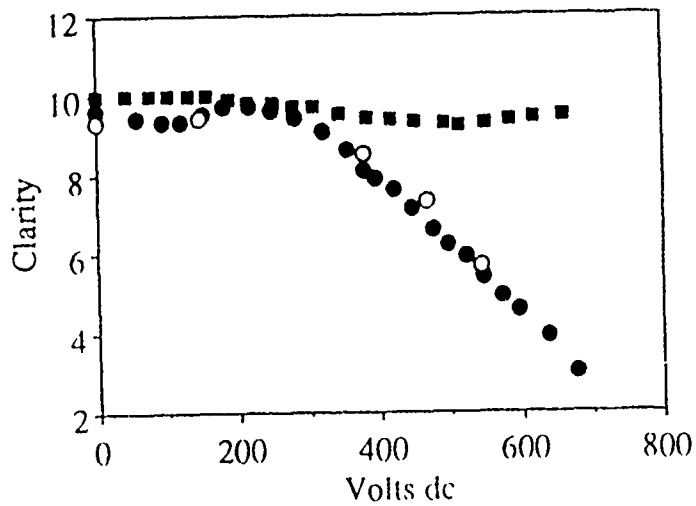
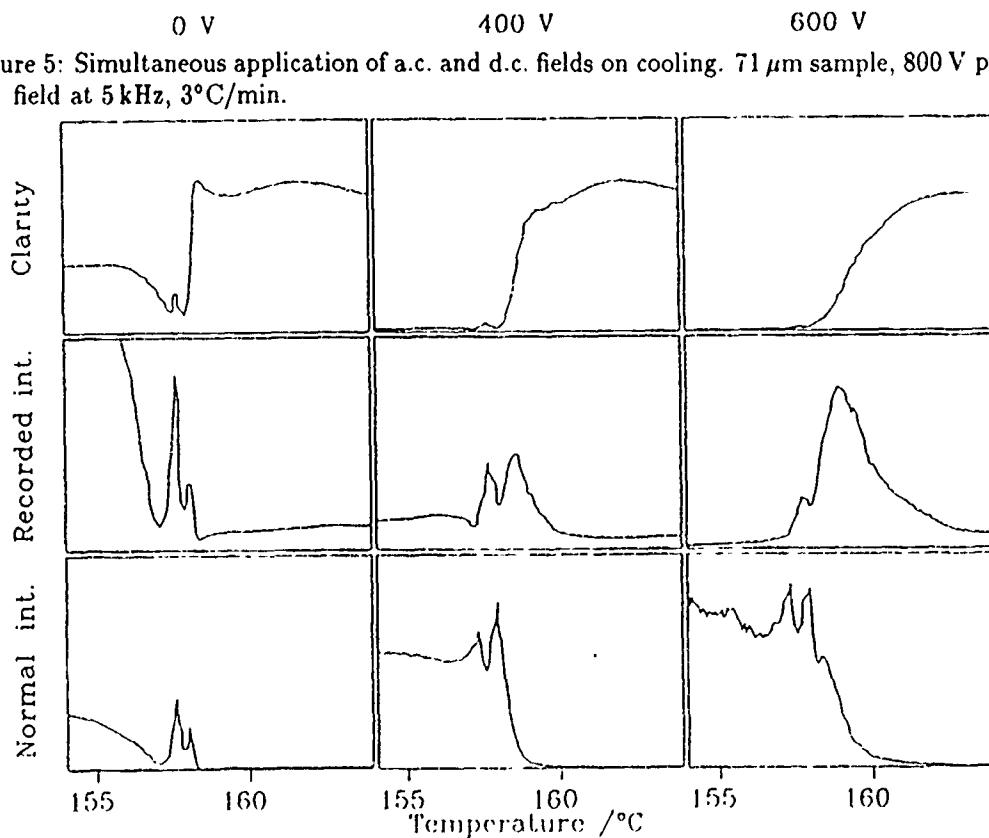


Figure 4: Dependence of clarity on d.c. voltage at 6.5°C (top curve) and 10°C (lower curve) above the transition temperature. (closed circles are on increasing the voltage, open circles are on reducing voltage, to show reversibility). 71 μm sample.

Figure 5: Simultaneous application of a.c. and d.c. fields on cooling. 71 μm sample, 800 V peak-peak a.c. field at 5 kHz, 3°C/min.



WAXS ANALYSIS OF POLY(MO6ONS-CO-MMA) COPOLYMERS

A careful study of unaligned polymers, using samples of the same size and corrected for weight differences, has shown that the MMA-rich members of the series are not segregated. Figure 7 compares experimental and results simulated on the basis of assumed segregation (calculated by adding the homopolymer and PMMA results in the appropriate ratios). High-temperature experimental results are included to allow comparison between the simulated results and samples which are at too high a temperature to be segregated simply by being smectic.

The lack of agreement between simulation and experiment in the poly(MO6ONS_{0.3}MMA_{0.7}) sample and those with lower concentrations of active groups, suggests that segregation does not occur in these cases. Mixed amorphous systems are difficult to model, however, and the question remains open.

The evidence for segregation in the poly(MO6ONS_{0.5}MMA_{0.5}) sample suggests that it would be better classed alongside the liquid crystalline members of the series (the two MO6ONS-rich members), which correlates with recent property measurements by Leeds University. However, attempts to a.c. align the 50/50 material have failed, with no evidence of homeotropy in the optical experiment described above, or in a WAXS experiment to detect alignment.

CONCLUSIONS

Detailed studies of the poly(MO6ONS) material have shown that a.c. fields applied on cooling through the isotropic-smectic transition give excellent alignment and clear smectic monodomains. There was no detectable pretransitional effect in a.c. D.c. fields gave significant pretransitional alignment (and instability stirring) but no smectic monodomains after cooling through the transition. The evidence is that the smectic phase is interdigitated and this militates against poling fields. This conclusion provides a structural explanation for the detailed properties measurements of the Leeds group.

Preliminary data on poly(MO4ONS) and poly(MO5ONS) show less evidence for interdigitation, and future studies may reveal structures which will enhance, rather than oppose, polar ordering.

The work suggests that radical changes in the method of attachment of the active group to the backbone could be advantageous, and the molecular design collaboration with the Hoechst Celanese group will explore these possibilities.

ACKNOWLEDGEMENTS

We would like to thank Hoechst-Celanese for funding and for much support, and particularly Tony East for synthesising the materials, and Ilmar Kalnin for electro-optic expertise; also the Science and Engineering Research Council, and Lt. Col. Chester Dymek of the US Air Force Office of Scientific Research for funding. We are indebted to Keith Page in our department for electronics support.

REFERENCES

1. D. Coates, W.A. Crossland, J.H. Morrissy and B. Needham, *J. Phys. D: Appl. Phys.* **11**, 2025-2034 (1978)
2. by Simon Martin, Cavendish Laboratory, University of Cambridge.

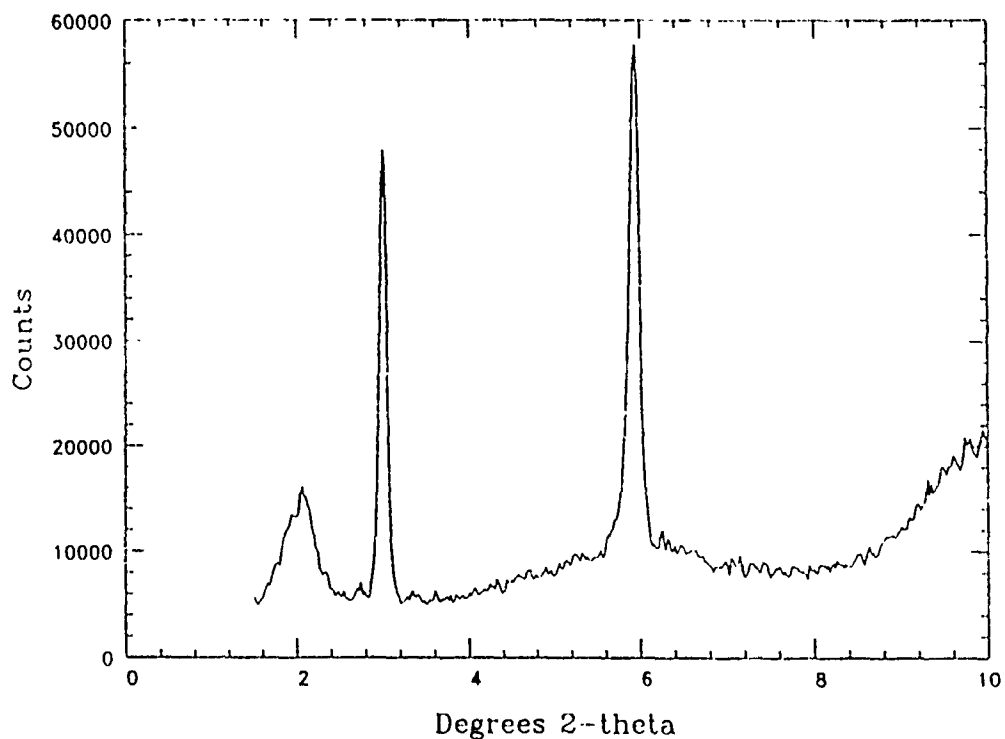


Figure 6: Meridional WAXS pattern of aligned poly(MO5ONS), using $\text{CuK}\alpha$ radiation.

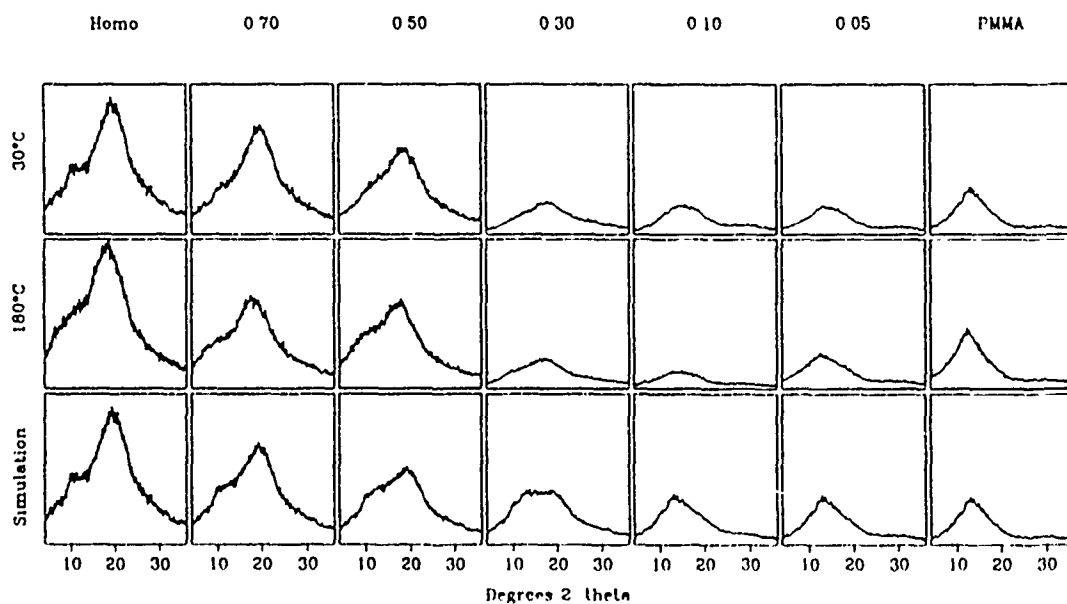


Figure 7. Experimental WAXS data, corrected for sample mass, at 30°C and 180°C, and simulated WAXS at 30°C. (180°C data unreliable for the 10% material, as the sample curled when heated)

Three Dimensional Packing Problems Associated with Molecular Materials

D. Michael P. Mingos
Inorganic Chemistry Laboratory
University of Oxford
South Parks Road, Oxford OX1 3QR

Introduction

The development of molecular electronics depends not only upon the synthesis of molecules with the desired physical properties but also on the way in which these molecules pack in the solid state. In recent years co-ordination and organic chemists have used their synthetic skills to synthesise donor-acceptor combinations which would result in the following bulk properties :

1. Organic metals and superconductors

The most dramatic advances have been obtained when sulphur based planar conjugated donor molecules have been combined with organic or inorganic anions which may function as acceptors. This has led to conducting metals and in some cases superconductors, although the transition temperatures are not as dramatic as those recently established for ceramic high temperature superconductors.

2. Non-linear optical materials

Following on from the successful design of non-linear optical materials based on conjugated organic molecules considerable work has been done on the development of chromophores based on inorganic and organometallic compounds. In our own laboratories we have concentrated on co-ordination compounds based on pentadionate ligands and carboranes. Although molecules with large changes in dipole moment between the ground and excited states may be successfully made the requirement that the molecules crystallise in a non-centrosymmetric space group is not generally easy to engineer.

3. Molecular ferromagnets

Ferro-, meta- and antiferromagnetic materials based on organometallic donor-acceptor molecules have attracted considerable attention in recent years. All these compounds contain chains of alternating donors and acceptors and the difference in magnetic properties depends on the metals present, their spin states and also the size and shape of the co-crystallising anion.

In all of these areas the structures of the individual molecules and their synthesis can be predicted from well established chemical principles. The manner in which these molecules come together in the crystallisation process is not very well understood and certainly the packing modes in the solid state are not currently governed by a set of simple structural principles. This arises, of course, from the rather weak and non-directional nature of the van der Waals' and coulombic interactions between the molecules in the solid state. As part of our general programme into the design of inorganic and organometallic materials which display non-linear optical and ferromagnetic interactions we have initiated a theoretical programme designed to understanding the packing of such molecules in the solid state.

The analysis starts with the definition of size and shape parameters for organic and organometallic ions of interest to the development of non-linear optical materials. The

relevant structural parameters are the molecular volume, surface area and moments of inertia. From the volume an effective radius of the ion may be calculated if the ion is approximately spherical.

The effective radii serve as a basis for a set of radius ratio rules which define the primary co-ordination numbers of the cations and anions in the structure. The moments of inertia represented graphically as ellipsoids then provide an estimate of the non-regularities of the structures. In the molecular salts illustrated in Figures 1 and 2 the radius ratios suggest co-ordination numbers of six and the sodium chloride and nickel arsenide structures are indeed adopted. The nickel arsenide structure is also adopted in the molecular salt illustrated in Figure 3, however when the same salt is crystallised from acetone a layer structure results with the acetone molecules forming distinct layers. The ions in these salts are not perfectly spherical and their shapes can be better represented as ellipsoids. The resulting co-ordination sphere based on ellipsoids shown in Figure 5 provides a basis for understanding the distortions in the structure from the idealised NaCl and NiAs structures. The analysis is completed by specific calculations of the van der Waals' and coulombic interactions in the solid state. The results of such an analysis are summarised in Figure 6 for a range of molecular salts. It is noteworthy that as the ions become larger the coulombic interactions diminish, but are effectively replaced by matching van der Waals' interactions leading to an approximately constant total lattice energy.

Design of Molecular Ferromagnets

Joel Miller of Central Research at Du Pont characterized in 1987 a ferromagnetic interaction in the organometallic donor-acceptor complex of decamethylferrocenium tetracyanoethenide, which was obtained from $\text{Fe}(\text{C}_5\text{Me}_5)_2$ and tetracyanoethylene. The crystal structure of an acetonitrile solvate (Figure 7) consists of alternating metallocene and TCNE units with an Fe-Fe separation along the chain of 10.52Å. [TCNE] lies between essentially parallel Me_5C_5 rings.

All the magnetic data are consistent with a strong coupling of spin 1/2 systems associated with the donor and acceptor ions along the chain in a ferromagnetic fashion. The ferromagnetic chains are weakly coupled at the scale of the crystal lattice again in a ferromagnetic fashion. The compound therefore exhibits bulk ferromagnetism with a spontaneous magnetization below $T_c = 4.8\text{K}$. Miller have attributed the ferromagnetic interaction to McConnell's mechanism, however Kahn has raised severe objections to the mechanism.

In order to resolve some of the questions associated with the mechanism we have recently synthesised and characterised some donor-acceptor complexes based on decamethylferrocene cations but with transition metal carborane anions. These combinations provide a much wider range of possibilities for testing the mechanism than the Miller compounds because the anions can also have a range of spin states. A typical synthesis and structure is shown in Figure 8. The measurement of magnetic properties is still at an early stage but preliminary results suggest that the model is not sufficiently general to cover this class of compound.

Summary

The research described in these paper has attempted to provide a more rational basis for understanding the structures of molecular salts in the solid state. The general features can be understood using simple concepts derived from the size and shape characteristics of the ions. Future work will attempt to find methodologies for predicting the more subtle aspects of the structures. The synthesis of the new donor acceptor complexes based on metallocenes and sandwich carborane anions should provide a better test of the current models for designing molecular ferromagnets.

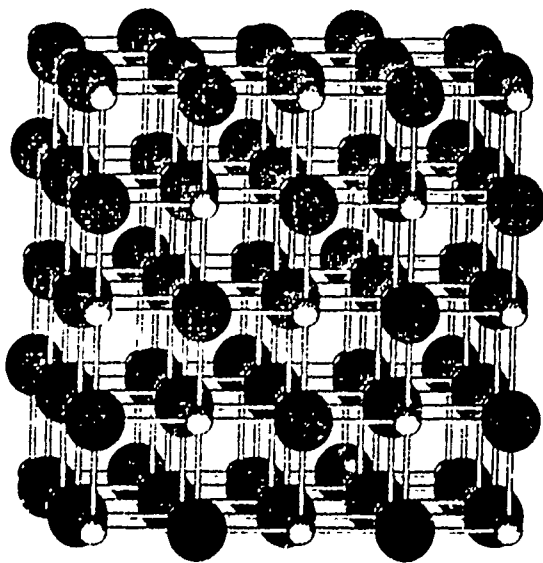
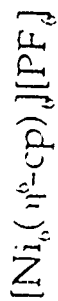


Figure 1

The space of the cation is very spherical and therefore the structure is very close to the NaCl structure.

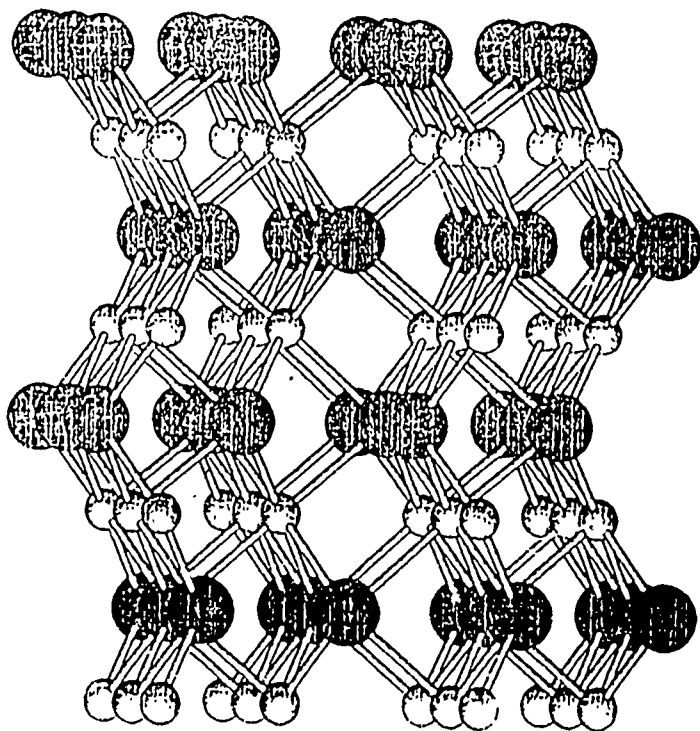
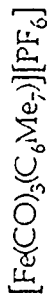


Figure 2

This salt adopts the anti-nickel arsenide structure based on the relative sizes of the cation and anion this is correct. The non-spherical nature of the cation lead to distortions away from the ideal structure.

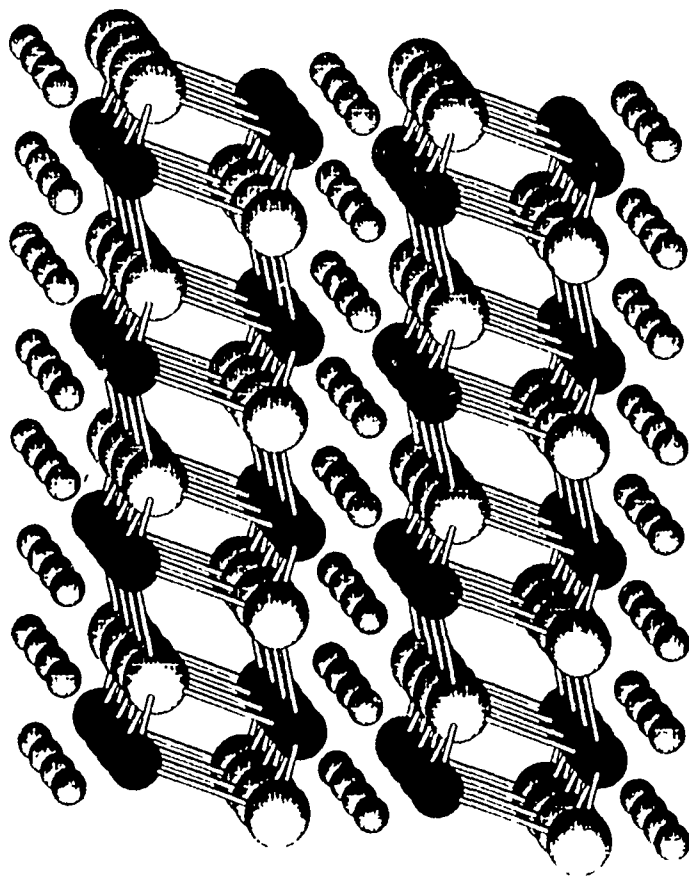
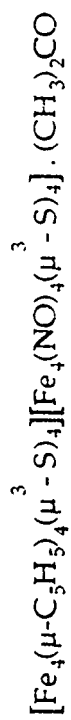


Figure 4

The presence of solvent molecules of acetone leads to a distortion of the nickel arsenide structure into 3 layer structure with the acetone molecules occupying complete layers.

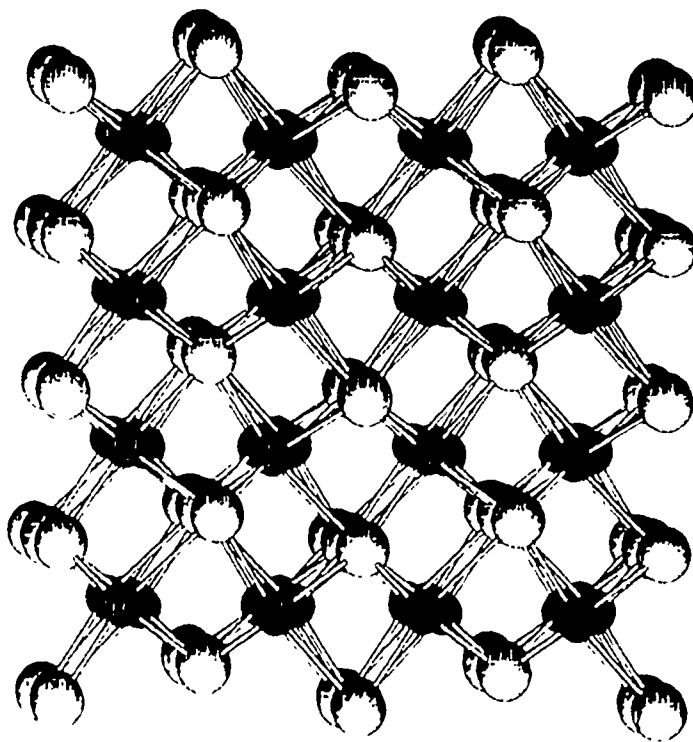


Figure 3

Fe²⁺ salt adopts the anti-nickel arsenide structure.

Figure 6

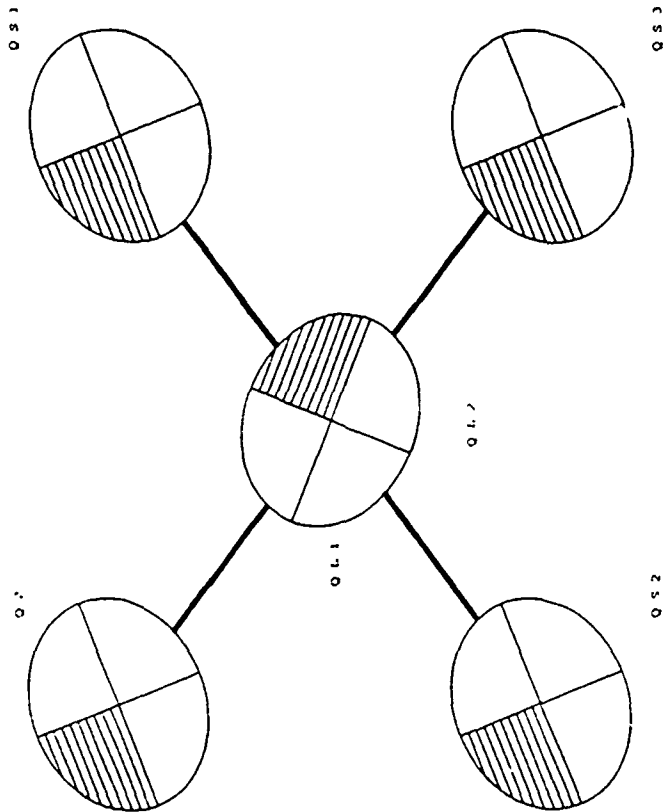
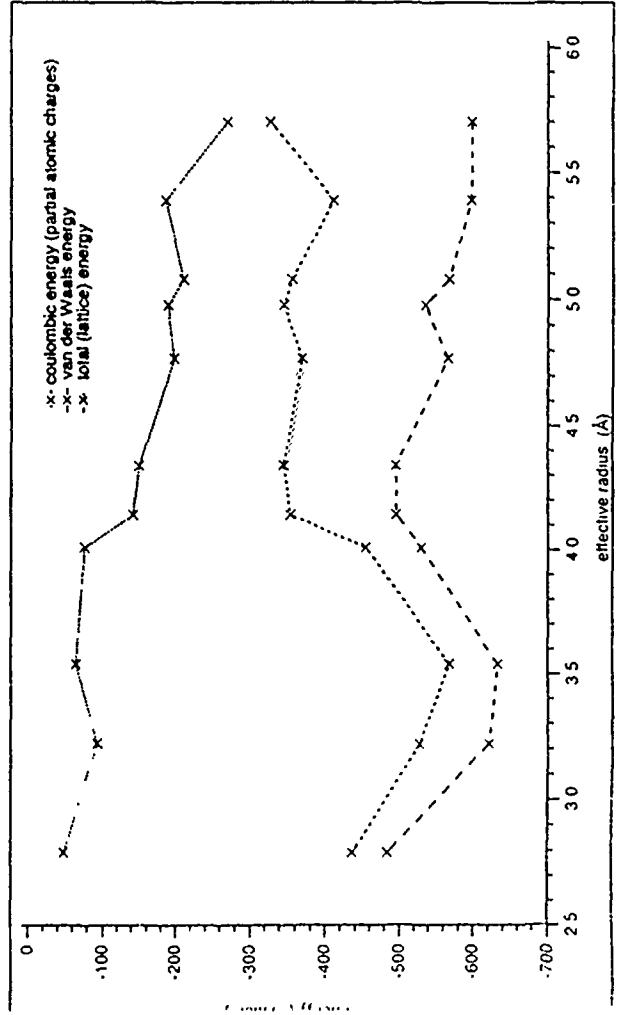
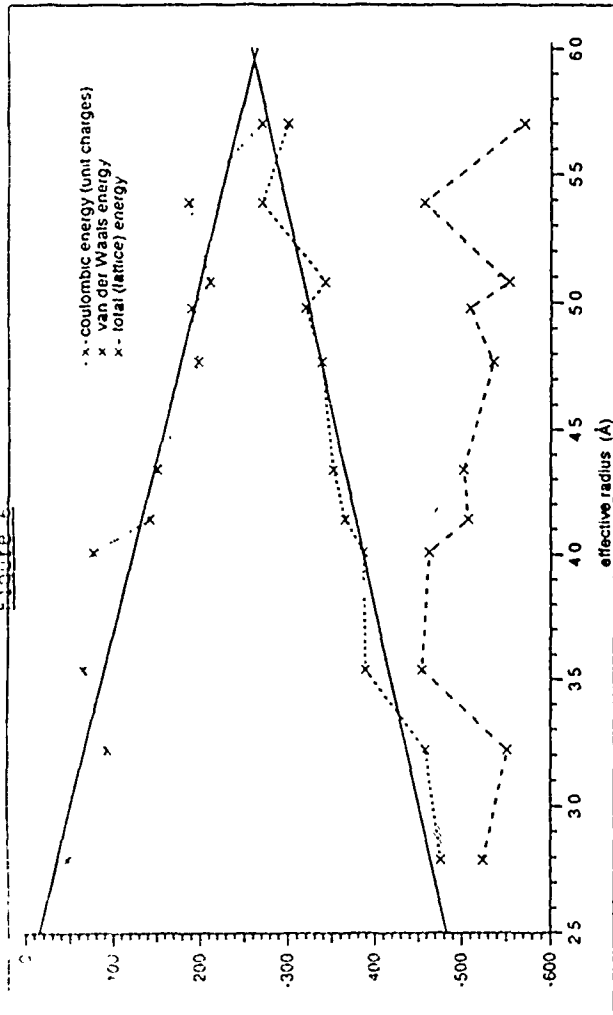


Figure 5

Illustration of the manner in which the shape ellipsoids can be used to account for the structural distortions in the structure and the relative orientations of the ions.

Acknowledgements

Andrew Rohl completed the theoretical studies on the molecular salts and Jennifer Forward did the magnetic and synthetic work on the new molecular salts based on carboranes. The SERC and AFOSR are thanked for financial support.

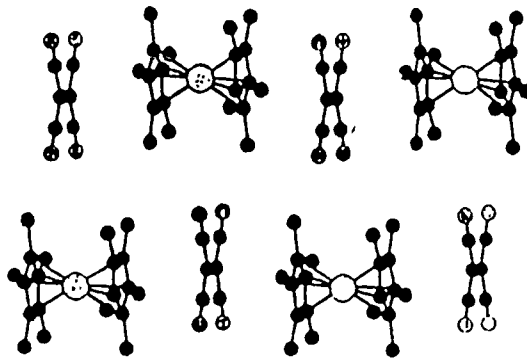
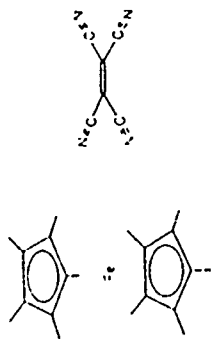


Figure 7

Structure of a molecular ferromagnet based on $\text{Fe}(\text{C}_5\text{Me}_5)_2$ and TCNE

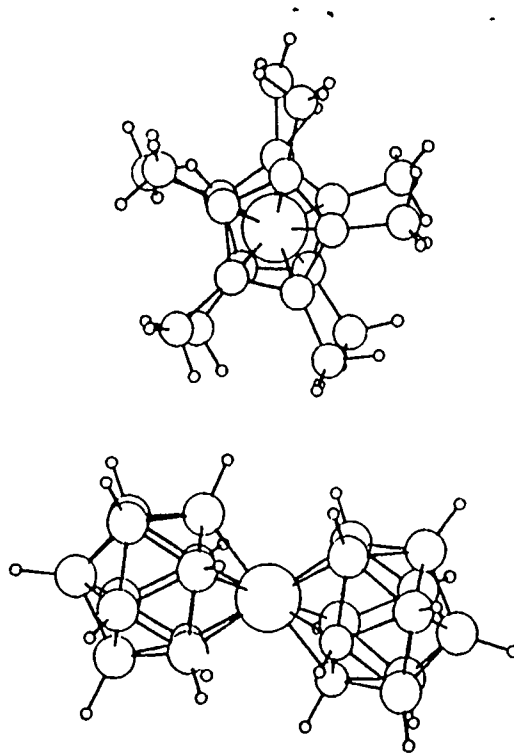
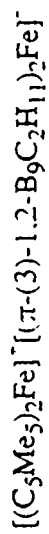
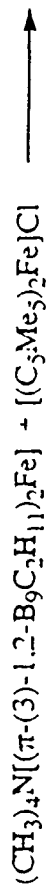


Figure 8

Synthesis and structure of the novel charge transfer salts involving organometallic and carborane sandwich compounds.

Progress Report, 1990-1991

Semiconductor Quantum Dot Materials

Principal Investigator: Professor John D. Mackenzie, UCLA

Ph. D. Student: Chia-Yen Li

Collaborator: Professor Masayuki Yamane, Tokyo Institute of Technology

1. Background

The NLO properties of these semiconductor-glass composites (SGC) have been widely studied since 1983 [1]. Because the small size of the semiconductor crystals is on the order of the size of exciton, one may utilize the quantum size effects to preserve the exciton at room temperature to enhance nonlinearity [2-4]. CdS and CdS_xSe_{1-x}-doped filter glasses have been observed to exhibit a large $\chi^{(3)}$ of 10^{-9} esu to 10^{-8} esu [1]. Time-resolved measurements of experimentally prepared CdS SGC samples show that the population relaxation time is 300 fs for a 30 Å sample and 500 fs for a 44 Å sample [5]. In addition to large nonlinearity and fast switching speed, the isotropic character of these materials make them suitable candidates for use in optical switching applications.

The high temperature processes used in conventional glass fusion methods have three main disadvantages: (a) the solubility of the semiconductor components are limited to only a few weight percent; (b) the compositions of the final product are difficult to control because of the different vapor pressure of various species in the melt; and (c) the chemical modification of the semiconductor microcrystallites is extremely difficult. The sol-gel process to prepare semiconductor-doped glasses is superior to the conventional melt-quench method, since the size and the amount of semiconductor dopant can be better controlled. The sol-gel method can also give glasses with new compositions, high purity and good homogeneity at temperatures significantly lower than those required by the melting method [5-10]. A low temperature route based on sol-gel method to obtain these quantum-dot materials has been explored in our project.

Research Objectives

- (a) Prepare glass-semiconductor nanocomposites with high $\chi^{(3)}$ at room temperature.
- (b) Develop an understanding of how fabrication processes affect the final size, size distribution, composition and crystal structure of semiconducting microcrystallites.
- (c) Determine experimentally the relation between non-linear optical properties and nanostructure of

quantum dots in semiconductor-oxide nanocomposites as a function of the matrix chemistry.

(d) Understand the interplay between quantum confinement effects arising from the nanostructure of the semiconductor clusters and the structure of matrices.

2. Research Progress

(A). Fabrication of semiconductor-oxide nanocomposites by the sol-gel process

Various methods of obtaining semiconductor-oxide nanocomposites have been studied. Two different matrix systems were investigated to prepare these nanocomposites. In the first multicomponent silicate glass system, the sols containing Cd^{2+} were prepared by adding aqueous solution of Cd salt and sodium acetate to the methanol solutions of partially hydrolyzed mixture of tetramethylorthosilicate and boron ethoxide. Gelation of the sols was accomplished by ultrasonic agitation. The obtained gels were heat-treated at around 430°C to decompose the remaining organics and, subsequently, expose to a H_2S stream to sulfidize CdO in the heat-treated gel. The CdS-doped porous glasses were fully densified at a temperature as low as 550°C .

The second type of matrix used was organically modified silica (Ormosils). Part of the bridging oxygen bond in ormosils were replaced by alkyl groups by adding 10 wt.% of polydimethylsiloxane (PDMS) into a tetraethylorthosilicate (TEOS) alcohol solution. Cadmium salt was then incorporated into the sol solution. The resulting ormosils were highly transparent. The organic groups present decrease the risk of fracture on drying. After heat treatment at 300°C , Cd^{2+} containing Ormosils samples were reacted with H_2S . CdS microcrystallites were then formed well within quantum confinement size range.

Fig. 1 shows the CdS semiconductor-oxide nanocomposites prepared by the methods described above.

(B). Characterization of the semiconductor-oxide nanocomposites

Ormosils derived from polydimethylsiloxane (PDMS) and tetraethoxysilane (TEOS) show high optical transparency and enhanced mechanical properties which allow cutting, grinding and polishing prior to heat-treatment. Disc samples with diameters of 1 inch have been routinely prepared in our lab. An equivalent CdO concentration up to 20 wt.% has been achieved and the quantum confinement effects are clearly shown in Fig. 2 where the peaks of the samples with smaller particles are shifted toward shorter wavelengths. Ormosils also provide an advantage to prepare high quality films with enough thickness by spin coating for waveguide device applications. The thickness of spin coated single layer Ormosils is two to three times higher than that in normal sol-gel process. The Ormosils used are thermally stable up to 340°C which is

higher than normal integrated circuits processing temperatures. X-ray diffraction (XRD) patterns of the CdS-doped Ormosils shows the CdS crystallites have a hexagonal wurtzite structure.

The CdS crystal structure in fully densified sodium borosilicate glass is the same as in the Ormosils. The pore free glass by sol-gel process contains CdS up to 8 wt.%. The average microcrystallite diameter observed by transmission electron micrograph was in the range of 25 Å to 42 Å. Fig. 3 shows the CdS crystallites with an average size of 35 Å were monodispersed in glass matrix.

(C). Nonlinear optical characterization

Preliminary DFWM experiments of CdS-doped Ormosils by using 25 ps pulsewidth YAG laser at 532 nm showed that the damage threshold is higher than 2 GW/cm². As shown in table 1 and Fig. 4, The off-resonance $\chi^{(3)}$ values are on the range of 10⁻¹³ to 10⁻¹¹ esu, and the relaxation time is less than 25ps (laser limit). The $\chi^{(3)}$ values can be enhanced by resonance conditions as the laser wavelength was tuned to the bandgap of semiconductor microcrystallites. The $\chi^{(3)}$ value as high as 6.3x10⁻⁷ esu at wavelength 460nm was measured by the DFWM technique with a 7 ns laser pulsewidth for the CdS-doped sodium borosilicate glass (see table 2).

3. Future Plans

- (a) Improve Ormosils transparency through chemistry.
- (b) Improve semiconductor crystal quality through heat-treatment and chemistry.
- (c) Investigate the relationships between the particle sizes (also the size distributions) and the processing parameters.
- (d) Correlate the relationships between the optical properties and the semiconductor microcrystallite size.
- (e) Conduct femtosecond DFWM experiments to determine the transient behavior of these quantum-dot materials.
- (f) Study the frequency dependence of the third-order nonlinear properties by using tunable dye laser.
- (g) Fabricate and test nonlinear optical device made of the quantum-dot materials by sol-gel processing.

Reference

1. R. K. Jain and R. C. Lind, J. Opt. Soc. Am., 73 (1983) 647-653.
2. Research on Nonlinear Optical Materials: An Assessment, Appl. Opt. 26 (1987) 211-234.

3. Research Opportunities on Clusters and Cluster-assembled Materials - a panel report, *J. Mater. Res.*, 4 (1989) 704-736.
4. M. L. Steigerwald and L. E. Brus, *Annu. Rev. Mater. Sci.*, 19 (1989) 4471-495.
5. N. Peyghambarian, S. W. Koch, H. M. Gibbs, H. Huang, *Nonlinear Optics and Optical Computing*, Ed. by S. Martellucci and A. N. Chester, Plenum Press, New York 1990 99-116.
6. C. M. Bagnall and J. Zarzycki, *SPIE Proc.*, 1328 (1990) 108-118.
7. M. Nogami, M. Watabe, K. Nagasaka, *ibid*, 119-124.
8. M. Nogami, K. Nagasaka, E. Kato, *J. Am. Ceram. Soc.*, 73 (1990) 2097-2099.
9. M. Nogami, Y. Zhu, Y. Tohyama, K. Nagasaka, T. Tokizaki, A. Nakamura, *J. Am. Ceram. Soc.*, 74 (1991) 238-240.
10. N. Tohge, M. Asuka, T. Minami, *SPIE Proc.*, 1328 (1990) 125-132.

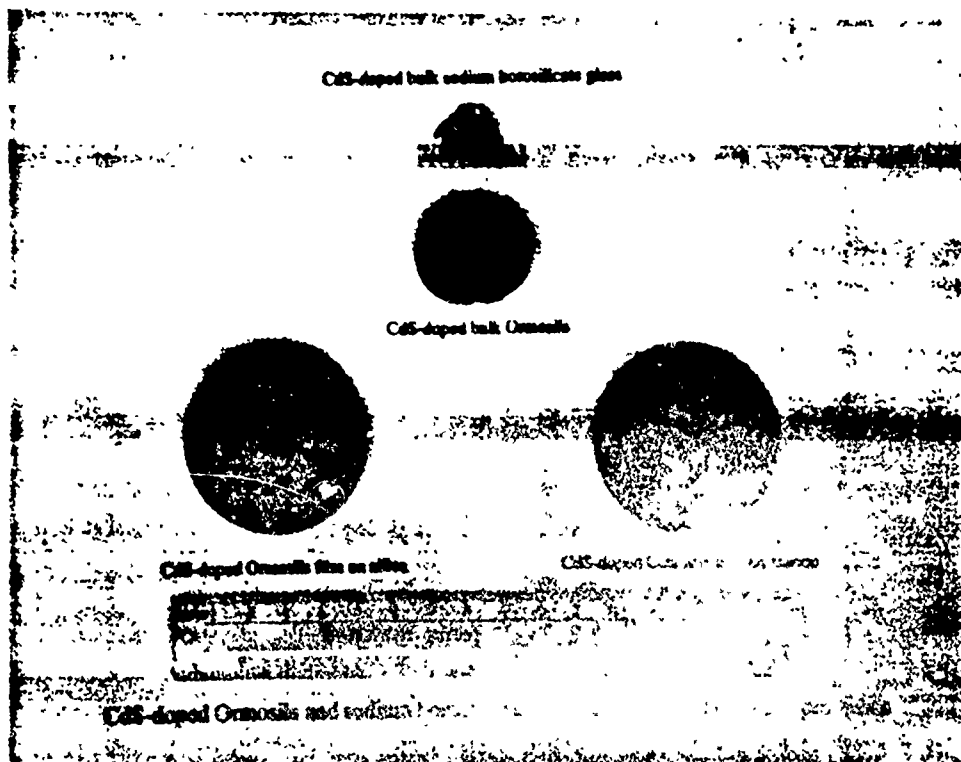


Fig.1 CdS-doped Quantum-dot composites by sol-gel methods.

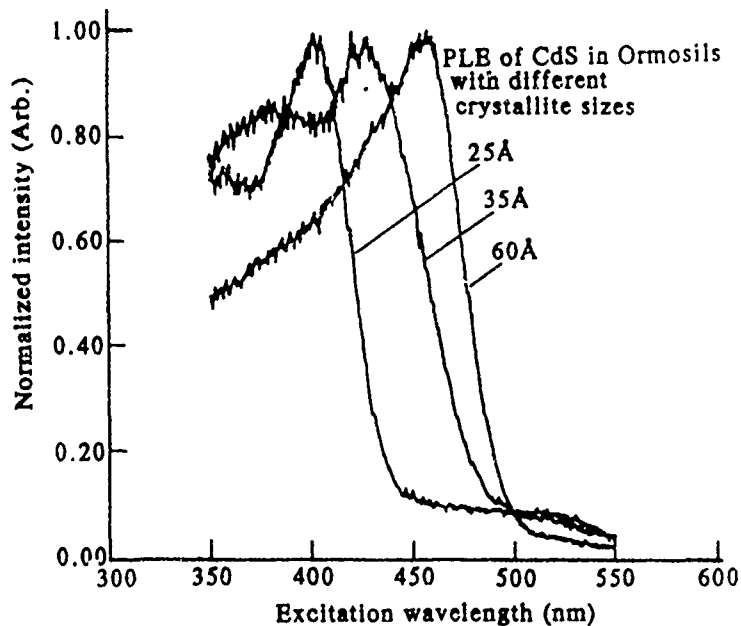


Fig. 2 Photoluminescence excitation (PLE) spectrum of CdS-doped Ormosils with different crystallite size of 60Å, 35Å and 25Å. The photoluminescence from the samples was monitored at 680nm, 4.2K. The position and width of the peaks can be used to correlate particle size and particle size distribution. CdS concentrations are 0.9 wt.% for 25 Å sample and 2.7 wt.% for 35Å and 60Å samples.

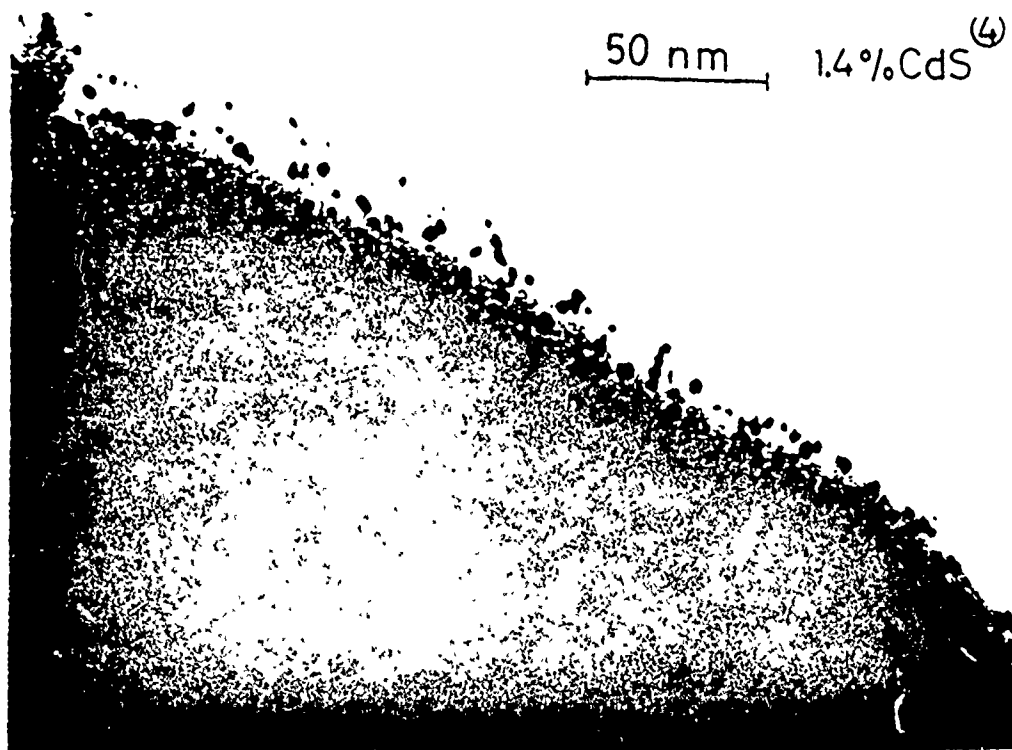


Fig. 3 Transmission electron micrograph of $\text{Na}_2\text{-B}_2\text{O}_3\text{-SiO}_2$ glass with 1.4 wt.% CdS. The CdS crystallites are seen as dark spheres with an average size of 35\AA .

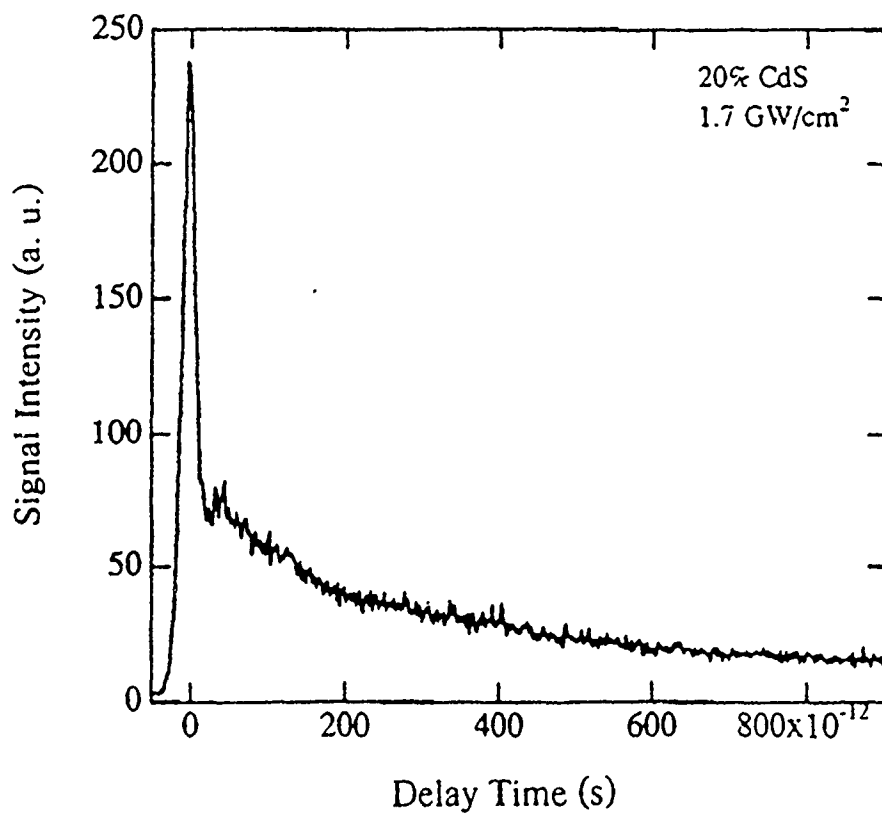


Fig. 4 $\chi^{(3)}$ response of the CdS-doped Ormosils as a function of time delay.

Table 1 Results of third-order responses of CdS-doped Ormosils.

Method: Degenerate Four Wave Mixing

Laser Wavelength: 532 nm

Laser Pulsewidth: 25 psec

CdS Concentration (nominal)	Average Particle Size, (Å)	Absorption Coefficient, (cm ⁻¹)	$\chi^{(3)}$ (esu)
2	25	1.1	1.5 x 10 ⁻¹³
4	40	1.3	1.6 x 10 ⁻¹³
6	55	2.6	5.1 x 10 ⁻¹³
15	60	6.5	3.6 x 10 ⁻¹²
20	120	23	3.7 x 10 ⁻¹¹

Table 2 Third-order nonlinear optical responses of Na₂-B₂O₃-SiO₂ glasses by sol-gel processing.

Intensity of Exciting Light: 35 kW/cm² for Sample 1 and 2

10 kW/cm² for Sample 3, 4, and 5

Sample No.	Conditions of Sample preparation	CdS Concentration (wt%)	Wavelength 450 nm		Wavelength 460 nm	
			α (cm ⁻¹)	$\chi^{(3)}$ (esu)	α (cm ⁻¹)	$\chi^{(3)}$ (esu)
1	5N-20B-70Si-15CdO 430°C/24h;150°C/24h;580°C/24h	8.0	1736	4.7x10 ⁻⁷	1557	3.5x10 ⁻⁷
2	5N-20B-70Si-15CdO 430°C/24h;150°C/24h;580°C/12h	8.0	1833	4.5x10 ⁻⁷	1715	6.3x10 ⁻⁷
3	5N-20B-75Si-10CdO 500°C/24h;150°C/24h;580°C/24h	4.5	915	3.1x10 ⁻⁷	849	4.1x10 ⁻⁷
4	5N-20B-75Si-10CdO 520°C/24h;150°C/24h;580°C/12h	1.4	493	2.9x10 ⁻⁷	417	3.3x10 ⁻⁷
5	5N-20B-75Si-10CdO 500°C/24h;R.T/6h;590°C/12h	0.5	217	1.2x10 ⁻⁷	184	1.3x10 ⁻⁷

α : Absorption Coefficient

$\chi^{(3)}$: Third-Order Non-Linear Optical Susceptibility

Progress Report 1990-1991

Second Harmonic Generation (SHG) in Inorganic Materials

Principal Investigator: Professor John D. Mackenzie, UCLA

Associate Researcher: Yuhuan Xu

Ph. D. Student: Yu-Hua Kao

I. Background

The frequency of light traversing a material can be doubled via the $\chi(2)$ response. Since 1961 [1], only piezoelectric and ferroelectric crystals have been shown to have this property of SHG. Further, theoretically, only noncentrosymmetric materials would exhibit SHG. It was very surprising, therefore, that in 1986 [2], it was conclusively shown that a silica glass fiber actually emitted green light ($0.532 \mu\text{m}$) after injection with intense infrared light ($1.064 \mu\text{m}$) for several hours. This frequency doubling in a silica glass fiber doped with GeO_2 was totally unexpected. Since that time, many experiments have confirmed this surprising result [3-6] and the following facts have emerged:

- a. Frequency doubling is much enhanced if the fiber is first "seeded" by injection of the green light [7]. Figure 1 shows the typical experimental arrangement for studying SHG.
- b. The efficiency of frequency doubling is dependent on time [2] and seeding energy [4, 6] and reaches some maximum value which varies with different fibers [2, 8].
- c. Application of an electric field on the fiber can significantly increase the efficiency of the frequency doubling [9].
- d. Although the conversion efficiency from infrared to green is relatively low (13% maximum to date [10]), some workers were able to use the emitted green light to successfully pump a dye laser [2].
- e. Although almost all the observations were made with silica fibers, there was also one report involving vapor-deposited thin silica films in a planar waveguide [11].
- f. All the samples showing SHG were silica glass doped with Ge with or without P [2, 8].
- g. The SHG capability is erasable by exposure to green or blue light alone [12].

There is absolutely no doubt that the structure of the glass has been slowly modified during preparation [13, 14]. This modified structure can be destroyed via high-frequency light. Numerous models have been developed to explain the origin of the SHG effect. All models can be classified into two types [15, 16]. One type proposes that the laser beam can somehow orient dipoles in the glass, thereby destroying its symmetry to produce macroscopic $\chi^{(2)}$. The dipoles present are assumed to occupy the proper positions of spatial periodicity for phase-matching. However, the small amount of dipoles (Ge E' centers) available appears to be insufficient to account for the high level of green light observed experimentally, and this has caused many to doubt the accuracy of this model [15, 16]. The other model proposes that the laser beam directly destroys the glass symmetry and induces macroscopic charge separation, thereby creating a strong, spatially periodic dc field.

The origin of frequency doubling in glass fibers is still unresolved. This discovery has created a wealth of scientific challenge for the glass scientist. Furthermore, one can immediately inquire as to the possibility of other glasses and amorphous solids.

Recently in 1991, amorphous ferroelectricity has been shown to occur in amorphous lithium niobate thin films made by the sol-gel process [17]. Because ferroelectricity arises from the alignment of existing dipoles in the material after poling, they are expected to show frequency doubling.

This research involves the investigation of amorphous ferroelectric materials and other oxide glasses for second harmonic generation and linear EO applications. In addition to materials fabrication, this research will address the device fabrication of these materials into planar waveguides by photolithography, as well as the processing of bulk solids.

2. Research Objectives

1. Determine the relationship between amorphous oxides and amorphous ferroelectric materials (such as composition and structure) and frequency doubling.
2. Obtain an understanding of the mechanism of SHG in amorphous materials (such as the creation of dipoles by intense laser irradiation) for improving NLO properties.
3. Fabrication of amorphous thin films and bulk solids having the property of SHG.
4. Fabrication of planar waveguide devices (such as modulators and switches) out of the above-mentioned materials.

3. Research Progress

(A). Amorphous Ferroelectricity

Amorphous ferroelectric thin films have been successfully fabricated by the sol-gel process. The structure of the films have been proven to be amorphous by X-ray diffraction and electron diffraction. Furthermore, electrical properties such as P-E hysteresis loops and pyroelectric currents were measured. The ferroelectric hysteresis loop of amorphous $\text{LiNb}(\text{OC}_2\text{H}_5)_x\text{O}_{3-x/2}$ (where $x < 0.01$) thin film on conductive polypyrrolle substrate is shown in Fig 2. The pyroelectric coefficient as a function of temperature for this same film on Si made at room temperature is shown in Fig. 3.

(B). Second Harmonic Generation From Oxide Glass

Frequency doubling in optical glass fibers has been performed with a Nd:YAG laser at UCLA. Conversion efficiency was roughly $10^{-3}\%$ (coupling efficiency of 19%) at an average IR power of 75mW (peak power of about 2kW) in the fiber. Furthermore, planar waveguides made with Ge doped silica are being fabricated by photolithography.

4. References

1. P. Franken, A. Hill, C. Peters, and G. Weinreich, Phys. Rev. Lett. 7, 4, pp. 118-119, (1961).
2. U. Osterberg and W. Margulis, Opt. Lett. 11, 8, pp. 516-518, (1986).
3. U. Osterberg and W. Margulis, Opt. Lett. 12, 1, pp. 57-59, (1987).
4. A. Krotkus and W. Margulis, Appl. Phys. Lett. 52, 23, pp. 1942-1944, (1988).
5. F. Ouellette, Opt. Lett., 14, 17, pp. 964-966, (1989).
6. B. Batdorf, C. Krautschik, U. Osterberg, G. Stegeman, J. Leitch and J. Rotge, Opt. Commun. 73, 5, pp. 393-397, (1989).
7. R. Stolen and H. Tom, Opt. Lett. 12, 8, pp. 585-587, (1987).
8. M. Saifi and M. Andrejco, Opt. Lett. 13, 9, pp. 773-775, (1988).
9. M. Bergot, M. Farries, M. Fermann, L. Li, L. Poyntz-Wright, P. Russell, and A. Smithson, Opt. Lett., 13, 7, pp. 592-594, (1988).
10. M. Farries, Laser Focus World 10, p. 12 (1988).
11. R. Kashyap and B. Ainslie, Electron. Lett. 25, 3, pp. 206-208, (1989).
12. F. Ouellette, K. Hill, and D. Johnson, Opt. Lett. 13, 6, pp. 515-517, (1988).
13. A. Kamal, D. Weinberger, and W. Weber, Opt. Lett. 15, 11, pp. 613-615, (1990).

14. T. Tsai, M. Saifi, E. Friebele, D. Griscom, and U. Osterberg, *Opt. Lett.* 14, 18, pp. 1023-1025, (1989).
15. V. Mizrahi, Y. Hibino, and G. Stegeman, *Opt. Commun.* 78, (3, 4), pp. 283-288, (1990).
16. V. Mizrahi and J. Sipe, *Optics & Photonics News*, p. 16-20, (1991).
17. R. Xu, Y. H. Xu, and J. Mackenzie, *Phys. Rev. B* (submitted).

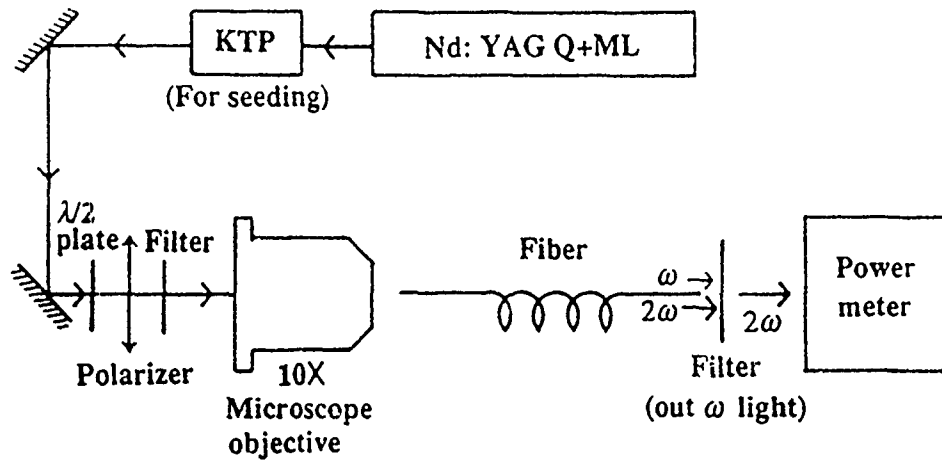


Fig. 1. Schematic of the experimental setup showing the measurement of the second harmonic power generated in the fiber.

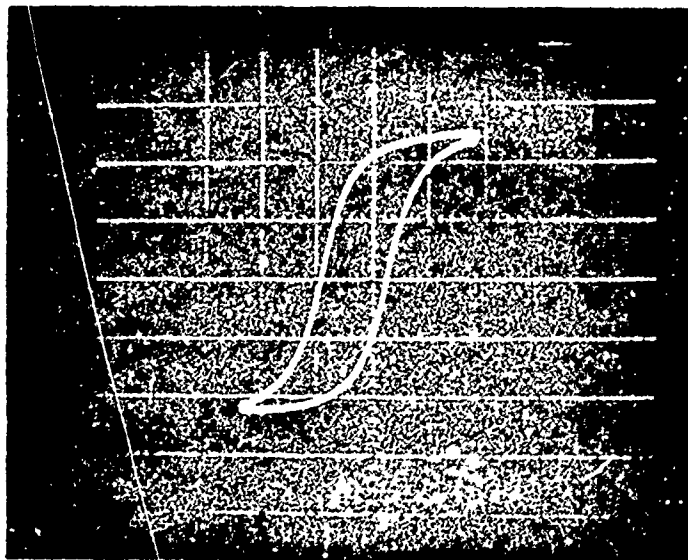


Fig. 2. P-E hysteresis loop of amorphous $\text{LiNb}(\text{OC}_2\text{H}_5)_x\text{O}_{3-x/2}$ (where $x < 0.01$) thin film on conductive polypyrrolle substrate.

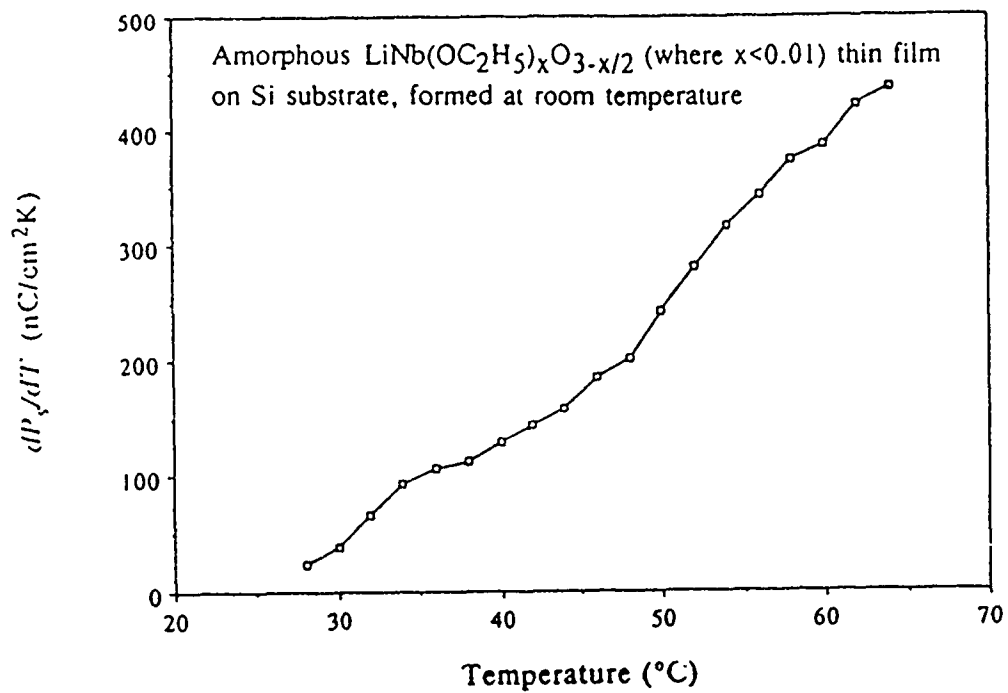


Fig. 3. Pyroelectric coefficient as a function of temperature for amorphous $\text{LiNb}(\text{OC}_2\text{H}_5)_x\text{O}_{3-x/2}$ (where $x < 0.01$) thin film.

STRUCTURALLY ENGINEERED POROUS SOL-GEL SILICA FOR OPTICAL COMPOSITES

Larry L. Hench
Advanced Materials Research Center
University of Florida
One Progress Blvd., #14
Alachua, FL 32615

Abstract

Two methods are described for preparation of optical composites: (A) a sol method where an organic phase is mixed with an inorganic precursor and (B) an impregnation method where an optical transparent inorganic Type VI gel-silica matrix is first prepared and stabilized thermally, then an optically active polymer is impregnated into the interconnected 3-D pore network. Comparisons of relative processing merits, mechanical properties and optical applications are presented with emphasis on multifunctional optical applications.

For centuries optical components have been primarily single phase materials with or without chemical dopants to produce specific optical characteristics. Examples include glasses and single crystals for lenses, mirrors, lasers, filters; polycrystalline ceramics for optoelectronics; and glass-ceramics for mirrors.¹ During the last few years the use of sol-gel chemical processing has made it possible to develop optical composites which have two or more phases, and thereby possess unique optical properties. The composites are usually an optically active organic phase and a sol-gel derived oxide matrix. Because of the chemical stability of an oxide network such optical composites offer substantial advantages in processing, reliability, and performance over the organics by themselves. Many of the organics of interest are liquid at ambient temperature and are therefore restricted in use in an optical system. By using the composites approach these restrictions are circumvented.

Several groups have pioneered the growing interest in optical composites including Reisfeld, Avnir and colleagues in Israel;^{2,3,4} Mackenzie⁵ and Dunn⁶ and co-workers at UCLA; King and colleagues at the University of Manchester, U.K.;⁷ Prasad and Karasz at SUNY at Buffalo and University of Massachusetts⁸ and Noguez and co-workers at the University of Florida and Geltech, Inc.⁹ Their developments will be reviewed as examples of this new field along with recent results from our laboratory.¹⁰

Our current research emphasis is on producing optical matrices with a narrow distribution of pore sizes that are carefully controlled from an average of 1.4 nm to 12 nm and a volume fraction of porosity from 0.2 to 0.7. These matrices will make it possible to match the specific requirements of molecular size and loading factor for a broad range of organic phases. Thermal and chemical treatments are being used to tailor the surface chemistry of the pores to match polymer requirements.

Testing of the matrices is being done in the OGAMMS program by King, et al., in Manchester and Phillips, et al., at Loughborough. Characterization and process development of matrices to meet specific requirements of the organic phases is being done at the University of Florida.

Introduction

Two alternative pathways are used in making optical composites, as illustrated in Figure 1. In Method A, termed *sol processing*, the metal organic sol-gel precursor is mixed with the optical organic molecules. Hydrolysis and polycondensation reactions occur in Process Steps 1-3, see References 11 and 12 for details, which results in formation of a highly porous, interconnected 3-D oxide network, the gel, containing the organic within the framework of the gel. Removal of the alcohol-water liquid from the pores of the gel, Step 5, produces a dry and moderately strong two phase material. The size and volume fraction of pores containing the organic phase are influenced greatly

OPTICAL COMPOSITES PROCESSING

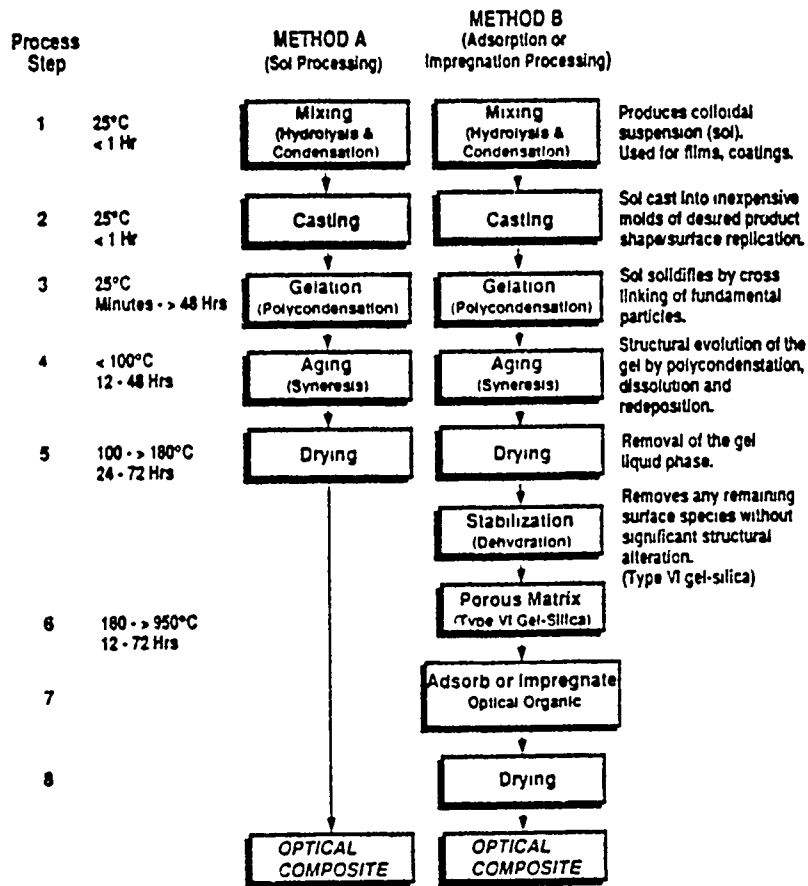


Figure 1 Process steps for two methods of making optical composites

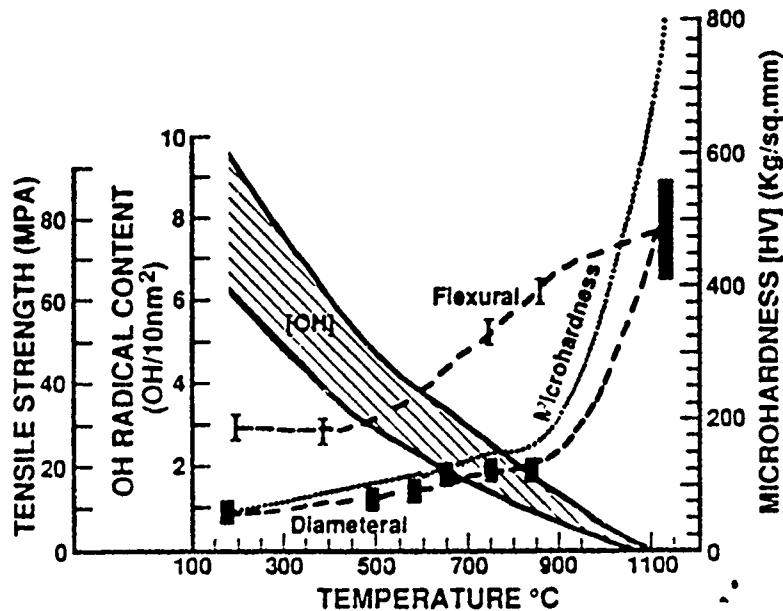


Figure 2 Effect of stabilization temperature on properties of Type VI gel-silica optical matrices with 1.2 nm pores. OH content, ref.: flexural strength (MPa), ref.: diametral tensile strength (MPa), ref.: Microhardness (Kg/mm²), ref. X = flexural strength for fully dense vitreous silica, ref.

by the amount of water or alcohol used in making the gel and the Ph of the solution. The mechanical and chemical behavior of a composite made in this manner is restricted by the temperature limitation of drying imposed by the thermal stability of the optical polymer. Figure 2 illustrates the range of microhardness, flexural and diametral tensile strength, and hydroxyl content of silica gel monoliths dried at 180°C. The improvement in mechanical properties with increased processing temperature is also illustrated in Figure 2.

Method B is a two part process, termed *absorption or impregnation processing*, which circumvents the thermal stability limitation on processing. The first part, Steps 1-6, uses the sol-gel method to make an optically transparent gel-silica matrix with a very large volume fraction of interconnected porosity with a very small average pore radius (<10nm). This type of material is termed Type VI gel-silica. (For a discussion of Type I-IV silicas see Bruckner,¹³ for a description of the processing of Types V and VI gel-silica see references 11 and 14.) The Type VI matrix is chemically stabilized by a thermal treatment, see Figure 1, Step 6, and then ground or polished, if necessary, to produce an optical element. In the second part, Steps 7 and 8, the optical organic phase is diffused or impregnated into the porous matrix where it is chemically or physically absorbed within the pore network. The extent of chemical interaction between the optical organic phase and the network is strongly influenced by the stabilization treatment which controls the silanol concentration on the surface of the pores.^{15,16}

There are advantages and disadvantages of both process options. The primary advantage of Method A is its simplicity. There is relatively little information on the mechanical, and thermal properties of composites made by Method A. Likewise data on ultrastructural or textural characterization of composites made by Method A is limited.

The primary advantages of optical composites made by Method B, Table 1, is that the textural properties such as volume fraction and pore size distribution can be tailored for specific applications. Also, the chemical nature of the pore network, largely controlled by pore radius, silanol concentration, and adsorbed water layers can be varied during stabilization, Step 6, and optimized for a particular organic impregnate. For example, Nikiel, et al. have shown¹⁷ that the rotational relaxation times for acetonitrile in a Type VI gel-silica matrix is an order of magnitude larger when the molecules are adsorbed in the first monolayer compared with molecules that completely fill the pores. Perry and Li¹⁸ and Hench and West¹ and Wang¹⁹ have shown that the extent of pore surface hydration affects the ligand fields of elements adsorbed in the pores.

Table 1
Advantages of Type VI Gel-Silica as a Laser Dye Host

1) Fabricability into laser rods, slabs, or Brewster angle segments	2) Wide range of volume fraction of porosity
3) Polishability	4) Wide range of pore sizes
5) High mechanical strength	6) High thermal stability
7) Net shape and net surface casting	8) High chemical stability
9) High purity	10) Excellent transmission over wide range of wavelengths
11) Ability to tailor chemically the surface to control the dye-matrix interface	

Characterization of Commercial Gel-Sil™

In order to be able to compare results and design the next phases of optical composite research, commercial sol-gel silica monoliths were purchased from Geltech.* The overall characterization program is summarized in Table 2. These investigators have received porous Gel-Sil™ samples processed from 180°C to 1000°C in ambient air. The characterization included: surface area, total pore volume average pore radius and bulk density. Structural density, genus (pore connectivity), Vickers hardness, UV cutoff, visible and near infrared transmission will be reported in a subsequent paper. All results presented are compared to porous Type VI gel-silica produced in the University of Florida Advanced Materials Research Center laboratories.

Types of Optical Composites

Reisfeld has reviewed^{4,20} the use of Method A sol processing to form a very large variety of optical composites and discussed in detail several of those developed by her Institute. Table 2 (in Ref. 26) summarizes several of the optical composites made by either Method A or Method B and their potential applications.^b It is clear that the versatility of these methods is extraordinary. However, in most cases considerable effort is still required to optimize the composite systems and make them commercially viable. Two systems that have received considerable attention, solid state dye lasers made by both Methods A and B, and scintillators and detectors, Method B, are reviewed here.

Solid-State Dye Lasers

Incorporation of laser dyes in a solid matrix has been studied for many years with the goal of obtaining a lightweight, portable solid state system which is inexpensive to fabricate, is reliable, and is safe to handle. Organic dyes are attractive for use in lasers because they offer tunability. In contrast to tunable lasers based on transition elements, such as chromium III, doped in crystals which operate only in the near IR,²¹ organic dyes can emit in the entire visible spectrum. The potential advantages of solid state dye lasers over their liquid dye counterparts are listed in Table 3.

In most solid state dye laser systems, inorganic crystals, glasses and polymers are used as host materials or saturable absorbers.⁴ Recently, porous structures made by Method A sol processing have been used to incorporate dye molecules in the solid state systems.^{2-7,22} Type VI gel-silica made by Method B has also been studied by King⁷ and Shaw, et al.²³ and Hench, et al.¹⁰ for lasing characteristics using two different types of dyes. Controlling the chemical environment of the dye molecules is likely to be essential to achieve high photostability, based upon comments by Reisfeld.⁴

In the recent work by Zhu, et al.²⁴ and Hench, et al.¹⁰ rectangular gel-silica specimens of 6 X 6 X 10 mm were stabilized to 800°C for 4 hrs. The ends of the rectangles were polished to 600 grit and are parallel to each other. Other surfaces of the specimens were not polished and were kept in an as-cast condition.

The laser dye used in this study developed by Lee and Robb²⁵ was 4-{2-(5-phenyl-oxazolyl)}-1-methylpyridinium p-toluenesulfonate (4PyPO-MePTS).** This dye is water soluble which is a major advantage in the processing of the composite. The dye also has exceptionally high photostability.²⁵

Type VI gel-silica monoliths with pore sizes ranging from 1.2 to 8 nm were filled with the dye solution, and tested using methods discussed in another publication.²⁴ The impregnated gel-silica monoliths exhibited good environmental, chemical and thermal stability.

*Gel-sil™ is a registered trademark of Geltech, Inc., Alachua, Florida.

**Aldrich Chemical Company, Inc., Milwaukee, Wisconsin.

Table 2
Characterization Study

Characterization Test	Institution	Status
TGA, DMA, DSC, DTA	UF	Feb. 92
Dilatometry	UF	Feb. 92
Microhardness	UF	Complete
Nitrogen Adsorption Isotherm Analysis	UF	Complete
Neutron Activation	UF	Feb. 92
Index of Refraction	UF, Loughborough U. of Tech.	Feb. 92
Optical Dispersion	Subcontract	
Surface Finish and Figure	UF	
Dimensional Tolerance	UF, Loughborough U. of Tech.	
Homogeneity (Zygo Interferometer)	UF	
FTIR	UF, Brunel University	Complete
UV, VIS, NIR	UF, Brunel University	Complete
Vacuum UV	UF, Subcontract	
AFM	Digital Instrument	Complete
Raman Spectroscopy	UF, Brunel University	
Inorganic Doping	Brunel University, UF	Feb. 92
Organic Doping	University of Manchester University of Buffalo Loughborough U. of Tech., UF	Feb. 92
Positronium Decay	TCU	
Neutron Scattering	University of Reading	
Synchrotron Scattering	University of Montpellier	
X-ray Small Angle Scattering	University of Sao Paolo	
Pressure IR	University of Illinois	
Vapor Stabilization	University of Wisconsin	
Gas Permeability	UF	Complete
Liquid Diffusivities	UF	
AC Impedance Spectroscopy	UF	

Table 3
Advantages of Solid State Dye Lasers

Advantage	Consequences
1) Eliminate fluid pumping and flow system	Compatness, ease of handling, less expensive
2) Isolation of dye molecules by pore walls	Minimizes dimerization and aggregation
3) Increase thermal stability	Operate at higher power
4) Isolate dye molecules	Inhibits destructive photo processes
5) Steric hindrance of dye molecules by porous silica matrix	Reduces rational modes that cause non-radiative loss
6) Easy substitution of laser rods with different dyes	Wide selection of wavelength throughout uv, visible and NIR
7) Higher thermal conductivity	Higher pumping thresholds than liquids

Conclusions

Two methods of preparing optical composites have been developed. Both are extremely versatile processes. Method A, where the organic is mixed directly with the sol offers the advantage of simplicity. Method B, where the organic is adsorbed or impregnated into a porous gel-silica matrix, offers the advantage of superior mechanical properties and considerable control over the interfacial chemistry of the pores and organic phase. It is too early to establish which is preferable for commercially viable optical devices.

Acknowledgements

The author acknowledges the Air Force Office of Scientific Research Directorate of Chemical and Atmospheric Sciences for financial support under contract #F49620-88-C-0073.

References

1. L. L. Hench and J. K. West, Principles of Electronic Ceramics, Chap. 8, Wiley, New York, 1990.
2. D. Avnir, D. Levy and R. Reisfeld; J. Phys. Chem. 88, 5956 (1984).
3. D. Avnir, V. R. Kaufman and R. Reisfeld, "Organic Fluorescent Dyes Trapped in Silica and Silica-Titania Thin Films by the Sol-Gel Method. Photophysical, Film and Cage Properties," J. Non-Cryst. Solids 74, 395 (1985).
4. R. Reisfeld, J. Non-Cryst. Solids 121, 254-266 (1990).
5. E. J. A. Pope and J. D. Mackenzie, "Incorporation of Organic Dyes in Polymer/Oxide Composites," MRS Bulletin, March 17/May 15, 29-31 (1987).
6. B. Dunn, J. D. Mackenzie, J. I. Zink, O. M. Stafsudd, "Solid-State Tunable Lasers Based on Dye-Doped Sol-Gel Materials," SPIE Sol-Gel Optics Conf., San Diego, July 1990.
7. T. A. King, SPIE High Power Solid State Lasers Conf., The Hague 1990, Vol. 1277.
8. P. N. Prasad, F. E. Karasz, Y. Pang and C. J. Wung; U.S. Patent Appl. #312132.
9. J. L. Noguez, S. Majewski, J. K. Walker, M. Bowen, R. Wojcik and W. V. Moreshead, J. Am. Ceram. Soc., 71[12], 1159-1163 (1988).
10. L. L. Hench, J. K. West, B. F. Zhu and R. Ochoa, "Gel-Silica Hybrid Optics," SPIE Sol-Gel Optics Conf., San Diego, July 1990.
11. L. L. Hench and J. K. West, "The Sol-Gel Process," Chem. Rev. 90, 33-72 (1990).

12. C. J. Brinker and G. W. Scherer, Sol-Gel Science, Academic Press, New York, 1990.
13. R. Bruckner, "Properties and Structural of Vitreous Silica. I," J. Non-Cryst. Sol. 5, 121-170 (1970).
14. L. L. Hench, S. H. Wang and J. L. Noguez, "Gel-Silica Optics", Multifunctional Materials 878, 76-85, Robert L. Gunshor, ed., SPIE, Bellingham, WA (1988).
15. V. Ya. Davydov, A. V. Kiselev and L. T. Zhuravler, Trans. Faraday Soc. 60, 2254 (1964).
16. S. Wallace, "Porous Silica Gel Monoliths, Structural Evolution and Interactions with Water," Ph.D. Dissertation, University of Florida, 1990.
17. L. Nikiel, T. W. Zerda and L. L. Hench, "Molecular Motion in Porous Silica", Am. Cer. Soc. Composites Conf., Orlando, FL, Nov. 1990.
18. C. Perry and X. Li, "NIR Studies of Monolithic Silica Gels," to be published.
19. S. H. Wang, "Sol-Gel Derived Silica Optics," Ph.D. Dissertation, University of Florida (1988).
20. R. Reisfeld, "Theory and Application of spectroscopically Active Glasses Prepared by the Sol-Gel Method," SPIE Int. Symp. on Sol-Gel Optics, San Diego, CA, July 8-13, 1990.
21. R. Reisfeld and C. K. Jorgensen, Structure and Bonding 69, 63 (1988).
22. T. S. Efendiev, Y. V. Kostennich and A. N. Rubinov, Appl. Phys. B33, 167 (1984).
23. D. J. Shaw, C. Whitehurst and T. A. King, "Sol-Gel Glass Solid State Lasers Doped with Organic Molecules," SPIE Sol-Gel Optics Symp., San Diego, CA, July 8-13, 1990.
24. B. F. Zhu, R. Ochoa and L. L. Hench (to be published).
25. L. A. Lee and R. A. Robb, IEEE J. Quantum Electronics, QE-16, 7, 777 (1980).
26. L. L. Hench, "Optical Composites", Am. Cer. Soc. Composites Conf., Orlando, Fl. Nov. 1990, M. Sachs, ed.

A report to the fourth OGAMM meeting
Ilkley, Yorkshire, August 1991

Progress in the optical technology of gel-silica and polymer materials

Nicholas J Phillips
Spencer Modica
Ce Wang*

Department of Physics, Loughborough University

* On leave from the University of Suzhou
Peoples Republic of China

ABSTRACT

We summarise local developments in the area of uses of imaging photopolymer and gel-silica technology. Thermal expansion measurements of gel silica have been undertaken using an in-house interferometer. These results are reported. Progress has also been made in the important area of embedded imaging polymer in a gel-silica matrix. The first results are reported. Finally, we report a novel aspect of holographic recording which emphasises the roles of coherence and incoherence in the use of the recording light. What are believed to be the first experiments using incoherent light to record holograms are reported.

1. Thermal expansion of gel-silica monoliths

Our decision to build an interferometer in which to measure the thermal expansion of gel-silica was based on our early experimental observations of unusual intra-cavity etalon effects using primitive gel-silica etalons. Such structures were uncoated and probably no more than 85% dense so that Rayleigh scattering was significant.

The full characterisation of etalons can only be achieved if both thickness and refractive index can be measured as the temperature is changed. Measuring the index is relatively easy but because of the low values of thermal expansion in silica, the thickness measurement requires extreme care.

An interferometer head was constructed as shown in Figure 1.

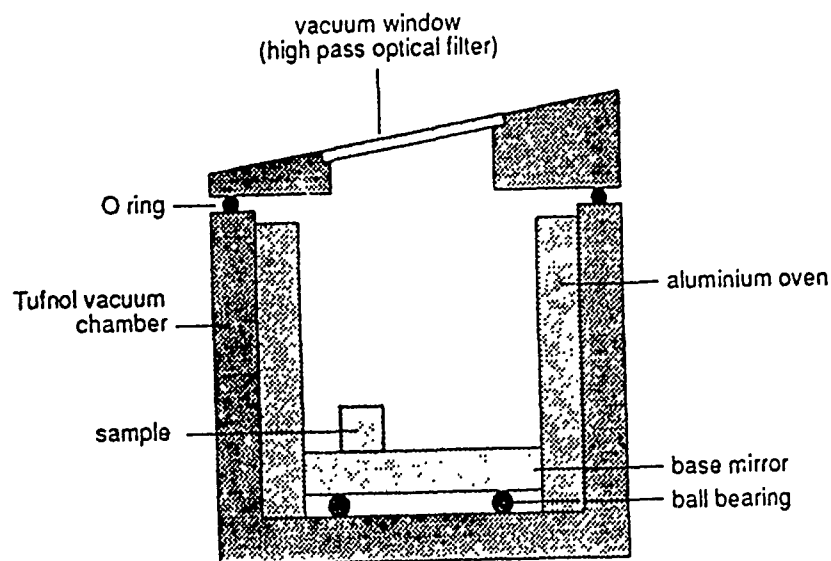


Figure 1 Interferometer Head

The materials were carefully chosen and the obvious aspect of the mode of operation lies in the reference of one of the reflected beams to the support surface of the lower mirror. The interferometer thus measures the relative movements of top and bottom surfaces of the sample.

The optical aspects of measurement are constrained by certain features of the optical feed process (see Figure 2). The incoming beam is first filtered by passing it through a single-mode optical fibre. This has the effect of removing transverse modal noise thus providing a marked clean-up of the beam. At the same time, reflected light from the experiment finds it geometrically difficult to re-enter the fibre and hence cause extraneous cavity effects; a major bugbear of laser based interferometry. The incoming beam is then split and divided into two by a polarizing beam splitter B. The s and p division is controlled by an input half wave plate P_1 . Light that travels to the sample and reference surface is then converted from the linearly polarized

form to one of circular polarization by a quarter wave plate QWP. This has the effect of converting the returned beam from the reflective surfaces into linearly polarized light orthogonal in direction to the input polarizations. The beams are then recombined by B and travel on to be analysed at the analyzer A. Since they approach the analyzer with orthogonal polarizations, the analyzer must be set to bisect the relative directions of the respective electric vectors.

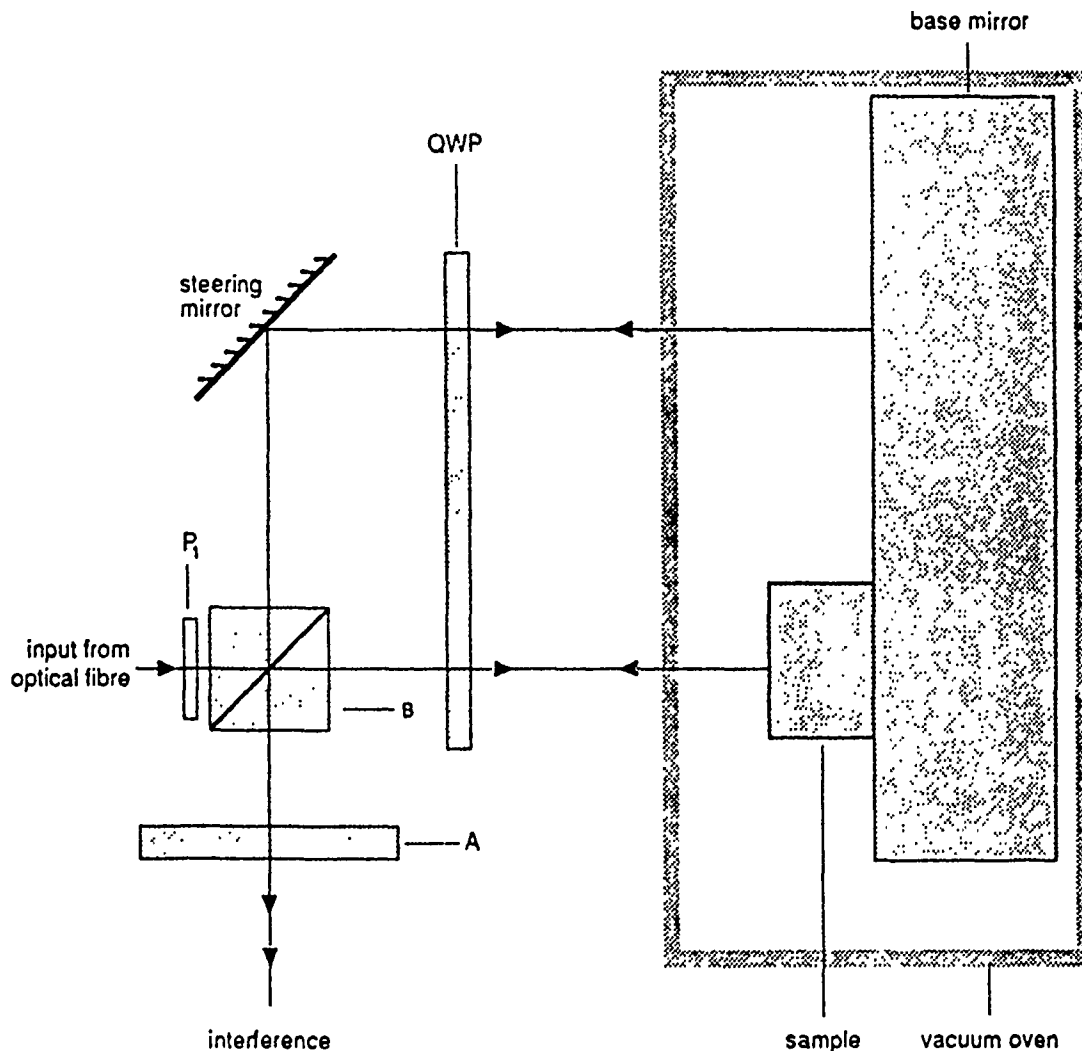


Figure 2 Optical Principles of the Dilatometer Interferometer

This system has an added advantage in that if a quarter wave plate is interposed prior to the analyzer (Figure 3), then a bias can be applied to create an interference pattern in phase quadrature to that originally perceived. This effect is vital to avoid instrumental sensitivity difficulties when the pattern is at a peak black or peak white condition.

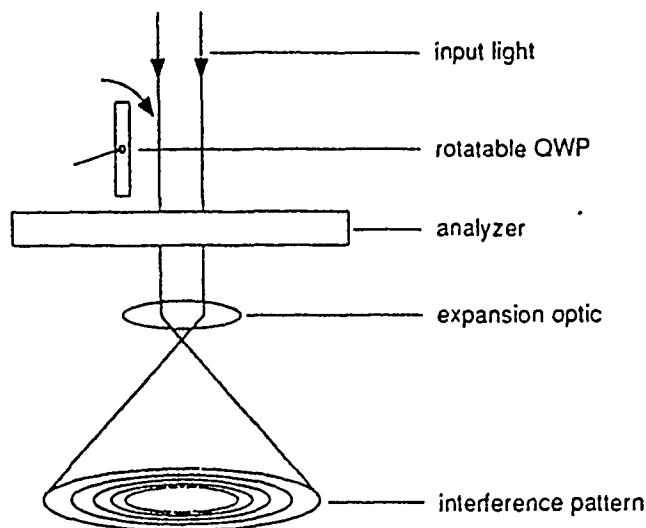


Figure 3 Introduction of a Quarter Wave Plate prior to the analyzer provides a quadrature bias to the pattern (a phase shift of 90°)

Essentially, the interferometer will deliver information of the form $\sin \phi$ and $\cos \phi$ where ϕ is the optical phase difference along the two branches of the interferometer.

Problems occur if we are near a peak or trough of these trigonometric functions. The lack of sensitivity corresponds to the vanishing of the differentials. This problem is overcome if we take the ratio eg $\sin \phi / \cos \phi$. The tangent function does not suffer from this problem. We have used a system in which the quarter wave plate is rotated into position after the intensity measurement in the interferometer is made. A second reading is taken thus satisfying the phase quadrature condition above. The overall system can be considered as in Figure 4.

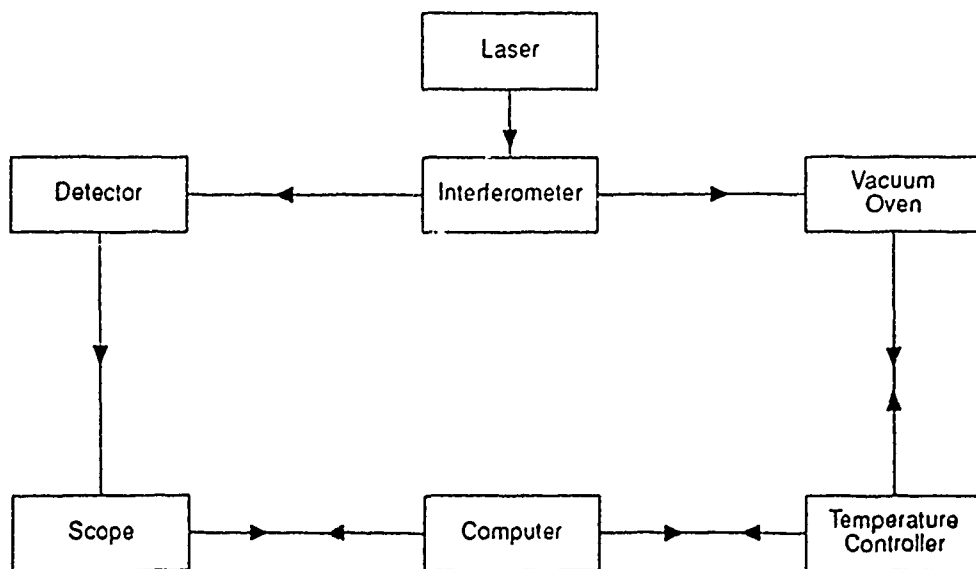
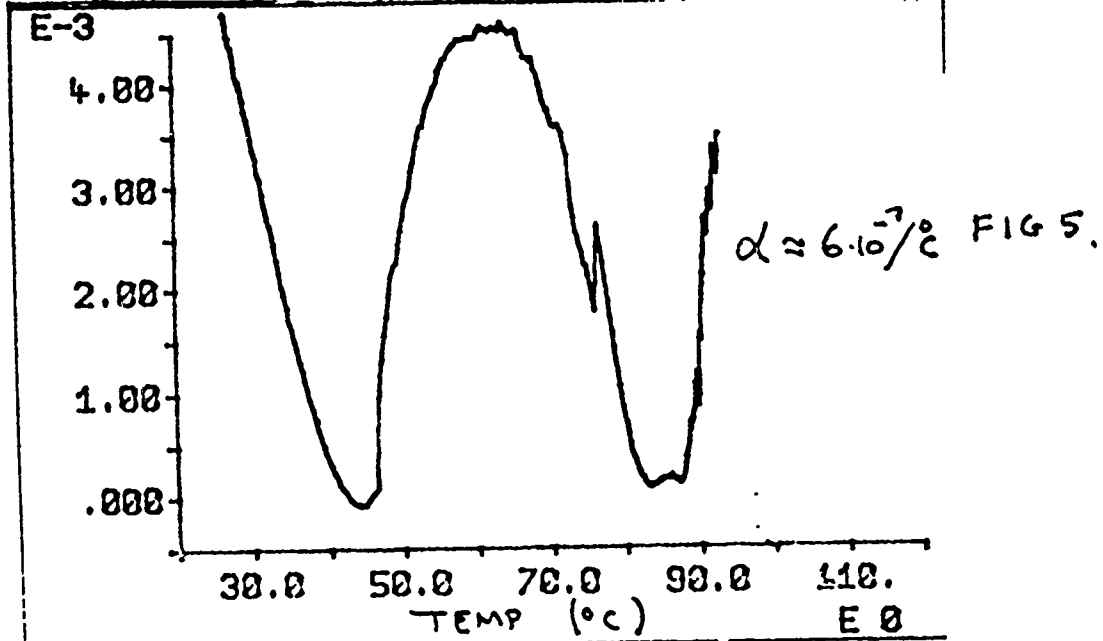


Figure 4 Schematic Block Diagram

Typical results show the output of say the single $\sin \phi$ or $\cos \phi$ pattern and plotted against temperatures give results typically specified as in Figure 5.



At this time, we find that gel-silica in its fully densified form does not show significant difference when compared to a reference 'Dynasil' high temperature prepared silica etalon. However, the subtleties of our investigation are only just underway and we expect novel developments in the next round of work.

2. Embedding of Du Pont's imaging monomer into the pores of gel-silica

This work has made considerable progress. A vacuum oven has been built with the advice of Larry Hench and Jon West of the University of Florida, leading to the system as shown in Figure 6.

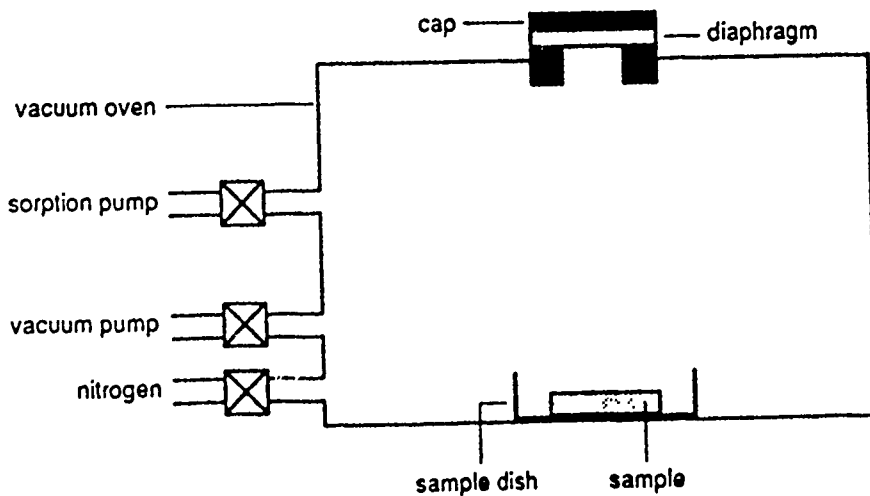


Figure 6 Monomer Embedding Oven

We evacuate the chamber at a temperature of 120°C and incorporate a large sorption pump at the rear of the chamber. Once good rough vacuum is achieved (after a number of hours) we inject liquid monomer over the sample using a diaphragm let into the ceiling of the oven. A plastic disc of rupturable material is penetrated by a syringe inserted through the top of the chamber. The sample is covered with liquid monomer and then the chamber is raised to atmospheric pressure in dry Nitrogen. After a suitable time, ranging from hours to days, the sample is removed and stored whilst immersed in further liquid monomer covered by a heavy inert organic gas. Eventually, solvent evaporation 'dries out' the encasing monomer and the sample is withdrawn. Surface dry polymer/monomer is peeled off and the sample exposed as in Figure 7.

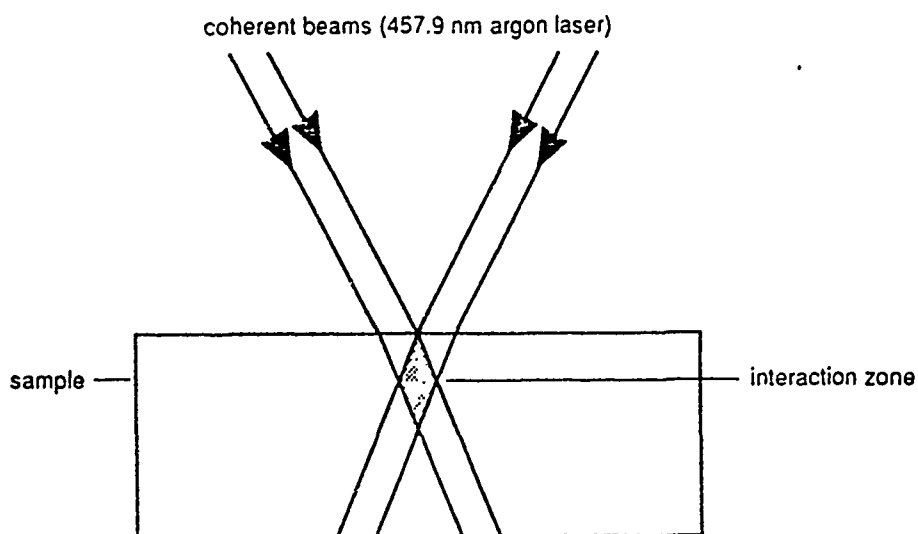
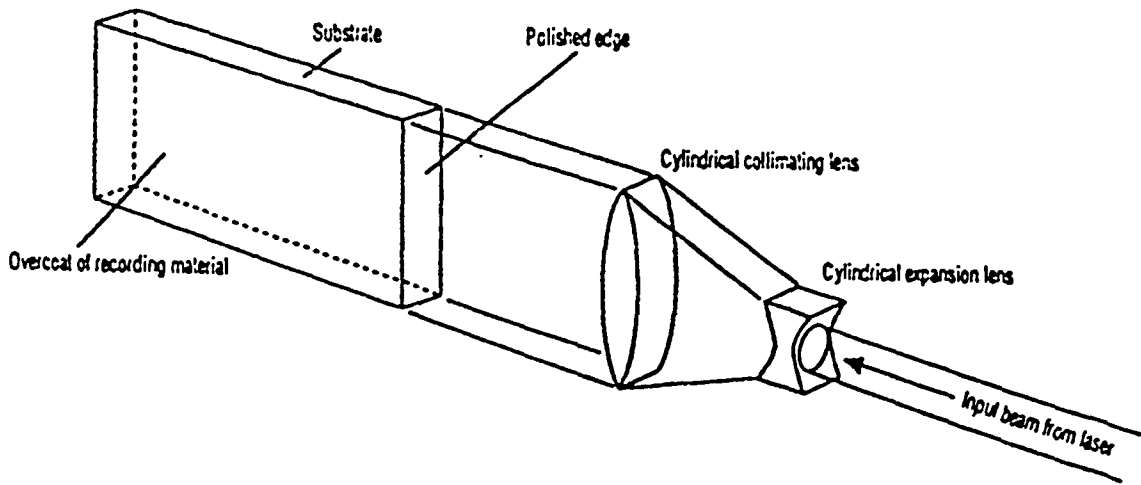


Figure 7 Showing Exposure Regime

Promising results have been obtained but it is apparent that the solvent based migration of monomer induced by the action of coherent light is a complex process which makes severe demands on the optical integrity of the matrix. The most subtle area of difficulty is related to the choice of solvents for the monomer. Thus methyl ethyl ketone and toluene have been used in preference to volatile solvents such as methylene chloride. Excess solvent volatility leads to micro cracking of the matrix and hence scattering levels that are undesirable.

We have recently introduced MMA (methyl methacrylate) as a solvent with the proposal that it is polymerizable and should cooperate in the polymer mechanisms of the Du Pont material. So far, we have seen the materials to be compatible and imaging results are in the process of study.

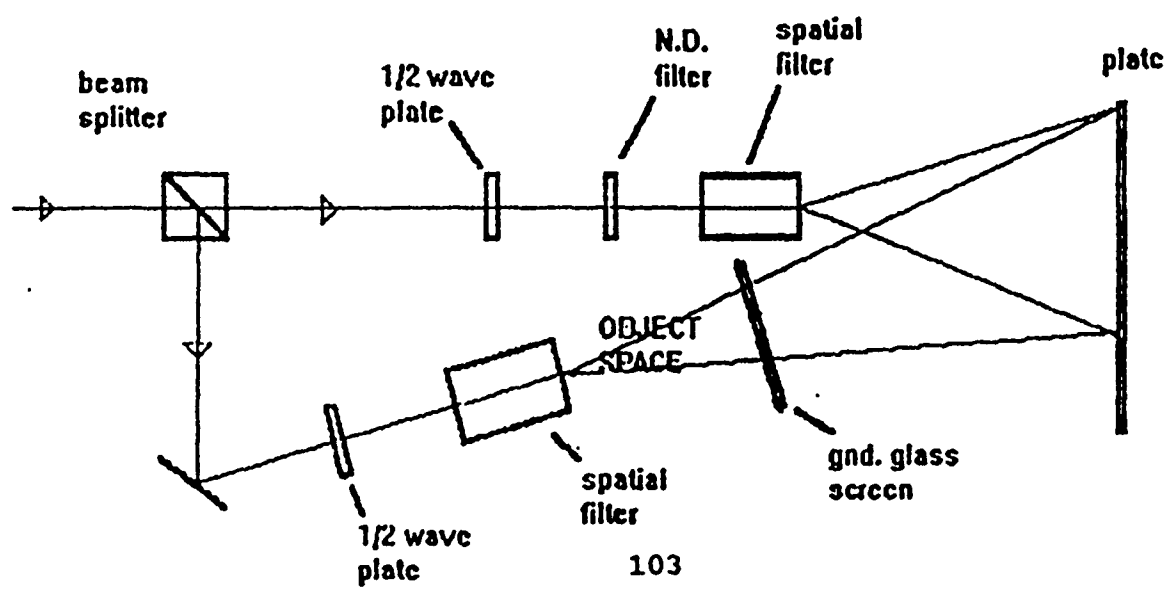
In the generality of uses of thick polymer-gel-silica composites, we have predicted the use of such materials in the important area of edge-illuminated holograms (Figure 8). We have made a study of such holography by contacting coated sheets of Du Pont's polymer against a glass substrate. The results are very positive and give rise to great promise for this new area of display holography. The transference of our work into the thick polymer-silica composites will follow when the problems of embedding are satisfactorily overcome.



3. New forms of holography-coherence and incoherence in the recording process

What is seen as a new area of holography has been opened up by our polymer studies. We have first formed a hologram in the Du Pont photopolymer using a conventional recording regime (Figure 9).

NO-REFERENCE BEAM HOLOGRAPHY



The material responds by creating a recording in real-time.

We argued that if the correct exposure is given in this first stage it might be possible to switch off the reference beam thus permitting the recording of object information without the usual coherence. In fact, the incoming light from the object is split into zero and first order components by the hologram previously formed. These components then interfere in the material that is not used up in the first exposure. The real point of this invention is that it may create relaxed conditions for the stability of the recording process and may have implications in readers for optical computing.

We do not claim to have made holograms using incoherent light but in principle, the second recording should be possible with filtered natural light.

Acknowledgement

The authors would like to thank AFOSR and SDI for the provision of funds. The early help from Dr Don Ulrich was a memorable experience and more recently we should like to thank Larry Hench and John West of the University of Florida and Dr Charles Lee at AFOSR in Washington.

GEL-SILICA LASERS AND OPTICS

A.Charlton, M.A.Meneses-Nava, D.J.Shaw and T.A.King

Physics Department
Schuster Laboratory
University of Manchester
Manchester
M13 9PL
United Kingdom

1. Laser Development.
2. Laser Enhanced Densification.
3. Basic Properties of Adsorbed Molecules.

Laser Development

Introduction

Work in this area has concentrated on the requirement to develop new and more practical gel-silica laser devices including improved performance from doped sol-gel lasers in various cavity configurations. The production of polymer and active dye gel-silica composites by a post doping method offers several potential advantages over the conventional ORMOSIL preparative methods, and should significantly enhance the basic mechanical and optical properties of undensified gel-silica.

Doped gel-silica lasers

The wavelength range of doped gel-silica lasers has been extended significantly in this project from 360nm using phenyl-biphenyl-oxadiazole (PBD) dye to 630nm with Sulforhodamine 640. The pump laser used was a Nd:YAG with harmonic generator assembly giving outputs of 20mJ per pulse at 255nm, and 200mJ per pulse at 532nm. In both cases the gel-silica block of dimensions 5x5x20mm was placed in a simple laser cavity

consisting of a high reflector and output coupler of approximately 50% reflectivity. The output of the Nd:YAG laser was focused by a 20cm focal length cylindrical lens to a strip approximately 300 μ m wide at the surface of the gel-silica thereby producing a transversely pumped laser. Using pump energies of up to 5mJ per pulse, output efficiencies were <1% (PBD) and <5% (Sulforhodamine), with significant shot to shot fluctuations and relatively poor photostability (< 500 shots). These results are preliminary and should be improved significantly by optimisation of the laser parameters.

Extensive work has been carried out on rhodamine 6G doped gel-silica including tuning operation, narrow linewidth performance, and photostability studies involving comparison with doped ORMOSIL samples. Using a Littrow mounted grating cavity and a frequency doubled Nd:YAG pump laser, the R6G doped (1×10^{-4} M) gel-silica laser was tuned from 560nm-620nm (figure 1) with a maximum efficiency of 16% and a linewidth of 3nm.

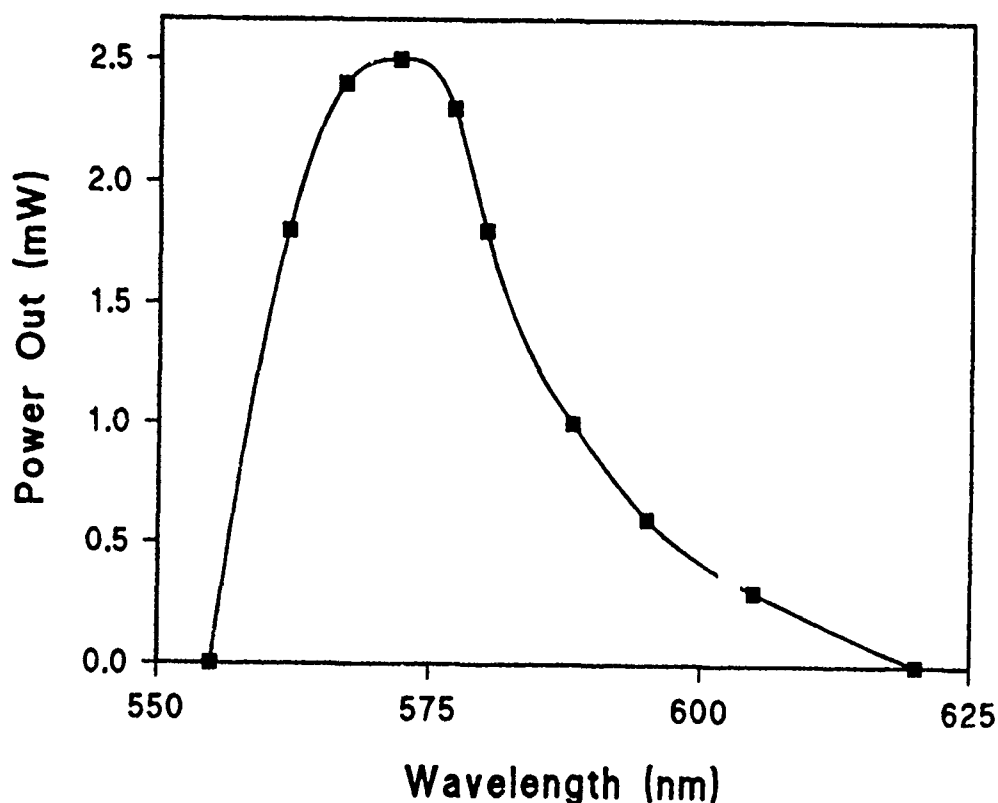


Figure 1.

Tuning curve for R6G doped gel-silica sample pumped by 15mW frequency doubled Nd:YAG laser.

In order to produce narrow linewidth performance another R6G doped sample (2×10^{-5} M) was placed in a Littman grazing incidence cavity designed for single mode operation and longitudinally pumped by the frequency doubled Nd:YAG laser. Although output efficiency was reduced significantly, the resulting linewidth was measured to be $< 0.05 \text{ nm}$, a considerable improvement over the Littrow cavity result.

Dye photostability was measured by placing the doped gel-silica and ORMOSIL samples in a plane cavity consisting of high reflector and output coupler ($R = 80\%$), pumping the laser transversely with a frequency doubled Nd:YAG laser, and monitoring the laser output. The results for post-doped gel-silica (R6G) with and without the use of water as index matching fluid, ORMOSIL (R6G and RB) and a solution of R6G in methanol (all 1×10^{-4} M) are presented in figure 2.

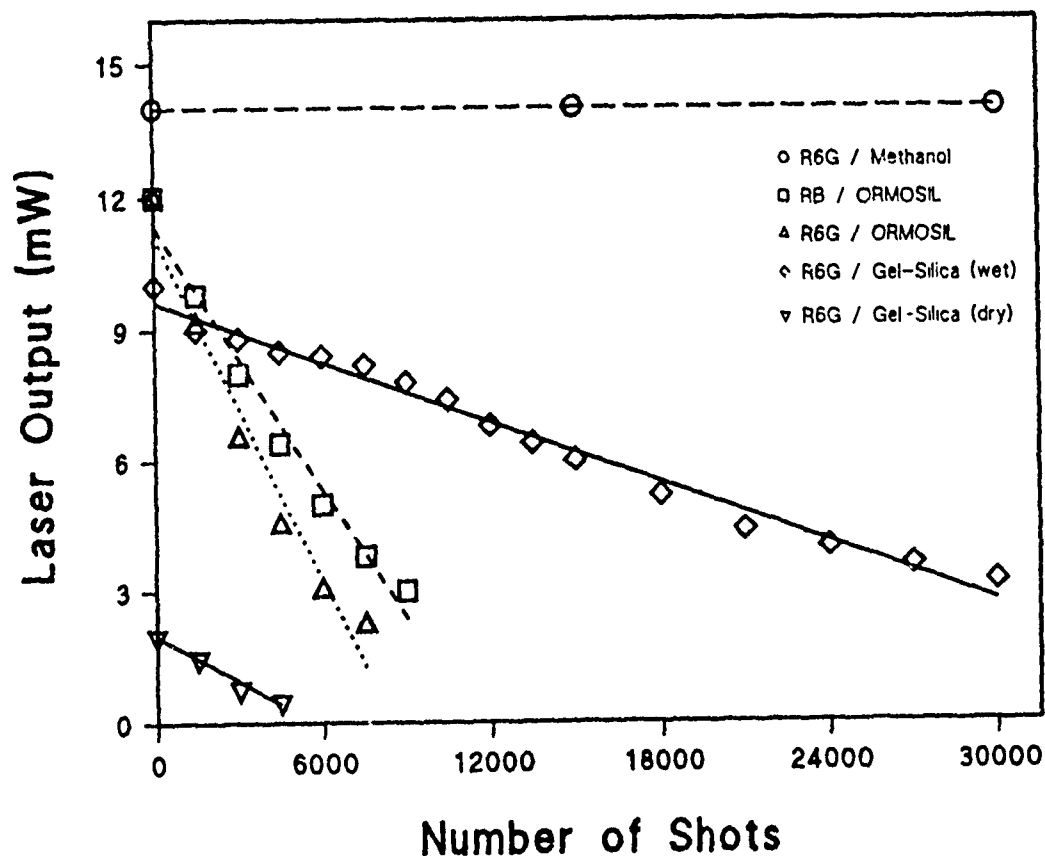


Figure 2.

Laser output versus number of shots for various laser hosts pumped with 3mJ/pulse at 10Hz from a frequency doubled Nd:YAG laser.

The apparent high photostability of the dye in solution is due to the large volume of the solution compared to the volume actually pumped (a factor of approximately 5000), and the mobility of dye molecules within the solution. From these results it is clear that index matched post-doped gel-silica compares favourably with the ORMOSIL host, giving similar peak efficiencies and greatly increased photostability of approximately 20,000 shots at a pump energy of 3mJ per pulse. This corresponds to a total input energy of 60J in a volume of approximately 0.5mm³, or 120kJ/cm³ compared to 10kJ/cm³ for the R6G doped ORMOSIL sample. This result, together with the greater flexibility of the post-doping method and the possibility of including polymer index matching after the dopant has been introduced, highlights the advantages and potential offered by the post-doping method.

Another aspect of post-doping which has is being studied is the distribution of dopant within the gel-silica sample and the dependence of the distribution on dopant size, doping conditions and gel-silica pore size. This question has been investigated using a fluorescence imaging technique to probe the dye concentration obtained within a gel-silica sample. The method involves the use of an argon ion laser ($\lambda=488\text{nm}$) as an excitation source and a scanning photodiode to detect the fluorescence as a function of position within the sample. This technique allows concentrations of up to 5×10^{-4} M R6G to be determined, as well as displaying the distribution of less concentrated samples. Using a solution of 2×10^{-4} M R6G in methanol and a standard 2.5nm pore size gel-silica sample it can be seen that the dye remains confined within 250 μm of the edge of the sample even after several days immersion in solution. In contrast, the results for a large pore size sample (4nm diameter) after 15 minutes and 7 hours immersion are presented in figure 3. This clearly shows the slow time dependence of the diffusion process into the sample, despite the fact that the solvent penetrates to the centre in a matter of minutes. The importance of relative pore size and dopant size, the choice of solvent, the processing of the gel-silica and the possibility of tailoring dopant distributions to meet specific requirements and applications are still under investigation.

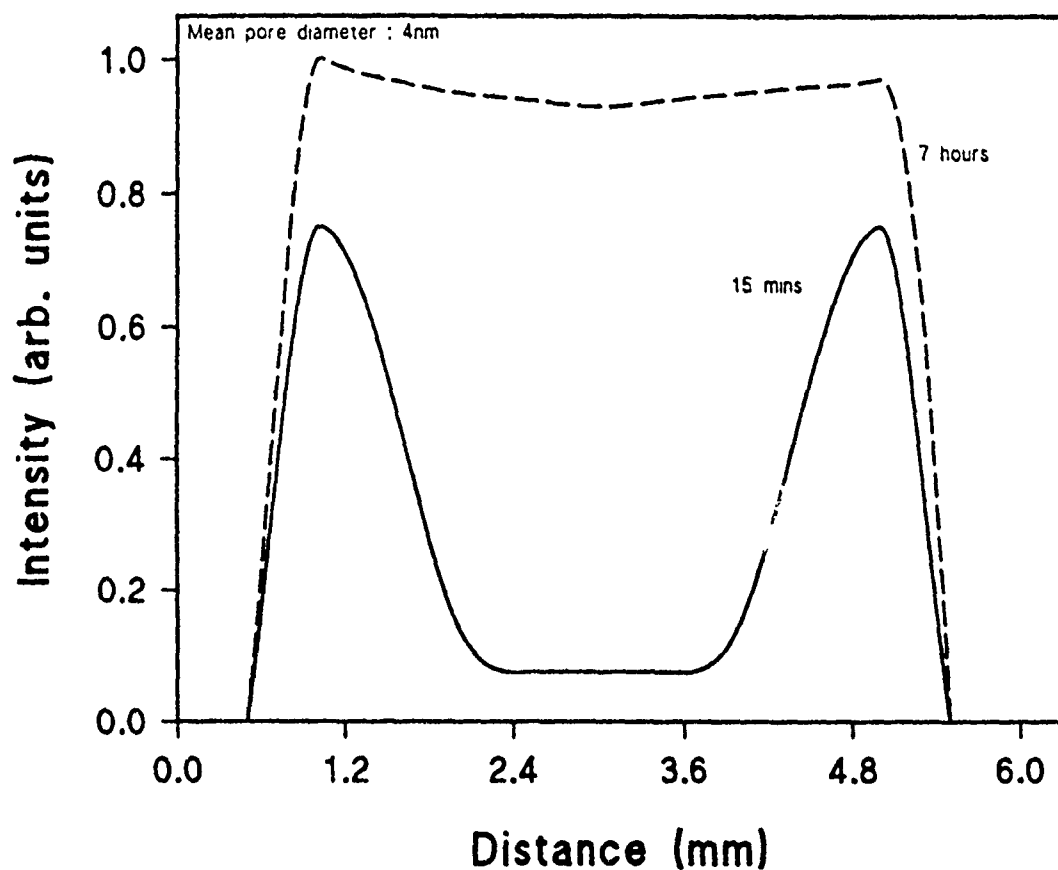


Figure 3.

Fluorescence intensity across a doped gel-silica sample after being immersed in R6G solution for a) 15mins and b) 7 hours.

Laser Enhanced Densification

Introduction

Previous studies on laser enhanced densification of gel-silica using a CO₂ laser have proved successful and thresholds for densification and damage to the gel-silica have been determined at 4.3J/cm² and 6.4J/cm² respectively. The main limitation of this technique is the difficulty in focusing the CO₂ laser radiation to a spot significantly smaller than 100μm, thus limiting the spatial resolution and minimum size of waveguide produced. One way of reducing this minimum size is to dope the undensified gel-silica with a suitable species which absorbs radiation at shorter wavelengths, e.g. from an argon ion laser, where radiation can

readily be focused to a spot size of $10\mu\text{m}$ or less. As well as producing greater resolution this also enables much higher intensities to be achieved with a modest power (3W) laser.

Results

Initial developments of this technique have involved the use of rhodamine 6G as the absorbing species doped into gel-silica partially densified to 1000°C . The dopant concentration of 5×10^{-3} M leads to an absorption coefficient of approximately 500cm^{-1} for the argon ion radiation, similar to that of CO_2 laser radiation in silica. The quantum efficiency of R6G is approximately equal to 1 and so the actual energy deposited in the dye is given by the energy difference between the excitation photon ($\lambda=488\text{nm}$) and the fluorescent photon ($\lambda=600\text{nm}$). This means that approximately 20% of the incident energy is transferred to heat and used to densify the gel-silica matrix, therefore the energy densities which follow have been adjusted to allow for this factor.

Using a 3W argon ion laser focused to a spot size of $100\mu\text{m}$, thresholds for damage to the gel-silica have been measured using two techniques. First the sample was held stationary and the exposure time and laser power varied to determine the damage threshold which in this way was measured at approximately $5\text{J}/\text{cm}^2$. The second technique involved translating the sample through a fixed laser beam at velocities between $10\text{cm}/\text{s}$ and $30\text{cm}/\text{s}$ to determine the velocity below which damage occurred. This was measured at $24\text{cm}/\text{s}$ corresponding to an energy density of $3.4\text{J}/\text{cm}^2$. These values agree well with those given for the CO_2 laser.

Reduction of the exposure energy below the thresholds determined above produced visible changes in the doped gel-silica samples in both the static and translation techniques. Preliminary measurements of the microhardness across these tracks and discs however showed no significant variation from the unexposed regions. These observations could be explained by one or more of the following:

1. The gel-silica sample at 1000°C was already near fully densified, allowing only a further 10% increase in microhardness - this is within the errors of the Riechart 2683 microhardness apparatus used.
2. The maximum temperature is produced below the surface of the gel-silica sample and so the surface hardness need not be significantly changed to produce densification below the surface. If this effect does occur then it suggests a method of producing cladded waveguide devices.

3. The damage produced is caused by evaporation of the organic species and does not necessarily correspond to a temperature sufficient to densify the gel-silica - reduction of the incident energy below this leads merely to a bleaching effect which can be observed optically.

Work is continuing to fully explain these results and to investigate the possibility of using inorganic species as an alternative dopant. Further studies will include densification at elevated temperatures to ensure no water is trapped in the gel-silica matrix and also the laser densification of thin films.

Basic Properties of Adsorbed Molecules

Introduction

The radiative properties of dye molecules adsorbed into gel-silica hosts can exhibit significant differences from traditional solvent hosts due to molecular isolation and immobility. Studies of absorption spectra, emission spectra and excited state lifetimes have confirmed these differences and an experiment to measure dye photostability in terms of these parameters and quantum efficiency has been designed and is presently under construction.

Results

The two dyes studied were rhodamine 6G and methylene blue, and in each case three different hosts of methanol, water and gel-silica were used. The concentration of all the samples was only 2×10^{-6} M in order to minimise any concentration quenching effects which might otherwise distort the results. The properties measured were the absorption spectra using an absorption spectrometer, the emission spectra using an argon ion laser excitation source and an optical multichannel analyser, and the excited state lifetime using a mode locked cavity dumped dye laser and photon counting technique.

In the case of rhodamine 6G no significant host dependent effects were observed, however with methylene blue there was a definite decrease in the absorption peak wavelength from water to methanol to gel-silica, and a similar decrease in the emission peak wavelength. The

most striking effect was the increase in the excited state lifetime from 285ps in water to 1.8ns in gel-silica. The measured lifetime in gel-silica actually had two components of 300ps and 1.8ns in approximately equal proportions, a fact which can be explained by the residual water deliberately present in the gel-silica sample for index matching purposes and to reduce scattered light. The detailed results for both dyes in each of the three hosts are presented in table 1.

		Absorption Peak +/- 1 nm	Emission Peak +/- 2 nm	Lifetime ns +/- 10%
	Water	525	551	4.6
Rhodamine 6G	Methanol	525	551	4.6
	Gel-silica	525	547	4.6
	Water	663	674	0.28
Methylene Blue	Methanol	652	671	0.57
	Gel-silica	644	668	1.8

Table 1.

Physical properties of dyes in water, methanol and gel-silica hosts.

These results are not unexpected because the high quantum efficiency of R6G in methanol cannot be significantly improved by molecular isolation, whereas methylene blue has a low quantum efficiency which is clearly increased in the gel-silica host. This is an significant result which demonstrates the importance of the interaction between the gel-silica host and the absorbed species. Further work is underway to develop an experiment which directly measures the quantum efficiency of the absorbed dye as well as the excited state lifetime. This experiment will also monitor the dye photostability, allowing the most favourable gel-silica doped system to be selected as well as probing the basic physics of the interaction.

Acknowledgements

This work was supported by a grant from the A.F.O.S.R. (Contract No. 90-0338). Gel-silica samples were supplied by the Advanced Materials Research Center, University of Florida, and GELTECH Inc. Discussions with Professor Larry Hench and Dr Jon West are gratefully acknowledged.

Structural Studies of Sol-gel Glasses

Carole C. Perry and Xiaochun Li

Chemistry Department

Brunel University

Uxbridge

Middlesex

UB8 3PH

Chemical/ spectroscopic studies have been performed on a range of sol-gel derived materials including;

(a) silica gel glasses (metal ion doped and dye doped)

(b) silica/ titania gel glasses

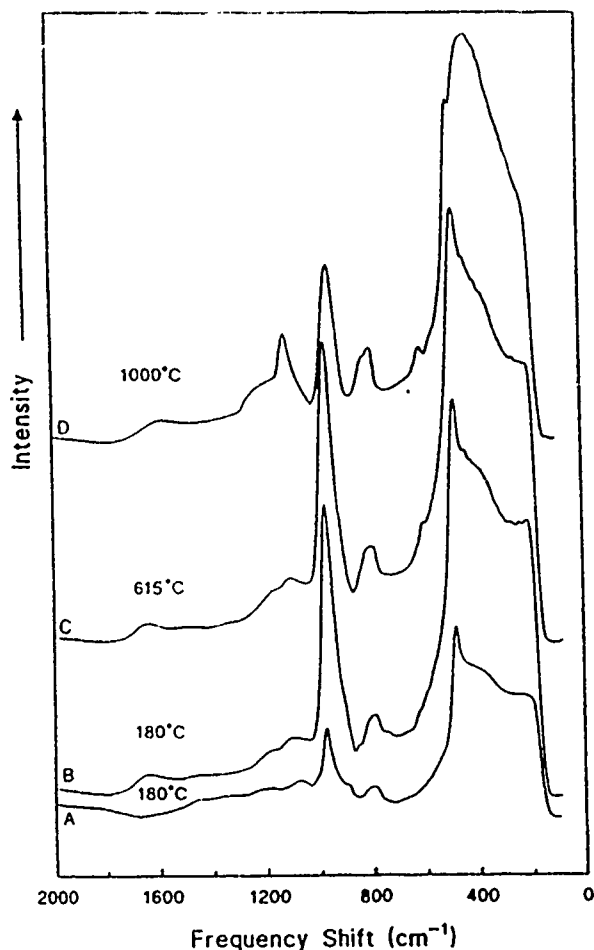
This report will detail information obtained from detailed studies of the silica/ titania gel glasses and preliminary information obtained from study of Rhodamine 6G dye doped silica gel glasses.

Spectroscopic Studies of Silica/Titania Gel Glasses

The addition of heteroatoms such as titanium at the gel synthesis stage leads to glasses with very low thermal expansion coefficients with increased refractive index. At the molecular level, introduction of titanium into the gel structure (average bond angles, Ti-O-Ti, 159° , Si-O-Si, 152° and bond length Ti-O, 1.8-1.86Å, Si-O, 1.6Å) yields more readily deformable structures although there are problems to contend with in the presence of elements with different coordination requirements. These problems become more apparent as thermal treatment temperatures are increased and solid state changes including ion migration occur. In addition, the incorporation of electropositive elements provides for variations in charge and surface functional groups. This may well be of importance, particularly for the porous gel glasses where potential applications in the areas of membrane technology, gas separation and catalysis all rely for their efficacy upon the structure and surfaces of the material which are presented to the reaction environment. For all of these applications, it is of fundamental importance to understand the nature of the chemical reactions which occur between gel-glass surface species and adsorbed species.

Transmittance and reflectance infrared studies of these materials in powdered form and as monoliths respectively have shown that thermal treatment up to 1000°C of glasses containing 3% titanium leads to the expected increase in mean Si-O bond strength but is not accompanied by a reduction in mean Si-O-Si bond angle and angular spread for this feature. The gel-silicas are more open and disordered, even in the presence of low levels of titanium. Evidence can be obtained for the formation of Si-O-Ti bonds, principally during the later stages of thermal treatment (above 600°C) but clear evidence was obtained from FT-Raman data discussed below.

The figure below shows Raman spectra for silica and silica/titania gel glasses. The corresponding table shows the peak positions for bands of interest.



FT-Raman spectra for silica and 3% titania/silica gel-glasses subjected to a range of thermal treatments. (a) silica, 180°C, (b) silica/titania, 180°C, (c) silica/titania, 615°C, (d) silica/titania, 1000°C.

Raman spectra for the silica gel glasses resemble those obtained for vitreous silica. The strongest line at ca. 430 cm^{-1} is due to in-plane Si-O-Si bending (weak or absent in the ir, though accidentally close to the out-of-plane bending vibration). This line shows no observable LO-TO splitting. The symmetric (ca. 800 cm^{-1}) and antisymmetric (ca. 1100 cm^{-1}) Si-O-Si stretching modes show such splittings, which become well developed in

higher temperature samples, and for both modes the LO component is assigned to the higher wavenumber feature of the pair.

SiO ₂ gel glasses						SiO ₂ / TiO ₂ gel glasses			assignment
180°C	600°C	700°C	1000°C	1100°C	1150°C	180°C	615°C	1000°C	
421	424	428	430	430	436	420	424	430	$\delta(\text{Si-O-Si})$, i.p.
486	487	488	488	486	488	483	485	484	D ₁ , 4-fold ring
—	601	601	601	601	601	596	596	597	D ₂ , 3-fold ring
800	795	796	796	794	795	796	796	795	$\nu_s(\text{Si-O-Si})$, TO
	818	818	817	818	818	816	816	817	$\nu_s(\text{Si-O-Si})$, LO
974	975	975	974	968	—	968	966	942	$\nu(\text{Si-OH, Ti-OH})^a$ $\nu_{as}(\text{Si-O-Ti})^b$
1061	1056	1058	1060	1064	1067	1090	1101	1108	$\nu_{as}(\text{Si-O-Si})$, TO ^a $\nu_{as}(\text{Si-O-Ti})^b$
1171	1170	1174	1176	1200	1192	1155	1163	1167	$\nu_{as}(\text{Si-O-Si})$, LO

^a Dominant < 1000°C. ^b Dominant at 1000°C.

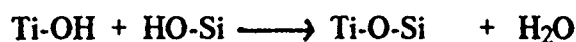
Observed FT-Raman frequencies (cm⁻¹) and assignments

The sharp bands at 490 cm⁻¹ (D1) and 605 cm⁻¹ (D2) (high temperature glasses only) have been ascribed to tetrasiloxane and trisiloxane rings in the gel glass. The spectra indicate that trisiloxane rings are absent from the low temperature samples but grow in abundance as the treatment temperature is increased. Tetrasiloxane rings, by contrast, are significant in the low temperature materials, where they originate from small molecule precursors, and persist to high temperatures.

Calculations using the 'centre of gravity' of the symmetric stretch and the peak maximum of the in-plane bend have shown that over the range 700 to 1150°C the calculated mean bond angle is of the order of 135°, although a small reduction (ca. 1.5°) in mean bond angle with increasing temperature was measured. This value is of the same order calculated for vitreous silica and suggests densification has little effect on the first coordination sphere of the silicon atom. The result gives independent support for the consolidation of the molecular framework accompanying the temperature treatment. Over the same temperature range, the angular spread changes from 14° to 12°, again similar to that calculated for vitreous silica and the change, though small, is qualitatively consistent with the known densification. We are not aware of other techniques which yield an estimate of the magnitude of this effect.

It must be noted that the structural changes observed on densification include changes in bond length, changes in mean Si-O-Si bond angle and in the distribution of bond angles.

The Raman spectra for the titanium-containing samples show differences similar to those observed in the ir although band broadenings are less marked, at least up to temperatures of 615°C. It is important to note that with increasing titanium content and increasing temperature bands arising from ring structures shift to lower frequency indicating that under these conditions, more titanium is incorporated into ring structures. Comparison with spectra obtained from the silica-only samples shows an enormous increase in significance of a band at ca. 970 cm⁻¹. A shoulder due to the formation of Si-O-Ti can be observed to the low frequency side, but the band derives predominantly from Si-OH and Ti-OH stretching vibrations. The relatively high intensity is readily explained by the larger polarizability change associated with the Ti-O bond. Above 615°C water loss occurs according to



such that, at 1000°C, Raman intensity at 970 cm⁻¹ declines and is replaced by Si-O-Ti features at 945 and 1110 cm⁻¹. Therefore, full incorporation of titanium atoms into the silica framework occurs only at the higher temperatures. Implicit in this statement is that the majority of titanium atoms must be situated at surface sites in order for this phenomenon to occur.

It must be noted that a band at ca. 685 cm⁻¹ due to octahedrally coordinated titanium is not observed at any of the sampling temperatures indicating that the materials do not contain any phase segregated titanium dioxide.

Near infrared studies have been performed on silica/ titania gel glasses after a range of thermal treatments in order to investigate the effect of 'foreign' ion incorporation on silica surface functional species. These studies have shown for the silica sample that in addition to a general strengthening of the matrix at high temperature, the O-H bond of the silanol group is also strengthened which leads to significant decrease in the ability of silanol groups in the high temperature samples to bind water. The importance of water molecules as secondary absorbing sites within the gel-glass is therefore increased.

The addition of titanium leads to a change in distribution of surface functionalities for the gel-glass material. A reduction in 'free' silanol levels and an increase in hydrogen bonded silanol groups, even after extended evacuation, occurs. In addition, the amount

of water remaining within the glass and the proportion of associated versus isolated water molecules also increases.

Thermal treatment of glasses containing even modest amounts of titania (3%) at 1000°C resulted in materials which contained fewer free silanol groups, most of which were found in the bulk rather than in the surface layers (in direct contrast to what has been observed for the silica only samples). In addition, the relative amounts of perturbed or hydrogen bonded silanol groups was higher. On hydration, all free silanol groups in the surface layers became hydrogen bonded to water although in the bulk of the glass low levels of silanol groups were unaffected by the hydration process. In addition, any increase in water levels on exposure of the sample to water vapour was significantly reduced in comparison to that observed for the silica only samples. These observations suggest that for glasses containing 3% titanium and heated to 1000°C the silanol groups are largely not accessible to the external environment. They are either perturbed by their immediate matrix environment or have been isolated within pores in association with water molecules. The implication is that the presence of titanium in the gel matrix leads to a tighter binding of water molecules to silanol groups. From these spectra it is not possible to say anything about the preponderance of SiOH vs. TiOH groups present within the sample as bands arising from titanium containing species would be very weak in comparison to those for silicon species.

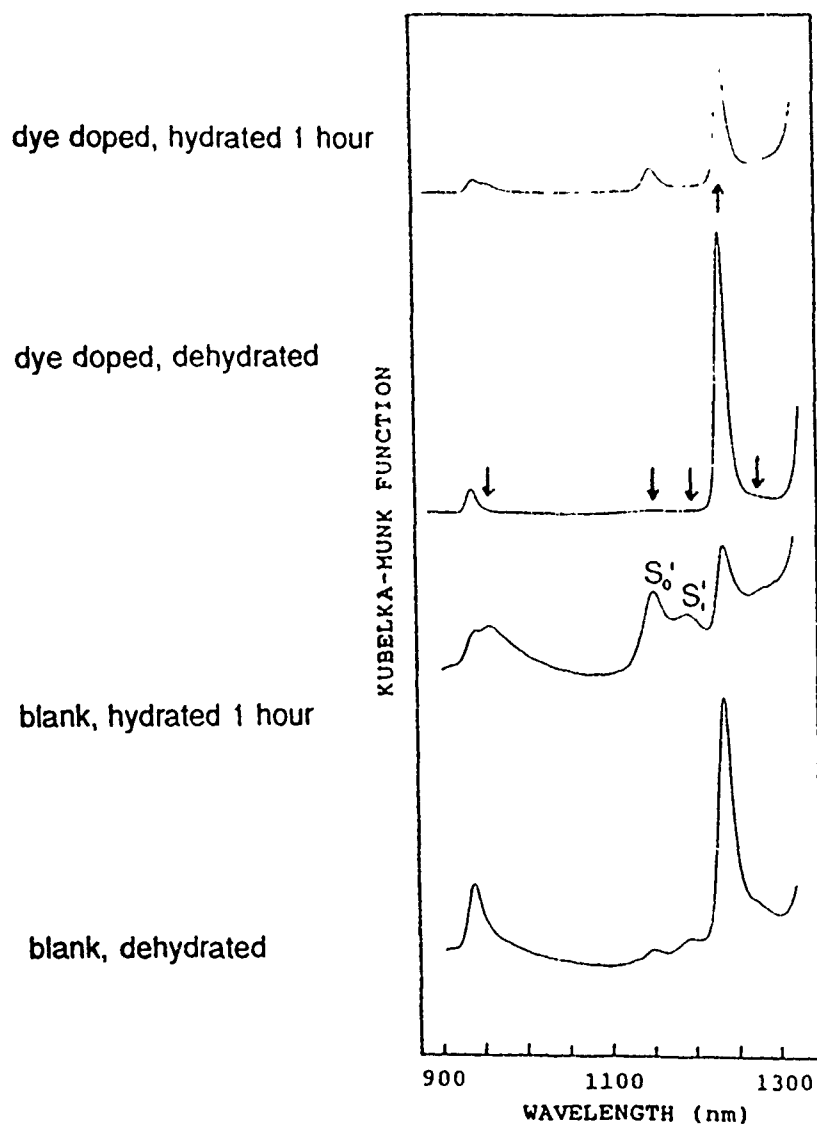
The principal conclusions resulting from this study are the following:

The addition of titanium atoms to gel glasses at the mixing stage leads to materials in which the majority of the metal ions are found at the surfaces of the fundamental particles making up the bulk phase. These 'foreign' ions affect the densification of the material and the surface chemistry of the resultant phases. It is only at higher temperatures that, for these systems, incorporation of the titanium ions into the matrix occurs fully. The addition of titanium leads to materials that are significantly more hydrophilic than for similar silica gel-glasses and leads to tighter binding of water molecules to silanol groups.

Spectroscopic studies of dye doped gel glasses

Initial studies on post doped Rhodamine 6G doped silica gel glasses thermally treated at 800 °C have concentrated on the behaviour of the dye molecule both in solution and within the pore matrix under a variety of reaction conditions. It is important to note that the absorption spectrum of the dye is dependent upon basic solution parameters such as concentration, pH and solvent used. Homogeneously doped glasses can be obtained if water is the solvent. If alcoholic solutions are used then the situation is identical to that observed for simple metal doped glasses. The alcoholated species do not diffuse well into the gel glass matrix (largely due to their large size) resulting in an inhomogeneous distribution within the sample. The uv/visible spectrum for the doped glass and solutions of the same concentration is the same and remains unaltered on dehydration of the gel glass.

An important phenomena which has been noted for the dye doped gel glasses is that the presence of the dye significantly reduces the amount of water present within the gel glass. Although the dye is absorbed from aqueous solutions, the levels of water present within the glass are significantly reduced. If a comparison is made of dye doped and blank glasses treated in an identical fashion (except for incorporation of the dye), see figure below, then we find that hydration takes much longer to accomplish for the dye doped gel glasses. It is important to note that the pattern of water speciation is different from that observed for blank glasses. The majority of the water present in the glass during the early stages of hydration is 'free' and bound only to silanol groups rather than being hydrogen bonded to other water molecules. This phenomenon may have a considerable role to play in determining the stability of such dye/ silica materials. It must be noted that the samples used for study had pores with average diameters of 24Å and the behaviour of gel glasses with much larger pores may show quite different behaviour to that presented above.



Near infrared spectra of silica and Rhodamine 6G doped silica glasses

S_0' corresponds to water molecules only bonded to silanol groups

S_1' corresponds to water molecules bonded to silanol groups and partially hydrogen bonded to other water molecules.

For further spectral assignments refer to the references listed below.

Acknowledgements

Support from the Air Force Office of Scientific Research Grant number AFOSR 89-0489 is gratefully acknowledged.

Publications

- (1) Perry CC, Li X, 1991 J. Chem. Soc. Faraday Trans. 87, 761
- (2) Perry CC, Li X, 1991 J. Chem. Soc. Faraday Trans., in the press
- (3) Perry CC, Li X, Waters DN, 1991 Spectrochimica Acta, in the press

PARTICIPANTS IN THE 4TH OGAMM MEETING
CRAIGLANDS HOTEL, ILKEY, YORKSHIRE
19-22 AUG 91

<u>NAME & ADDRESS</u>	<u>TELEPHONE NO</u>	<u>FAX NO</u>
Dr George Attard Department of Chemistry The University Southampton SO9 5NH UK	0703-559122 x2794	
Dr A Berry Physics Dept University of Manchester Manchester M13 9PL UK	061-275-4284	061 273 5867
Dr Alan Buckley Forschungsleitung Geb 8F-821 Hoechst AG Frankfurt, Germany		
Mr Paul L Carr Department of Physics University of Leeds Leeds LS2 3AR	0532-333808 (IMW)	
Dr Andrew Charlton Laser Research Group Physics Dept, Shuster Laboratory University of Manchester Manchester M13 9PL	(061) 275 4289	061 273 5867
Dr Larry R Dalton Department of Chemistry University of Southern California Los Angeles CA 90089-1062	(213) 743-7506	(213) 743-7757

<u>NAME & ADDRESS</u>	<u>TELEPHONE NO</u>	<u>FAX NO</u>
Dr Geoff R Davies IRC in Polymer Science & Technology University of Leeds Leeds LS2 3AR	0532-333815	0532-333846
Lt Col Chester J Dymek US Air Force European Office of Aerospace Research & Development 223/231 Old Marylebone Road London NW1 5TH	071-409-4384	071-402-9618
Mr Goerge Gallagher-Daggit Ministry of Defense Northumberland House Northumberland Avenue London WC2N 5BP	011-44-218-0545	071-218-4081
also at: Hayfield House 9 Tullis Close Sutton Courtenay Oxon OX14 4BD	0235-848288	
Mr Findlay Dept of Materials Science & Metallurgy Cambridge University Pembroke Street Cambridge CB2 3QZ, UK	0223-33-4300 (S'bd) 4355(Lab)	0223-334567
Dr Harris Goldberg Hoechst Celanese Research Division R L Mitchell Technical Center 86 Morris Avenue Summit New Jersey 07901	908-522-7523	908-522-7904
Mr S C Gratze GEC Marconi Research Center West Hanningfield Great Baddow Chelmsford Essex, UK	0245-73331	0245-75244

<u>NAME & ADDRESS</u>	<u>TELEPHONE NO</u>	<u>FAX NO</u>
Prof Dr Dietrich Haarer Lehrstuhl Experimental Physik IV Universitat Bayreuth Universitätsstrasse 30 Postfach 10-1251 8580 Bayreuth Germany	(0921)553240	(0921)553250
Dr Larry L Hench Advanced Materials Research Center University of Florida One Progress Boulevard, Box 14 Alachua, Florida 31615	904-462-5459	
Dr C T Imrie Department of Polymer Science and Engineering University of Massachusetts Graduate Research Center Amherst MA 01003	413-545-4783 or 0926	413-253-5295
Dr Frank E Karasz Department of Polymer Science and Engineering University of Massachusetts Graduate Research Center Amherst MA 01003	413-545-4783 or 0926	413-253-5295
Dr Terry King Physics Department Schuster Laboratory University of Manchester Manchester M13 3PL	061-275-4181	061-273-5867
Dr John D Mackenzie Department of Materials Science and Engineering School of Engineering and Applied Sciences Los Angeles, CA 90024	213-825-3539	

<u>NAME & ADDRESS</u>	<u>TELEPHONE NO</u>	<u>FAX NO</u>
Dr. D Michael Mingos Inorganic Chemistry Laboratory University of Oxford South Parks Rd Oxford OX1 3QR	(0865)272600	
Mr Spencer Modica Physics Department Loughborough University of Technology Loughborough Leicestershire LE11 3TU	0509-263171	0509-232772
Mr Naoya Ogata Dept of Chemistry Sophia University 7-1 K101-CHO Chiyoda-Ku Tokyo 102 Japan	81(Japan)-3(Tokyo)- 238-3447	81-3-264 0867
Dr Helen Ong Hoechst Celanese Research Division R L Mitchell Technical Center 86 Morris Avenue Summit, New Jersey 07901	908-522-7523	908-522-7904
Dr Carole C Perry Chemistry Department Brunel, The University of West London Uxbridge Middlesex UB8 3PH	0895-74000 x2293	0895-32806
Professor N J Philips Physics Department Loughborough University of Technology Loughborough Leicestershire LE11 3TU	0509-223303	0509-232772
Dr Prasad Department of Chemistry State University of New York, Buffalo Acheson Hall, Buffalo, NY 14214	716-831-3026	716-831-2960

<u>NAME & ADDRESS</u>	<u>TELEPHONE NO</u>	<u>FAX NO</u>
Dr Jim Stamatoff Hoechst Celanese Research Division R L Mitchell Technical Center 86 Morris Avenue Summit, New Jersey 07901	908-522-7785	908-522-3928
Dr Alan Windle Dept of Materials Science and Metallurgy Cambridge University Pembroke Street Cambridge CB2 3QZ UK	0223-334300/4321/4335	
Prof Graham Williams Department of Chemistry University of Wales University College Swansea, Singleton Park Swansea SA2 8PP	0729-205678	
Dr Mike R Worboys GEC-Marconi Research Centre West Hanningfield Road Great Baddow Chelmsford Essex, UK	0245-73331	0245-75244

DISTRIBUTION:

HQ AFSC/XT
/XTIC
IN TURN

HQ AFSC/XTR (Lt Col Larry Davis)

AFOSR/CC
/CD
/NC (Dr. Ball)
IN TURN

AFOSR/NC (Dr. Erstfeld)
NC (Dr. Gordon)
NC (Dr. Hedberg)
NC/Dr. C. Lee
NE (Dr. Schlossberg)

FJSRL/CA
/CD (Dr. John Wilkes)
IN TURN

FJSRL/NH (Dr. Kester)

PL/CA (Dr. Janni)

PL/WS/ARBM (Capt Corvo)

PL/XLI (Dr. Founds)

SDIO/IST (Dr. Len Caveny)

WL/CA (Dr. G. K. Richey)

WL/CA-M
/MLB (Dr. Dudis)
IN TURN

WL/MLB (Dr. Helminiak)
/MLB (Dr. Minges)
/MLBP (Dr. Evers)
/MLBP (Dr. Reinhardt)
/MLBT (Dr. Snyder)
/MLPJ (Dr. W. Adams)
/MLPO (Dr. G. Griffiths)
/MLPO (Mr. L. Riffie)

WL/CA-P
/POOS (Dr. Marsh)
IN TURN

WL/XO

USDAO LONDON
ODC/DCAO
IN TURN

SCIENCE OFFICER, US EMBASSY LONDON

ONREUR

USARDSG

EIDSON HOUSE LIBRARY

EOARD/CSX (3 copies)

Meeting participants